

**SYNTHESIS AND CHARACTERIZATION OF
GRAPHENE AND CARBON NANOTUBES FOR
REMOVAL OF HEAVY METALS FROM WATER.**

By

FORCE TEFO THEMA

Student number: 208014632

Dissertation submitted in fulfillment of the requirement for the degree of

MASTER OF TECHNOLOGY IN CHEMISTRY

FACULTY OF APPLIED AND COMPUTER SCIENCES

DEPARTMENT OF CHEMISTRY

Supervisor: Prof. E.D. Dikio

Co-supervisor: Prof. M.J. Moloto

June, 2012

DECLARATION

I hereby declare that this dissertation which I submit for the qualification of

Master of Technology Degree in Chemistry

To the Vaal University of Technology, Department of Chemistry, is apart from the recognized assistance of my supervisors, my own work and has not previously been submitted to any institution before for a research Diploma or Degree.

_____ On this _____ day of _____ 2012
Candidate

_____ On this _____ day of _____ 2012
Supervisor

_____ On this _____ day of _____ 2012
Co-supervisor

DEDICATION

I dedicate this work to my wife Margaret Mmasiako Thema, my son and daughter Batlhaping and Masa respectively, my late dad, mother, brothers, sisters, and relatives.

ACKNOWLEDGEMENTS

I would like to sincerely acknowledge people and organizations listed below for their immeasurable support and contribution for the success of this research project:

- First and foremost I thank and praise my Lord, God and my creator, who paved way for me to come this far, by giving me the strength, patience and intelligence to complete this research. In Jesus name, his mercy and glory be now and forevermore. Amen.
- My special thanks go to my supervisors Prof E.D. Dikio and Prof M. J. Moloto for all the moments spent together, the excellent guidance and encouragement during the period when the journey seemed endless and dark. Thank you a million times.
- It would be suicidal if I can forget to extend my specials thanks to Dr R.G. Chabo and Prof. M Maaza whose parental and technical assistance was respectively beyond any imagination.
- Million thanks go to Botswana College of Agriculture for sponsoring my study irregardless of how expensive it was and during the World economic meltdown times.
- Special thanks are also due to the Vaal University of Technology, particularly the research directorate and the Department of Chemistry for every support.
- Thanks to my fellow students N.D. Shooto, A.M. Farah and P.T. Ngoy for their good company and support.
- Special thanks go to my family, parents, my brothers and my sisters for all support, patience and prayers granted during the course of my study.
- Finally I would like to thank myself and all my friends.

PRESENTATIONS, WORKSHOPS AND PUBLICATIONS

Presentations

The work presented in this dissertation has been published in peer-viewed journals and presented at the following conferences.

1. Poster Presentation: **F.T. Thema**, E.D. Dikio, M.J. Moloto, M. Khenfouch, N.N. Nyangiwe, L. Kotsedi, M. Maaza, TechConnect World 2012 Conference and Trade Show, Santa Clara, California, United States of America. 18-21st June, **2012**, “Synthesis and characterization graphene thin films via Hummer’s method”.
2. Poster Presentation: **F.T. Thema**, E.D. Dikio, M.J. Moloto, M. Khenfouch, N.N. Nyangiwe, L. Kotsedi, M. Maaza, South African Nanotechnology Initiative (SANI) NanoAfrica 2012, University of the Free State, Bloemfontein, South Africa. 1-4th April, **2012**, “Synthesis and characterization graphene thin films via Hummer’s method”.
3. Oral Presentation: **F.T. Thema**, E.D. Dikio, M.J. Moloto, M. Khenfouch, N.N. Nyangiwe, L. Kotsedi, M. Maaza, South African Chemical Institute (SACI) young chemist symposium, Vaal University of Technology, Vanderbijlpark, South Africa. 14th October, **2011**, “Synthesis and characterization graphene thin films via Hammer’s method”.

Workshops

1. Indo-South Africa Symposium on Nanotechnology and Innovation, Unisa, Pretoria. 12-15th March, **2012**.
2. Summer Nano School, Nelson Mandela Metropolitan University, Port Elizabeth, 27-2nd November, **2011**.

Publications

1. **F.T. Thema**, M.J. Moloto, E.D Dikio, N.N Nyangiwe, L Kotsedi, M. Maaza, and M. Khenfouch. Synthesis and characterization of graphene thin films by chemical reduction exfoliated and intercalated graphite oxide. *E. J. Chem.* (2012) DOI: 10.1155/2012/150536.
2. **F.T. Thema**, M.J. Moloto, E.D. Dikio N.N. Nyangiwe, L. Kotsedi, M. Maaza, M. Khenfouch. Synthesis and characterization of graphene thin films via Hummers Method. Technical Proceedings of the Nano Science and Technology Institute, 2012, 1, 13-16. ISBN 978-1-4665-6274-5.
3. Abdullahi M. Farah, **Force T. Thema** and Ezekiel D. Dikio. Electrochemical detection of hydrogen peroxide based on graphene oxide/Prussian blue modified glassy carbon electrode. *Int. J. Electrochem. Sci.* 7(6) (2012) 5069 – 5083.
4. Abdullahi M. Farah, Ntaote D. Shooto, **Force T. Thema**, Johannes S. Modise and Ezekiel D. Dikio. Fabrication of Prussian blue/Multiwalled carbon nanotubes modified glassy carbon electrode for electrochemical detection of hydrogen peroxide. *Int. J. Electrochem. Sci.* 7(5) (2012) 4302-4313.
5. **Force T. Thema**, Abdullahi M. Farah, Ntaote D. Shooto, and Ezekiel D. Dikio. One-step reduction, characterization and magnetic behaviour of exfoliated graphene oxide. *J. Mater. Sci. Pol.* (2012) **Submitted. Ref: 2012-375.**
6. Albert J. Kupeta, **Force T. Thema**, Charity W. Dikio and Ezekiel D. Dikio. A comparative study of the effect of MgO and CaCO₃ as support materials in the synthesis of carbon nanotubes with Fe/Co catalyst. *J. Synth. React. Inorg. Metal Org. Nano Metal Chem.* (2012) **Submitted. Ref: LSRT-2012-0089**
7. Ntaote D. Shooto, **Force T. Thema**, Abdullahi M. Farah, and Ezekiel D. Dikio. Raman and TGA study of carbon nanotubes synthesized over Mo/Fe catalyst on aluminium oxide, calcium carbonate and magnesium oxide support. *J. Mat. Chem. Phys.* (2012) **Submitted. Ref: MATCHEMPHYS-D-12-01003.**

ABSTRACT

The commercial flake graphite was prepared into functionalized graphite oxide (GO) by adopted chemical treatment. After the exfoliation and intercalation of graphite into functionalized graphene oxide that formed stable colloidal dispersion in polar aprotic solvent, the reduction process was undertaken by continuous stirring with hydrazine hydrate in a microwave at 35 °C for two hours. The reduced material was characterized by X-ray diffraction (XRD), attenuated total reflectance (ATR) FT-IR, Ultra-violet visible (UV-vis), atomic force microscopy (AFM), transmission electron microscopy (TEM), scanning electron microscopy (SEM), Raman microscopy and magnified optical microscopy that confirm the oxidation of graphite and reduction of graphene oxide into graphene sheets.

Carbon nanomaterials were synthesized from Co-Sn, Co-Sr and Co-Zn as catalysts supported on Al₂O₃, CaCO₃ and MgO. The as-prepared nanomaterials were characterized by thermogravimetric and derivative thermogravimetric analysis (TGA & DTA), Raman spectroscopy, scanning electron microscopy (SEM) and energy dispersive spectroscopy (EDS) and the transmission electron microscopy. The intensity ratios (I_D/I_G) of the D- and G- bands were found to be the same that is averagely at 0.83. The TGA & DTA curves have shown Co-Sn/Al had significant weight loss, Co-Sr/Mg weight loss and decomposition, Co-Sr/Al decomposition and Co-Zn/Mg weight loss. However these weight losses were not significant. The EDS analysis showed all elements which took part in the reaction confirming the success of each synthesis. The SEM images show carbon nanotubes only on samples that have been synthesized on MgO as confirmed by TEM images. Finally the XRD showed some characteristic peaks at desired peaks except that they were other peaks attributed to impurities and amorphous carbon. It was also observed that Co-Sn/Al and Co-Sn/Mg XRD curves showed broad peaks at $\theta = 24.3^\circ$ & 42.6° and $\theta = 23.9^\circ$ & 43.1° respectively which are lattice structure characteristic peaks.

TABLE OF CONTENTS

Declaration	i
Dedication	ii
Acknowledgements	iii
Presentations and publications	iv
Abstract	v
Table of content	vi
List of figures	x
List of table	xi
List of abbreviations	xii

CHAPTER ONE

INTRODUCTION AND PROBLEMMENT STATEMENT

1.1. Introduction	2
1.2. Graphene	2
1.3. Carbon nanotubes	4
1.4. Problem statement	6
1.5. Objectives	7
1.6. Value of research	7
1.7. Outline of the dissertation	8
References	9

CHAPTER TWO

LITERATURE REVIEW

2.1. Introduction	14
2.2. Properties of graphene	16
2.2.1. Electronic properties	15
2.2.1.1. Optical properties	16
2.2.1.2. Relativistic Charge carriers	17
2.2.1.3. Anomalous Quantum Hall Effect	17
2.2.2. Thermal properties	18
2.2.2.1. Intrinsic Thermal properties	19
2.2.3 Mechanical properties	19
2.3. Potential Applications/Uses of graphene	20
2.3.1. Water Purification	20
2.3.2. Single molecule gas detection	21
2.3.3. Graphene transistors	22
2.3.4. Graphene biodevices	23
2.3.5. Transport conducting electrodes for replacement of Indium tin oxide (ITO)	23
2.4. Carbon nanotubes (CNTs)	24
2.5. Types of CNTs	25
2.5.1 Single walled carbon nanotubes	25
2.5.2 Multi walled carbon nanotubes	26
2.6. Properties of Carbon Nanotubes (CNTs)	26
2.6.1. Optoelectronic properties	26
2.6.2. Thermal properties	26
2.6.3 Atomic and Electronic structure of disordered carbons	27
2.6.4. Mechanical properties	27
2.7. Potential application/Uses of Carbon Nanotubes	27
2.7.1. Water purification	27
2.2.5. Reinforcement for polymer nanocomposites	28
References	29

CHAPTER THREE

EXPERIMENTAL METHODS

3.1 Introduction	35
3.2 Chemicals and Materials	35
3.3 General experimental procedure and characterization techniques	35
3.3.1 Synthesis of graphene oxide	35
3.3.2 Reduction of graphene oxide	37
3.3.3 Sample preparation	36
3.4 Chemical reactions	36
3.4.1 Oxidation of graphite flake	36
3.4.2 Reduction of graphene oxide	37
3.4.3 Removal of metal ions	37
3.5 Carbon nanotubes	37
3.5.1 Synthesis of catalysts	37
3.5.2 Synthesis of carbon nanotubes	38
3.6. Analytical techniques used in this study	39
3.6.1 X-ray diffractometer (XRD)	39
3.6.2 Fourier transform infrared (FTIR) spectrometry	41
3.6.3 Ultraviolet visible (UV-Vis) spectrometry	42
3.6.4 Scanning electron microscopy (SEM)	43
3.6.5 Transmission electron microscopy (TEM)	44
3.6.6 Raman spectroscopy	45
3.6.7 Atomic force microscopy (AFM)	47
3.6.8 Optical microscopy	48
3.6.9 Thermogravimetric analysis (TGA)	50
References	61

CHAPTER FOUR

RESULTS AND DISCUSSION

4.1 Introduction	54
4.2 Synthesis of graphene oxide, reduced graphene oxide and carbon nanotubes	54
4.3 Physico-chemical measurements	54
4.4 Graphene/Graphene oxide characterization	55
4.4.1 X-ray Diffraction microscopy	56
4.4.2 Fourier transform infrared microscopy (FTIR-ATR)	57
4.4.3 Ultraviolet visible microscopy	58
4.4.4 Scanning electron microscopy	59
4.4.5 Transmission electron microscopy	60
4.4.6 Raman spectroscopy	61
4.4.7 Atomic force microscopy	62
4.4.8 Optical microscopy	64
4.5 Carbon nanotubes characterization	65
4.5.1 X-ray Diffraction microscopy	65
4.5.2 Raman spectroscopy	71
4.5.3 Thermogravimetric analysis	78
4.5.4 Scanning electron microscopy	83
4.5.5 Energy dispersive energy	88
4.5.6 Transmission electron microscopy	94
4.5.6 Heavy metals extraction analysis	97
References	100

CHAPTER FIVE

5.1 Introduction	102
5.2 Graphene and graphene oxide	102
5.2.1 Morphological analysis	103
5.3 Carbon nanotubes	104
5.3.1 Structural analysis	104
5.3.2 Morphological analysis	104
5.4 Recommendation	104

LIST OF FIGURES

Figure 1.1 Graphene top left is a honeycomb lattice of carbon atoms. Graphite top right can be viewed as a stack of graphene layers. Carbon nanotubes are rolled-up cylinders of graphene bottom left. Fullerenes C ₆₀ are molecules consisting of wrapped graphene by the introduction of pentagons on the hexagonal lattice	3
Figure 1.2 Presenting the formation of CNTs	4
Figure 2.1 Molecular structure of graphene	16
Figure 2.2 Pictures of brownish graphene oxide (GO) & blackish reduced graphene oxide (RGO)	16
Figure 2.3 Spike-like changes in Hall resistivity near neutral point. (Schedi, Nat. Mater. 6 (2007) 652)	23
Figure 2.4 Structures of the main types of carbon nanotubes	26
Figure 2.5 Carbon allotropes	27
Figure 3.1 A picture of synthesized but not calcined catalyst	41
Figure 3.2 Synthesis of carbon nanotubes	42
Figure 3.3 Diagram of the horizontal furnace used for synthesis of CNTs	42
Figure 3.4 Schematic diagram of X-ray diffractometer	43
Figure 3.5 Schematic diagram of fourier transform infrared	46
Figure 3.6 Schematic diagram of UV-Visible spectrophotometer	46
Figure 3.7 Schematic diagram of scanning electron microscope	47
Figure 3.8 Schematic diagram of transmission electron microscope	48
Figure 3.9 Schematic diagram of conventional Raman spectroscopy	49
Figure 3.10 Schematic diagram of atomic force microscope	51
Figure 3.11 Schematic diagram of Optical microscope	52
Figure 3.12 Schematic diagram of thermogravimetric analyser	54
Figure 4.1 XRD patterns of graphene oxide	60

Figure 4.2 XRD patterns of reduced graphene oxide	61
Figure 4.3 FTIR (ATR) patterns of graphene oxide and reduced graphene oxide	62
Figure 4.4 The structure model of the graphite oxide species.	63
Figure 4.5 Uv-vis spectra of graphene and graphene oxide.	64
Figure 4.6 Typical SEM images of GO and RGO.	65
Figure 4.7 Typical TEM images of GO and RGO.	66
Figure 4.8 Raman spectra of graphene oxide in the range of 250-2500 cm^{-1}	67
Figure 4.9 3D AFM topography of graphene oxide.	68
Figure 4.10 3D AFM topography of reduced graphene oxide.	69
Figure 4.11 Optical (a) graphene oxide and (b) reduced graphene oxide	70
Figure 4.1.3 XRD patterns of CNTs synthesized with Co-Sn catalysts supported on Al_2O_3 (b) CaCO_3 (c) MgO .	73
Figure 4.1.4 XRD patterns of CNTs synthesized with Co-Sr catalysts supported on (a) Al_2O_3 (b) CaCO_3 (c) MgO .	75
Figure 4.1.5 XRD patterns of CNTs synthesized with Co-Zn catalysts supported on (a) Al_2O_3 (b) CaCO_3 (c) MgO .	77
Figure 4.1.6 Raman spectra of CNTs synthesized with Co-Sn catalyst supported on (a) Al_2O_3 (b) CaCO_3 and (c) MgO .	80
Figure 4.1.7 Raman spectra of CNTs synthesized with Co-Sr catalyst supported on (a) Al_2O_3 (b) CaCO_3 and (c) MgO .	82
Figure 4.1.8 Raman spectra of CNTs synthesized with Co-Zn catalyst supported on (a) Al_2O_3 (b) CaCO_3 and (c) MgO .	84
Figure 4.1.9 Thermo gravimetric and derivative thermo gravimetric analysis of CNTs obtained from Co-Sn catalyst supported on (a) Al_2O_3 (b) CaCO_3 and (c) MgO	87
Figure 4.2.0 Thermo gravimetric and derivative thermo gravimetric analysis of CNTs obtained from Co-Sr catalyst supported on (a) Al_2O_3 (b) CaCO_3 and (c) MgO .	89

Figure 4.2.1 Thermogravimetric and derivative thermogravimetric analysis of CNTs obtained from Co-Zn catalyst supported on (a) Al ₂ O ₃ (b) CaCO ₃ and (c) MgO.	91
Figure 4.2.2 SEM images for CNTs synthesized with Co-Sn catalysts supported on (a) Al ₂ O ₃ (b) CaCO ₃ (c) MgO.	93
Figure 4.2.3 SEM images for CNTs synthesized with Co-Sr catalysts supported on (a) Al ₂ O ₃ (b) CaCO ₃ (c) MgO.	95
Figure 4.2.4 SEM images for CNTs synthesized with Co-Zn catalysts supported on (a) Al ₂ O ₃ (b) CaCO ₃ (c) MgO.	97
Figure 4.2.5 Energy Dispersive Spectroscopy analysis of CNTs obtained from Co-Sn catalyst supported on (a) Al ₂ O ₃ (b) CaCO ₃ and (c) MgO.	99.
Figure 4.2.6 Energy Dispersive Spectroscopy analysis of CNTs obtained from Co-Sr catalyst supported on (a) Al ₂ O ₃ (b) CaCO ₃ and (c) MgO.	101
Figure 4.2.7 Energy Dispersive Spectroscopy analysis of CNTs obtained from Co-Zn catalyst supported on (a) Al ₂ O ₃ (b) CaCO ₃ and (c) MgO.	103
Figure 4.2.8 depicts TEM image for Co-Sn/Ca and it shows that carbon nanotubes were not synthesized but only carbon spheres.	104
Figure 4.2.9 TEM image for Co-Sr/Ca	105
Figure 4.3.0 TEM image for Co-Sr/Mg	106
Figure 4.3.1 TEM image for Co-Zn/Ca	107
Figure 4.3.2 TEM image for Co-Zn/Mg	108

◆—————◆

LIST OF TABLES

Table 4.1 shows T-band peak height and intensity, D and G band peak heights and intensities and the ratios of D and G bands obtained from Raman spectra of CNTs synthesized with various catalyst and support materials.	85
Table 4.2 showing pH for $\text{Pb}(\text{NO}_3)_2$ before and after filtered through graphene oxide.	109
Table 4.3 showing pH for $\text{Pb}(\text{NO}_3)_2$ before and after filtered through reduced graphene oxide.	109
Table 4.4 showing pH for $\text{Pb}(\text{NO}_3)_2$ before and after filtered through carbon nanotubes.	109

Equations

Equation 2.1	17
Equation 2.2	18
Equation 2.3	18
Equation 3.1	36
Equation 3.2	36
Equation 3.3	36
Equation 3.4	36
Equation 3.5	36
Equation 3.6	37
Equation 3.7	37
Equation 3.8	37
Equation 3.9	37
Equation 3.10	37
Equation 3.11	39
Equation 3.12	39
Equation 3.13	40
Equation 3.14	43

LIST OF ABBREVIATIONS

- FTIR: Fourier transform infrared
- TGA: Thermo gravimetric analysis
- UV-Vis: Ultraviolet-Visible
- TEM: Transmission electron microscope
- SEM: Scanning electron microscope
- FE-SEM: Field emission scanning electron microscope
- EDS: Energy dispersive spectroscopy
- AFM: Atomic force microscope
- XRD: X-ray Diffractometer
- GO: Graphene oxide
- RGO: Reduced grapheme oxide
- CNTs: Carbon nanotubes
- SWNTs: Single walled nanotubes
- DWNTs: Double walled nanotubes
- MWNTs: Multi walled nanotubes
- SLG: Single layer grapheme
- BLG: Back-gated bilayer grapheme
- PB: Prussian blue
- GCE: Glass carbon electrode
- ITO: Indium tin oxide
- FTO: Flourine tin oxide
- PECVD: Plasma-enhanced chemical vapour deposition
- CCVD: Catalytic chemical vapour deposition
- MFC: Mass flow controller
- H₂SO₄: Sulphuric acid
- HNO₃: Nitric acid
- HCl: Hydrochloric acid
- KCl: Potassium chloride

- H_2O_2 : Hydrogen peroxide
- KMn_2O_4 : Potassium permanganate oxide
- Mn_2O_7 : Manganate heptaoxide
- H_2O_4 : Hydrazine hydrate
- ZnCl_2 : Zinc chloride
- CaCO_3 : Calcium carbonate
- Al_2O_3 : Aluminium oxide
- MgO : Magnesium oxide
- $\text{HC}\equiv\text{CH}$: Acetylene
- Na_2CO_3 : Sodium carbonate
- NaOH : Sodium Hydroxide
- N_2 : Nitrogen
- CoCl_2 : Cobalt chloride
- KBr : Potassium Bromate
- MnCl_2 : Manganese Chloride
- KCl : Potassium chloride
- H_2O : Water
- N_2H_4 : Hydrazine hydrate
- MnO_3^+ : Manganese oxide anion
- H_3O^+ : Hydronium
- OH : hydroxyl
- OH^+ : Hydroxyl cation
- COOH : Carboxylic
- $\text{C}=\text{O}$: Carbonal
- $\text{C}-\text{O}$: Carbonyl
- Co^{2+} : Cobalt anion
- Mn^{2+} : Manganese anion
- K^+ : Potassium anion
- H^+ : Hydrogen ion
- Cl^- : Chlorine cation

- Zn^{2+} : Zinc anion
- Ca^{2+} : Calcium anion
- Co: Cobalt
- Zn: Zinc
- Al: Aluminium
- Mg: Magnesium
- Ca: Calcium

**CHAPTER ONE: INTRODUCTION AND
PROBLEM STATEMENT**

CHAPTER ONE

INTRODUCTION AND PROBLEM STATEMENT

I.1 Introduction

The conventional methods of heavy metal removal from water include chemical oxidation or reduction, chemical precipitation, ion exchange, membrane technology, filtration, electrochemical treatment and adsorption, etc. [1]. As an economical and efficient method, adsorption techniques have been widely applied to remove heavy metal ions from wastewater [1]. Numerous materials have been used as adsorbents for the removal of heavy metals such as activated carbon, silica, ion-exchange resins, rock materials, activated slag, agricultural wastes, microbial and plant derived biomass and chitin, etc. [2]. All these techniques have shortcomings, for example the main disadvantages of precipitation are the generation of unwanted chemicals and waste disposal issue [3, 4]. It is therefore, fundamentally important to develop a low-cost, easily available, high adsorption capacity material for wastewater treatment in order to remediate heavy metal environmental problems [1].

Although carbon nanotubes and graphene derivative have been discovered just a few years they have attracted tremendous research interests not only in the electronics and energy fields [5-6], but also in environmental applications [7-10]. For example, it has been reported that graphene oxide (GO) and carbon nanotubes could be used for heavy metal removal [7]. In addition, graphene composites have been used for arsenic and dye removal [8-10].

I.2 Graphene

Graphene, which is dubbed as the mother of all graphitic structures, is a single two dimensional carbon sheet with the same structure as an individual layer of graphite packed into a hexagonal pattern. Figure 1.1 shows all forms of graphene in different structural patterns. As a one atom-thick planar sheet of sp^2 bonded carbon atom, graphene has received much attention in the recent years in materials science due to its unusual properties, such as a half-integer quantum hall effect, ballistic and extraordinary electron transport [11]. Precisely, graphene based assemblies are also

gaining attention because of their potential in designing electronic, sensing and energy conversion devices [12-15]. Graphene oxide (GO) synthesized from chemical oxidation of graphite provides a simple and convenient method to obtain exfoliated, two dimensional carbon sheets [16]. Oxidation diminishes graphene's excellent conducting properties, so reduction of GO is desirable in order to partially restore its sp^2 network [17]. Reduced graphene oxide (RGO) can be produced through chemical [17-19], sonolytic [20], microwave [21-22] photo thermal [23-24], photo catalytic [25-28] and electrochemical methods [29-30]. Graphene oxide is a hydrophilic derivative of graphene to which biological micro molecules readily attach, with properties superior to those of amorphous carbon films commonly used in electron microscopy [31]. Hydrophobic, graphene can be functionalized by a chemical process producing hydrophilic substrates to which molecules can also readily attach.

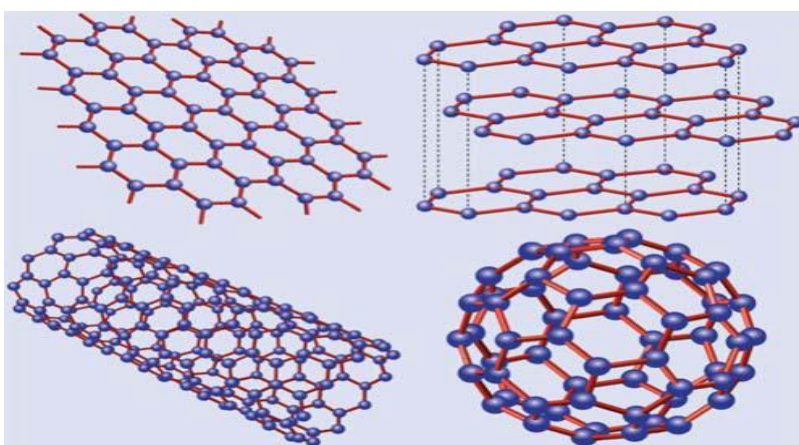


Figure 1.1: Graphene top left is a honeycomb lattice of carbon atoms. Graphite top right can be viewed as a stack of graphene layers. Carbon nanotubes are rolled up cylinders of graphene bottom left. Fullerenes C_{60} are molecules consisting of wrapped graphene by the introduction of pentagons on the hexagonal lattice.

Chemical reagents are critical to the reduction of GO, whether in the solid phase or liquid state [32-33]. It is therefore, critical to choose the method of synthesizing graphene taking into account its intended ultimate application. For instance, the introduction of chemical reagents is a significant disadvantage because the intrinsic response of graphene to trace analytes may be masked by the signals caused by impurities [31].

1.3 Carbon nanotubes

Research in the area of nanotechnology has also increased in recent years due to the unusual physical properties, large application and potential displayed by single wall carbon nanotubes (SWCNTs) [34]. This triggered interest by scientists and engineers ever since the discovery of carbon nanotubes (CNTs) in 1991 by S. Iijima and have shown great promise in a wide variety of applications such as strong composite material, nano electronic devices, catalysts and adsorbent for gas separation [34-35]. Formally derived from graphene sheets, CNTs exhibit unusual mechanical properties such as high toughness and high elasticity module [34]. Because of their electronic structure, CNTs exhibit semiconducting as well as conducting behaviour and thus cover a wide range of properties important for technology [34].

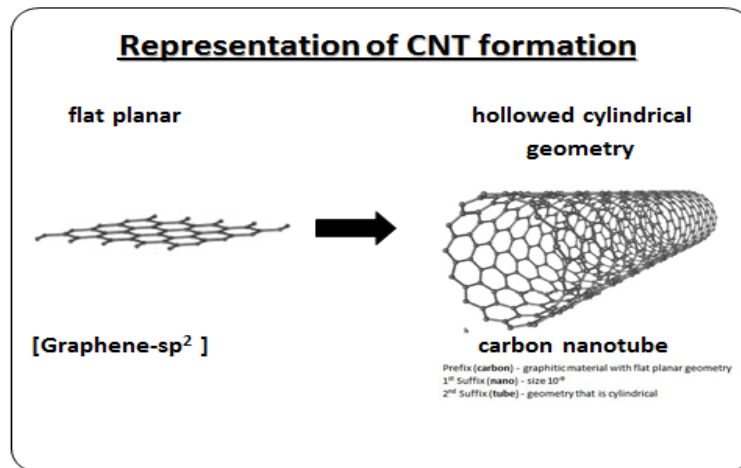


Figure 1.2: Representation of the formation of CNTs.

Since nanotubes have several of applications, some means must be developed to maximize their potential applications in real life. One of such processes is functionalization, which is to come up with a new class of material with more pronounced and desirable properties. One way of functionalizing carbon nanotubes is by substitution reactions. A substitution reaction is a reaction in which a couple of carbon atoms in the tube are replaced by boron or nitrogen atoms [36]. Another method of functionalizing nanotubes non-covalently is by using compatilizers like block or graft copolymers [37]. This method is desirable since it does not destroy the chemical structure of the CNTs and instead improves the interfacial property between the CNTs and the polymer matrix without reducing the excellent mechanical and electrical properties of the CNTs

[37]. And recently, covalently modified way would be by using carbodiimide SWCNTs coupling chemistry to create a wide range of tip functionality on the multi wall carbon nanotubes (MWCNTs) [38].

However, the manipulation and processing of CNTs have been limited by their insolubility in most common solvents. Pristine CNTs tend to aggregate rather than disperse in most solvents due to Van der Waals forces [39] and as for functionalizing CNTs with long polymers; the long chains increase the solubility in many solvents even with a low degree of functionalization [40]. Functionalization should also be possible from the inside of the tubes. This trend is quite desirable because intense demand for high performance and miniaturization of many electronic devices which exclusively need soft magnetic materials with high permeability and high electrical resistivity, mechanical hardness and chemical stability [41] are of fundamental importance.

Nanotechnology holds out a promise of materials of precisely specified composition and property, which could yield structures of high quality and strength. This phenomenon was significantly raised with the discovery of routes to grow them in high yields [40-42]. Although many nanostructures such as large molecules and quantum dots are of interest, at present, one of the most active areas is the study of nanotubes. The synthesis of nanostructures is currently one of the most active aspects of nanoscience. Controlling individual atoms and molecules is still a challenge, particularly when the process must be repeated for large numbers of atoms and molecules [43].

More recently, functionalizing of carbon nano materials (nanotube, graphene and graphite) have shown a promising approach in the development of metal-free, carbon-based catalysts with higher electro catalytic activity and long term operational stability than that of commercial platinum-based electrodes for oxygen reduction in fuel cells [44].

I.4 Problem statement

Heavy metal pollution is an environmental problem globally [45]. For instance, nickel is a non-biodegradable toxic heavy metal ion present in wastewater [1]. The main source of nickel pollution in water derives from industrial production processes such as galvanization, smelting, mining, dyeing operation, batteries manufacturing and metal finishing [46].

The dyes in effluents are of serious concern because of their adverse effects to human beings and the environment [47-48]. Besides, the colours of the dyes are easily recognized even at low concentrations, making them highly visible and undesirable [50]. Many technologies have been developed for dye removal from aquatic environments, including physical, chemical, and even biological approaches [49-50]. Among these approaches, absorption is regarded as an easy and economic process [50-51].

The most common symptom of chronic fluoride exposures is skeletal fluorosis, which can lead to the permanent bone and joint deformations and dental fluorosis [52]. The dental and skeletal fluorosis is irreversible and no treatment exists [41]. The only remedy is prevention by keeping fluoride ion intake within safe limits. It is reported that the permissible limit of fluoride in drinking water is 1.0 mg/l [53], and the superfluous fluoride should be removed from drinking water. So, it is imperative and significant to explore the suitable technique to remove excessive fluorides from water and the discovery of graphene is a blessing as is a promising candidate to be used to curb these mishaps because of its unique properties.

Lead is one of the most toxic and hazardous heavy metals because of its non-biodegradability [54-55]. For humans, lead is a neurotoxic metallic element, exposure to high concentrations causing health problems by accumulating in brain and kidney, the main source being the wastewater, where lead must be removed [56].

It is quite evident that we are in a global world of many diseases and there is an urgent need for academics to research and come up with remedial responses to counter act, prevent and cure all these illnesses, some of which are a result of contaminated and polluted environment from different sources. One of such sources being chemically contaminated water disposal in the environment after use. We have countless chemical laboratories worldwide, and the question is, are waste products disposed of safely? Drinking water is treated with chlorine as a disinfectant,

the chlorine reacts with water to form hypochlorous acid which is harmful for human consumption. Therefore there is a need to filter this water through an effective media for purification purposes before consumption. However, one problem for all carbon nanotubes is their insolubility in any solvent. Therefore solubility is an urgent property for processability even as far as it concerns purification [34]. Further exciting developments in nanoscale science and technology are expected. The remarkable properties of carbon nanotubes (CNTs) have prompted intense research into application where their deployment could have a major impact [57-58].

Multiwalled carbon nanotubes have been reported to effectively absorb dioxin, biphenyls and some inorganic pollutants [59]. Based on this report, we therefore need to devise and explore other safe, cheap and effective scientific means to prevent this mishap from happening if we are to live healthier. The aim of this study is to synthesize and characterize graphene, graphene oxide and carbon nanotubes using Hummers adopted method and chemical vapor deposition process and apply them on a possible separation applications that will result in having a safe environment.

1.5 Objectives

The objectives of this research are:

- 1.5.1 To synthesize graphene oxide from flake graphite powder.
- 1.5.2 To reduce graphene oxide to graphene.
- 1.5.3 To synthesize various catalysts on different support materials.
- 1.5.4 To synthesize carbon nanotubes with different catalysts on different support materials.
- 1.5.5 To characterize and study the morphological properties of graphene oxide reduced graphene oxide and carbon nanotubes.
- 1.5.6 To remove heavy metals from water.

1.6 Value of research

Some diseases and infections which are a result of polluted environment and contaminated water through poisonous heavy metals can be prevented. Efficient and tangible research should be done on the application of graphene, graphene oxide and carbon nanotubes as they have proved to be

the answer in some instances. Their improvement of organic substances when cross linked leaves us with the assurance that many illnesses will be curbed. As economical and efficient method, adsorption technique has been widely applied to remove heavy metal ions from wastewater [1]. But graphene and its derivatives have been reported to be more efficient, low cost, easily available, high adsorption capacity material for wastewater treatment that might remediate the heavy metal environmental problem [1]. Graphene which is more user friendly and compatible because of its unique properties can also be cross linked to environmentally friendly reagents like L-glutathione [60]. Again, apart from water purification, these kinds of composites open up wide application possibilities in diverse fields of science and engineering such as catalysis fuel cells and etc. [61]

1.7 Outline of the dissertation

This dissertation is outlined as follows:

Chapter One (Introduction and Problem Statement): This chapter gives insight into this research project. The problem statement, objectives and the value of research are being covered.

Chapter Two (Literature Review): This chapter covers literature related to graphene, and its derivatives, their properties and uses are being investigated.

Chapter Three (Experimental Methods): This chapter explains all experimental procedures and analytical techniques used in this study.

Chapter Four (Results and Discussion): All data obtained from this study is presented, explained, interpreted and discussed in this chapter.

Chapter Five (Recommendations and Conclusions): Recommendations and conclusions are drawn based on the initial aim/objective of this research in this chapter.

References

1. Y. Ren, N. Yan, Q. Wen, Z. Fan, T. Wei, M. Zhang, J. Ma, *Chem. Eng. J.* (2010), doi:10.1016/j.cej.2010.08.010.
2. S -T. Yang, J. X. Li, D. D. Shao, J. Hu, X. K. Wang, *J. Mater.* 166 (2009) 109-116.
3. S. Ayoob, A. K. Gupta, V. T. A. Bhat, *Crit. Rev. Environ. Sci. Technol.* 38 (2008) 401-470.
4. K. Zhang, V. Dwivedi, C. Chi, J. Wu, *J. Hazard. Mater.* 182 (2010) 162-168.
5. A. K. Geim, *Sci* 324 (2009) 1530-1534.
6. C. N. R. Rao, A. K. Sood, K Subrahmanyam, S. A. Govindaraj, *Angew. Chem. Int. Ed.* 48 (2009) 7752-7777.
7. S -T. Yang, Y. Chang, H. Wang, G. Liu, S. Chen, Y. Wang, Y. Liu, A. Cao, *J. Colloid. Inter. Sci.* 353(2) (2011) 588-592.
8. S. Chandra, S. Bag, P. Das, D. Bhattacharya, P. Pramanik, *Chem. Phys. Lett.* 519 (2012) 59-63.
9. H. Zhang, X. Lu, Y. Li, Y. Wang, J. Li, *ACS. Nano.* 4 (2010) 380.
10. F. He, J. Fan, D. Ma, L. Zhang, C. Leung, H. L. Chan, *Carbon* 48 (2010) 3139.
11. L. Feng, Y. Chen, S. Ren, X. Qu, *Bio. Mater.* 32 (2011) 2930-2937.
12. P. V. Kamat, *J. Phys. Chem. Lett.* 2 (2011) 242-251.
13. C. N. R. Rao, A. K. Sood, R. Voggu, K. S. Subrahmanyam, *J. Phys. Chem. Lett.* 1 (2010) 572-580.
14. M .H. Liang, B. Luo, L. J. Zhi, *Int. Energy Res.* 33 (2009) 1161-1170.
15. P. V. Kamat, *J. Phys. Chem. Lett.* 1 (2010) 520-527.
16. W. S. Hummers, R. E. Offeman, *J. Am. Chem. Soc.* 80 (1958) 1339-1439.

17. S. Park, R. S. Ruoff, *Nat. Nanotechnol.* 4 (2009) 217-224.
18. R. Muszynski, B. Seger, P. V. Kamat, *J. Phys. Chem. C* 112 (2008) 5263-5266.
19. B. Seger, P.V. Kamat, *J. Phys. Chem. C* 113 (2009) 7990-7995.
20. K. Vinodgopal, B. Neppolian, I.V. Lightcap, F. Grieser, M. Ashokkumar, P. V. Kamat, *J. Phys. Chem. Lett.* 1 (2010) 1987-1993.
21. H .M.A. Hassan, V. Abdelsayed, A .E. R. S. Khder, K.M. AbouZeid, J. Ternner, M.S. El-Shall, S.I. Al-Resayes, A.A. El-Azhary, *J. Mater. Chem.* 19 (2009) 3832-3837.
22. A. F. Zedan, S. Sappal, S. Moussa, M.S. El-Shall, *J. Phys. Chem. C* 114 (2010) 19920-19927.
23. V. Abdelsayed, S. Moussa, H. M. Hassan, H. S. Aluri, M. M. Collinson, M. S. El-Shall, *J. Phys. Chem. Lett.* 1 (2010) 2804-2809.
24. D. A. Sokolov, R. R. Shepperd, T .M. Orlando, *J. Phys. Chem. Lett.* 1 (2010) 2633-2636.
25. Y. H. Ng, I. V. Lightcap, K. Goodwin, M. Matsumura, P. V. Kamat, *J. Phys. Chem. Lett.* 1 (2010) 2222-2227.
26. Y. H. Ng, A. Iwase, A. Kudo, R. Amal, *J. Phys. Chem. Lett.* 1 (2010) 2607-2612.
27. G Williams, B. Seger, P. V. Kamat, *ACS Nano.* 2 (2008) 1487-1491.
28. G. Williams, P. V. Kamat, *Langmuir.* 25 (2009) 13869-13873.
29. G. K. Ramashe, S. Sampath, *J. Phys. Chem. C* 113 (2009) 7985-7989.
30. A. Kongkanand, K. Vinodgopal, S. Kuwabata, P. V. Kamat, *J. Phys. Chem. B* 110 (2006) 16185-16192.
31. R. S. Pantelic, J. C. Meyer, U. Kaiser, W. Baumeister, J. M. Plitzko, *J. Struct. Biol.* 170 (1) (2010) 152-156.
32. J. Fang, K. Wang, T. Weit, *J. Carbon.* 48 (5) (2010) 1686-1689.

33. S. Stankovich, D. A. Dikin, R. D. Piner, K. A. Kohlhaas, A. Kleinhammes, Y. Jia, Y. Wu, S. T. Nguyen, R. S. Ruoff, *J. Carbon*. 45 (7) (2007) 1558-1565.
34. H. Kuzmany, A. Kukovecz, F. Simon, M. Holzweber, C. Kramberger, T. Pichler, *Synthetic. Metals*. 141 (2004) 113-122.
35. S. Iijima, T. Ichihashi, *Nat. London*. 363 (1993) 603-605.
36. D. Golberg, Y. Bando, W. Han, K. Kurashima, T. Sato, *Chem. Phys. Lett.* 308 (1999) 337-342.
37. K. T. Kim, W. Ho Jo, *Carbon*. 49 (2011) 819-826.
38. S. S. Wong, A. T. Wooley, E. Joselevich, C. M. Lieber, *Chem. Phys. Lett.* 306 (1999) 219-225.
39. J. J. Park, D. M. Park, J. H. Youk, W-R. Yu, J. Lee, *Carbon*. 48 (2010) 2899-2905.
40. D. S. Kumar, K. C. Mouli, 4(1) (2010) 51-59.
41. M. S. Dresselhaus, G. Dresselhaus, P. C. Eklund, *Academic Press, San Diego*. (1996) 985.
42. H-X. Wu, R. Tong, X-Q. Qiu, H-F. Yang, Y.-H. Lin, R. F. Cai, S X. Qian, *Carbon*. 45 (2007) 152-159.
43. P. Benito, M. Herrero, F. M. Labajos, V. Rives, C. Royo, N. Latorre, A. Monzon, *J. Chem. Eng.* 149 (2009) 455-462.
44. S. C. Roy, A.W. Harding, A. E. Russell, K. M. Thomas, *J. Electrochem. Soc.* 144 (1997) 2323-2328.
45. G. Krishna, Y. Bhattachary, S. G. Susmita, *J. Chem. Eng.* 136 (2008) 1-13.
46. Z. Al-Qodah, *Desalination* 196 (2006) 164-176.
47. T. Robinson, G. McMullah, R. Marchant, P. Nigam, *Bioresour. Technol.* 77 (2001) 247.
48. E. Forgacs, T. Cserhati, G. Oros, *Environ. Int.* 30 (2004) 953.
49. S-T. Yang, S. Chen, Y. Chang, A. Cao, Y Liu, H. Wang, *J. Colloid. Int. Sci.* 359 (2011) 24-29.
50. G. Crini, *Bioresour. Technol.* 97 (2006) 1061-1085.

51. M. Rafatullah, O. Sulaiman, R. Hashim, A. Ahmad, *J. Hazard. Mater.* 177 (2010) 70-80
52. Y. Li, P. Zhang, Q. Du, X. Peng, T. Liu, Z. Wang, Y. Xia, W. Zhang, K. Wang, H. Zhu, D. Wu, *J. Coll. Inter. Sci.* (2011), doi:10.1016/j.jcs.2011.07.032.
53. S. S. Tripathy, J. L. Bersillon, K. Gopal, 50 (3) (2006) 310-317.
54. L. Patrick, *Altern. Med. Rev.* 11 (2006) 2.
55. N. C. Papanikolaou, E. G. Hatzidaki, S. Belivanis, G. N. Tzanakakis, A. M. Tsatsakis, *Med. Sci. Monit.* 11 (2005) 3239.
56. V. K. Gaur, S. K. Gupta, S. D. Pandey, K. Gopal, V. Misra, *Environ. Monit. Assess.* 102 (2005) 419.
57. T. Morishita, M. Matsushita, Y. Katagiri, K. Fukumori, *Carbon.* 48 (2010) 2308-2316.
58. E. D. Dikio, F. T. Thema, C. W. Dikio and F. M. Mtunzi, *Inter. J. Nanotechnol. Appl.* 4 (2) (2010) pp. 117-124.
59. D. Yu, E. Nagelli, F. Du, L. Dai, *J. Phys. Chem. Lett.* 1 (2010) 2165-2173.
60. T. A. Pham, J. S. Kim, J. S. Kim Y. T. Jeong, *Colloids. Surf. A: Physiochem. Eng. Aspects* 384 (2011) 543-548.
61. T. S. Sreeprasad, S. M. Maliyekkal, K. P. Lisha, T. Pradeep, *J. Hazard. Mater.* 186 (2011) 921-931.

CHAPTER TWO: LITERATURE REVIEW

CHAPTER TWO

LITERATURE REVIEW

2.1 Introduction

Preparation of graphene nanosheets from graphene oxide by chemical reduction is one of the important topics in the area of nanotechnology because graphene-based nanomaterials have potential applications [1]. However, green and facile approach to produce graphene by using an environmentally friendly reagent as a reducing reagent is fundamentally important.

In 1859 Brodie obtained graphitic oxide by repeated treatment of Ceylon graphite with oxidation mixture consisting of potassium chlorate and fuming nitric acid [2]. Staudenmier, in 1898 produced graphitic oxide by the oxidation of graphite in concentrated sulphuric acid and nitric acid with potassium chlorate [3]. In 1958 Hummers and Offenman oxidized graphite in water free mixture of sulphuric acid, sodium nitrate and potassium permanganate [4].

The discovery of CNTs by lijima in 1991 has attracted considerable attention in the recent years, not only due to the remarkable physical and chemical properties of these materials, but also because of their versatility of their potential applications [5]. The synthesis of molecular carbon structures in the form of C₆₀ and other fullerenes has then stimulated intense interest in the structures accessible to graphitic carbon sheets [6].

Carbon nanotubes can be produced by different methods, eg.arc discharge, and laser-ablation or by plasma-enhanced chemical vapor deposition (PECVD) as well as by thermal chemical vapor deposition [7]. A technique for the synthesis of carbon nanotubes by catalytic decomposition of hydrocarbons was recently reported in which hydrocarbons are decomposed directly into hydrogen and carbon. Catalytic chemical vapor deposition (CCVD), arc discharge and laser ablation remain the three major synthesis routes for CNTs production [7]. In this research, Catalytic chemical vapor deposition was used,

2.2 Properties of graphene

2.2.1 Electronic properties

Figure 2.1 and 2.2 below show molecular structure of graphene and pictures of brownish graphene oxide and blackish reduced graphene oxide respectively. From literature, the brownish colour confirms the presence of oxidized graphite while the blackish colour confirms the reduced graphitic material. Graphene is a material with a host of unusual properties [8-17] including among others high electron mobility [18-19]. Besides its purely fundamental importance, researchers view graphene as a promising new material for electronic [20], chemical [21], or electromechanical [22] applications, where graphene's unique properties may be of substantial benefit. Graphene is a practically perfect two-dimensional crystal with a conductivity mediated by electrons with zero effective mass [23]. It is this feature that gives one grounds to consider graphene as a possible basis for solid state electronic for the future [24]. Although theory has been studying the electronic properties of two-dimensional crystals for a long time now, the true surge of interest in graphene has been spawned by an experimental demonstration that it can exist in a free stable state [23]. The high carrier mobility in graphene reaching $104 \text{ cm}^2/\text{Vs}$, which had been verified in the very first experiments, and observation of the room temperature quantum Hall effect [25] have provided strong support for the basic theoretical concepts bearing on this material and paved way to numerous studies of its properties and attempts at developing tentative structures of the corresponding electronic devices.

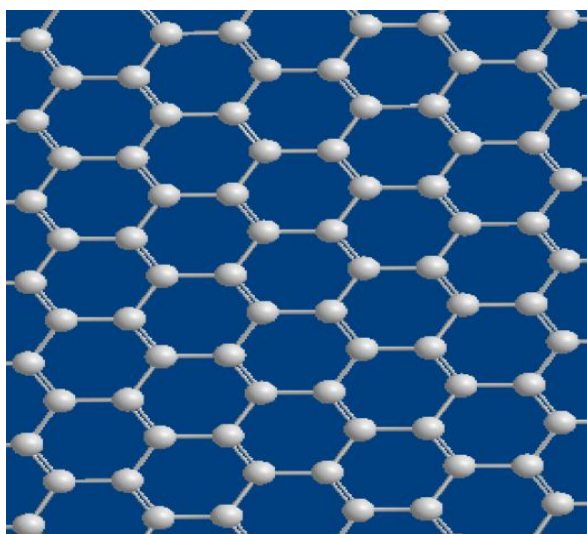


Figure 2.1 Molecular structure of graphene



Figure 2.2 Pictures of brownish graphene oxide (GO) and blackish reduced graphene oxide (RGO)

The electronic properties of graphene are exceptionally novel, for instance, the low-energy quasi particles in graphene behave as massless chiral Dirac fermions which has led to the experimental observation of many interesting effects similar to those predicted in the relativistic regime [26]. Graphene also has immense potential to be a key ingredient of new devices such as single molecule gas sensors, ballistic transistors and spintronic devices [26]. Bilayer graphene, which consists of two-energy band structures which generate very different scattering properties from those of monolayer [26]. It also presents the unique property that is tunable band gap can be opened and controlled easily by a top gate [26]. These properties have made bilayer graphene a subject of intense interest and research. It is further reported from literature that thermo power has been as a powerful tool to probe transport mechanisms in metals and semiconductors, but recently, the thermoelectric properties of graphene sheets and ribbons have attracted experimental as well as theoretical attention.

2.2.1.1 Optical properties

It has been measured that monolayer graphene absorbs 2.3 % of light [24] that is 97.7 % transmittance, quite a sizable fraction for an ultimately thin material. What is even more exciting is the fact that this number is given solely by the combination of fundamental constants [27].

$$\pi\alpha \quad (\pi = e^2/hc \approx 1/137) \quad [2.1]$$

Where α is the fine structure constant.

Such combination of high conductivity (sheet resistance of doped graphene can be as low as 10 Ohm) and low light adsorption makes this material an ideal candidate for transparent conductive coating. Graphene utilization for this type of applications has been recently demonstrated by constructing graphene-based liquid crystal [28] and solar cells [29].

2.2.1.2 Relativistic charge carriers

Historically, it is the electronic properties which attracted most of graphene attention. Electrons in graphene behave like massless relativistic particles, which govern most of its electronic properties. Probably one of the most spectacular consequences of such unusual dispersion is such combination of high conductivity (sheet resistance of doped graphene can be as low as 10 Ohm). Generally crystals of graphene could be prepared with very few defects (consequence of ultra-strong carbon-carbon bonds), which, in conjunction with the absence of localization and high Fermi velocity ensures very high mobility of the charge carriers and short time of flight in ballistic regime [30]. First prototypes of high-frequency transistors have been recently developed and demonstrated very encouraging characteristics [30]. Apart from the high technological potential, the relativistic nature of charge carriers in graphene provides the opportunity to address fundamental questions in condensed matter physics not accessible in any other material [31-36]. Unlike massive charge carriers governing conduction in semiconductor materials, electrons and holes in graphene obey a linear energy dispersion relation and behave as chiral massless particles [37-38].

2.2.1.3 Anomalous quantum Hall Effect

Hall Effect is the most widely used technique to measure the transport properties and assess the quality of epitaxial layers. For semiconductor materials, it yields the carrier concentration, its type, and carrier mobility. More specifically, experimental data on Hall measurements over a

wide temperature range (4.2–300K) provide quantitative information on impurities, imperfections, uniformity, scattering mechanisms, and so on. The Hall coefficient and resistivity (r) are experimentally determined and then related to the electrical parameters through (for n-type conduction).

$$R_H = r_H / ne \quad [2.2]$$

$$m_H = R_H / r. \quad [2.3]$$

Where n is the free electron concentration

e is the unit electronic charge

m_H is the Hall mobility and

r_H is the Hall scattering factor

The r_H depends on the particular scattering mechanism. The drift mobility is the average velocity per unit electric field in the limit of zero electric field and is related to the Hall mobility. Elation is the observation of half-integer quantum hall effect and the absence of localization [8]. The later might be very important for graphene-based field effect transistors.

2.2.2 Thermal properties

Heat is created when atoms or molecules are in motion. In gases, the molecules fly between occasional collisions with each other. In solids, by contrast, they vibrate about their mean positions; the higher the temperature, the greater the amplitude of vibrations. From this perception emerges all our understanding of the intrinsic thermal properties of solids, their heat capacity, expansion coefficient, conductivity, even melting. Heat affects mechanical, electrical, and optical properties too. As temperature rises, materials expand, the elastic modulus decreases, the strength falls, and the material starts to creep, deforming slowly with time at a rate that increases as the melting point is approached until, on melting, the solid loses all stiffness and strength. The electrical resistivity rises with temperature, the refractive index falls and colour may change

2.2.2.1 Intrinsic Thermal Properties

It is further reported that two temperatures, the melting temperature T_m and glass temperature T_g (units for both: Kelvin, K, or Centigrade, C), are fundamental points of reference because they relate directly to the strength of the bonds in the solid. Crystalline solids have a sharp melting point, T_m . Noncrystalline solids do not, the glass temperature T_g characterizes the transition from true solid to very viscous liquid. It is helpful in engineering design to define two further temperatures.

The maximum and minimum temperatures T_{max} and T_{min} (units for both: K or C). The first shows us the highest temperature at which the material can be used continuously without oxidation, chemical change, or excessive distortion becoming a concern. The second is the temperature below which the material becomes brittle or otherwise unsafe to use. It costs energy to heat a material. The energy to heat 1 kg of a material by 1°K is called the heat capacity or specific heat. It is reported that pristine graphite flake starts to lose mass at around 750 °C due to the carbon dioxide evolution. Thermal decomposition of graphene oxide is in two steps around 300 °C and 550 °C due to the removal of oxygen functional groups and carbon dioxide evolution respectively. Reduced graphene oxide sheets exhibit a weight loss at about 200 °C under dry atmospheric air. The weight loss percentage of graphene oxide is still about 60 % after thermal treatment under nitrogen atmosphere, but there is no loss in the weight percentage of reduced graphene sheets.

2.2.3 Mechanical properties

The mechanical properties of materials involve various concepts such as hardness, stiffness, and piezoelectric constants, Young's and bulk modulus, and yield strength. The solids are deformed under the effect of external forces and the deformation is described by the physical quantity strain. The internal mechanical force system that resists the deformation and tends to return the solid to its undeformed initial state is described by the physical quantity stress. Within the elastic limit, where a complete recoverability from strain is achieved with removal of stress, stress (s) is proportional to strain (e) [39].

It is these high mechanical, thermal and chemical properties of graphene that make it stable because of the strong covalent bonds between the carbon atoms. It is also reported that graphene has tensile Modulus and ultimate strength values as strong as 200 times as those of structural steel. Its theoretical Young modulus is around 1060 GPa that is one of the strongest known materials per unit weight and a theoretical surface area of around 2630 m²/g.

2.3 Potential application/uses of graphene

Because of its sp² hybridized cluster, graphene exhibits outstanding properties in various novel applications [40]. Particularly, sensing device is arousing continuous interests due to the low background noise and the surface activity [40]. The following are some its applications.

2.3.1 Water purification

A great challenge for this century lies in cleaning up the waste generated during industrial, domestic and agricultural activities [41]. Water as essential fluid on which all life depends is heavily affected by such activities [41]. Among the various contaminants found in water, heavy metals require special attention because of their toxic effect on human beings and the environment, even at very dilute concentrations [41]. Technologies like adsorption, precipitation, membrane separation, amalgamation and ion exchange have been used to remove such contaminants from water [26]. However, adsorption is proved to be economical and efficient over other technologies, especially for removing pollutants from dilute solutions [42-44].

Carbon is a versatile adsorbent that is heavily used in the removal of various pollutants including heavy metals from aqueous solutions [43, 45-49]. Various forms of carbon and their composites have been investigated to improve the adsorption efficacy [50-53]. Graphene [54], the latest member of the carbon family is believed to be one of the most interesting materials this century [41]. Graphene and its composites offer utility in several applications due to its unique two dimensional nature and associated band structure [55, 56]. Recent literature suggests that reduced graphene oxide (RGO), graphene oxide (GO) and their composites are getting into environmental remediation [53, 57-59]. RGO-magnetite and GO-ferric hydroxide composites were used for the removal of arsenic from water [57-59]. Iron based oxides and hydroxides are known to remove

arsenic from drinking water [60-62]. The reports show that RGO and GO supported materials have higher binding capacity compared to free nanoparticles [57]. The RGO is antibacterial [58] and this property may help in preventing the development of biofilm on the filter surface due to bacterial growth, which can cause unwanted tastes and odors or prematurely clogging of filters [63].

2.3.2 Single molecule gas detection

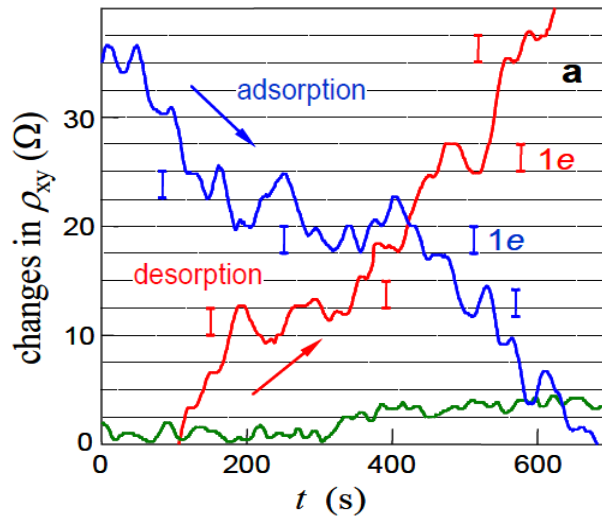


Figure 2.3 Spike like changes in Hall resistivity near neutral point. (Schedi et.al *Nat. Mater.* 6 (2007) 652)

Figure 2.3 shows sensors as critical components in all measurement and control systems. The need for sensors that generate an electronic signal closely followed the advent of the microprocessor and computers. Together with the ever present need for sensors in science and medicine, the demand for sensors in automated manufacturing and environmental monitoring is rapidly growing. In addition, small, inexpensive sensors are finding their way into all sorts of consumer products, from children’s toys to dishwashers to automobiles. Because of the vast variety of useful things to be sensed and sensor applications, sensor engineering is a multidisciplinary and interdisciplinary field of endeavour.

Graphene exhibits outstanding properties in various novel applications [64-68]. Particularly, sensing device is arousing continuous interests due to the low background noise and the excellent surface activity [59-70]. Various graphene nanosensors have been fabricated in previous works

[71-73], aiming to employ them in practical application. Actually, the industrial manufacturing of graphene nanosensors requires the preparation of graphene quantity [41].

Graphene is an ideal material for electrochemical [74] because of its very large 2D electrical conductivity, large surface area and low costs. The enlarged active surface area, its potential low manufacturing cost together with the unique features of Prussian blue (PB), a novel GO/PB hybrid film was electropolymerizinly constructed [74] on a modified glassy carbon electrode (GCE) and then used for electrochemical sensing applications [74]. It has also been reported that sensor devices utilizing epitaxially grown graphene have the potential to bypass the cumbersome removal of graphene and its subsequent redeposition onto a substrate, thus allowing for simple and reproducible devices. Single layer graphene sensors have every atom at the surface and demonstrate sensitivity down to single molecular level, functioning as low power, room temperature sensors [75]. Their sensitivity is due in part to their high metallic conductivity even when very few charge carriers are present [76-77]. Thus, changes in number of even few charge carriers can cause significant changes in conductivity and sensor signal [75].

2.3.3 Graphene transistors

The unique nanostructures and properties of graphene make it a promising candidate for the fundamental study as well as for potential device applications such as field-effect transistors, gas sensors and electromechanical resonators [74]. Crystals of graphene could be prepared with very few defects (consequence of ultra-strong carbon-carbon bonds), which, in conjunction with the absence of localization and high Fermi velocity ensures very high mobility of the charge carriers and short time of flight in ballistic regime. First prototypes of high-frequency transistors have been recently developed and demonstrated very encouraging characteristics [44].

Extraordinary properties of graphene [69] such as its extremely high room temperature electron mobility and thermal conductivity [69] make this material appealing for electronics and sensors. Very few studies of the low frequency noise in graphene devices were reported. Mostly, the previous works were focused on the back-gated bilayer graphene (BLG) devices. In contract to single-layer graphene (SLG), one can induce a band gap in BLG through the use of an external gate. There has been substantial recent progress in fabrication of graphene transistors with the top gate in addition to the conventional back gate [69]. The back gate is usually separated from

the graphene channel by 300 nm of SiO₂ required for graphene optical visualization [69]. The top gate enables better control of the electronic properties of graphene transistors and may achieve the current saturation characteristics [79].

2.3.4 Graphene biodevices

More recently, it is attractive to develop graphene-based nanocomposites films as enhanced sensing platform for constructing electrochemical sensors and biosensors, because these kinds of nanocomposites films may generate synergy on electro catalytic activity and thus enhance the sensitivity of the sensors [74].]. Furthermore, it has been communicated that an application of Graphene Oxide/Prussian Blue (GO/PB) hybrid film in the fabrication of an electrochemical glucose biosensor, which displayed favourable biosensing performances [74]. The results obtained showed that the GO/PB nanocomposites film could be used as enhanced sensing platform for developing novel types of highly sensitive and stable electrochemical sensors.

2.3.5 Transparent conducting electrodes for replacement of Indium tin oxide (ITO)

Indium tin oxide (ITO) and fluorine tin oxide (FTO) have been widely used as window electrodes in optoelectronic devices [81]. These metal oxides, however, appear to be increasingly problematic due to the following.

1. The limited availability of the indium on earth
2. Their instability in the presence of acids and base
3. Their susceptibility to ion diffusion into polymer layers
4. Their limited transparency in the near infrared region and
5. The current leakage of FTO devices caused by FTO structure defects [82]

As a result, the search for novel electrode materials with good stability, high transparency and excellent conductivity is therefore a crucial goal for optoelectronics [8]. Graphene, a two dimensional graphite, as a rising star in material science, exhibits remarkable electronic properties that qualify it for applications in future optoelectronic systems [82]. Recently, transparent and conductive graphene based composites have been prepared by incorporation of graphene sheets into polystyrene or silica [83]. However, the conductivity of such transparent composites is low, typically ranging from 10⁻³ to 1 S/cm depending on the graphene sheet

loading level, which makes the composites incapable of serving as window electrodes in optoelectronic devices [84].

2.4 Carbon nanotubes (CNTs)

Figure 2.4 below shows the structure of (a) multi-walled and (b) single-walled carbon nanotubes. As a result of wide range of applications in carbon allotropes, research in the area of nanotechnology has also increased in the recent years due to the unusual physical properties, large application and potential displayed by single wall carbon nanotubes (SWCNTs), that resulted in interest by scientists and engineers ever since the discovery of carbon nanotubes (CNTs) in 1993, [83-84]. Formally derived from graphene sheets, CNTs exhibit unusual mechanical properties such as high toughness and high elasticity module [85]. Because of their electronic structure, CNTs exhibit semiconducting as well as conducting behaviour and thus cover a wide range of properties important for technology [85]. Application in electronic devices, nanosensors, compound materials and gas storages are intensively explored and all these potential application require functionalization and characterization of the carbon nanotubes to enable processability and to fine tune their properties [85].

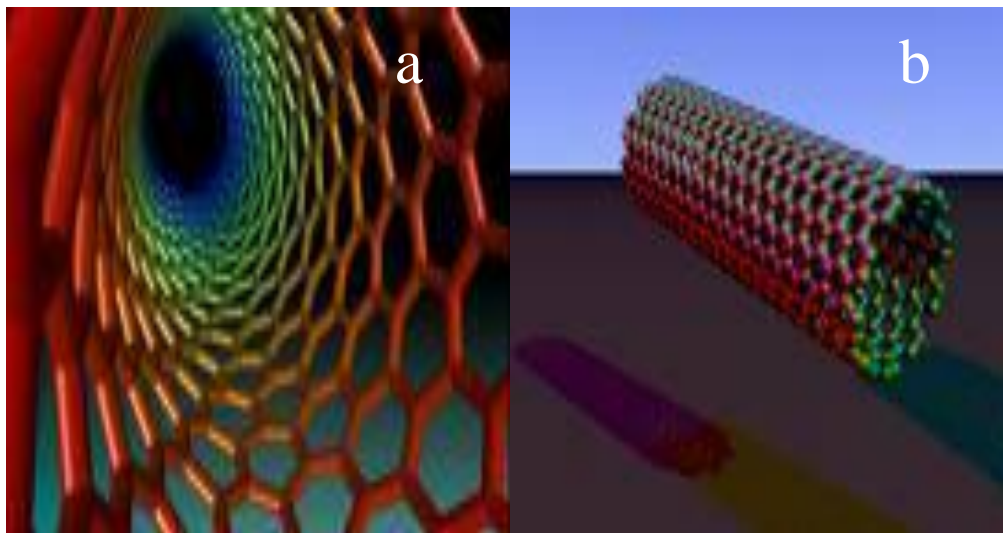


Figure 2.4 Structures of the main types of carbon nanotubes [84].

2.5 Types of carbon nanotubes

Carbon nanotubes are allotropes of carbon with a cylindrical nanostructure. Carbon is a unique element since it can catenate by hybridization forming sp , sp^2 and sp^3 bonds hence is capable of occurring in various forms.

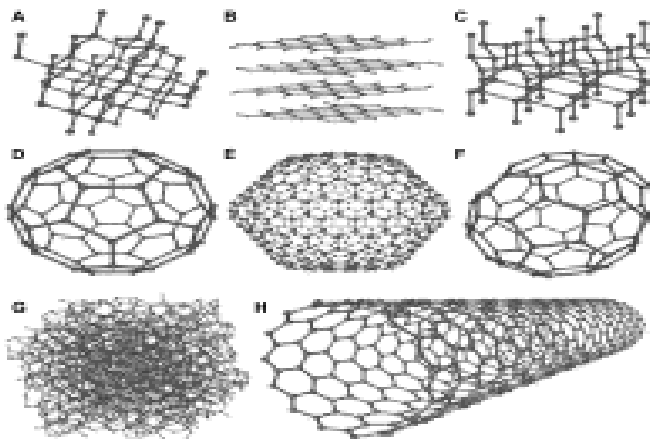


Figure 2.5 Allotropes of carbon: (a) Diamond, (b) Graphite, (c) Lonsdaleite, (d) C_{60} Buckminsterfullerene, (e) C_{540} Fullerene, (f) C_{70} Fullerene, (g) Amorphous carbon, and (h) Single-walled carbon nanotube (Adapted from *Arabian Journal of Chemistry*)

The nature of the bonding of a carbon nanotube is described by orbital hybridization in applied quantum chemistry. The chemical bonding of nanotubes is composed entirely of sp^2 bonds, similar to those of graphitic structure. This bonding structure provides the molecules with their unique strength and ability to conduct electrons through delocalized π -molecular orbitals that form from unhybridized $2p$ orbitals on carbon [86]. The growth mechanism is still a subject of research, with more than one mechanism being proposed to be operative [87]. Carbon nanotubes are categorized as single-walled nanotubes and multi-walled nanotubes.

2.5.1 Single-walled carbon nanotubes

Most SWNTs have a diameter in the range 1-2 nm, with a tube length that can be many million times longer. The structure of a SWNT can be conceptualized by wrapping a one atom thick layer of graphene into a seamless cylinder. The ends of some SWNTs are open while others are closed with fullerene caps. SWNTs are an important variety of CNTs because they exhibit electric properties that are not shared by the MWNT. SWNT are expensive to produce and the

development of more affordable synthesis techniques is vital to the future of carbon nanotechnology.

2.5.2 Multi-walled carbon nanotubes

MWNTs consist of multiple rolled layers of graphite. There are 2 models which can be used to describe the structures of MWNTs. In the *Russian Doll* model, sheets of graphite are arranged in concentric cylinders. In the *Parchment model*, a single sheet of graphite is rolled in around itself, resembling a rolled newspaper. The interlayer distance in MWNTs is close to the distance between graphene layers in graphite.

2.6 Properties of Carbon nanotubes

The great interest in the fundamental properties of carbon nanotubes and in their exploitation through a wide range of applications is due to their unique structural, optoelectronic, thermal, and mechanical properties [88].

2.6.1 Optoelectronic properties

Carbon nanotubes (CNTs) represent attractive materials for photovoltaic (PV) devices due to their unique electronic and optical properties. Single wall carbon nanotubes (SWNTs) layers can be directly configured as energy conversion materials to fabricate thin film solar cells, serving as both photo generation sites and charge carrier collecting/transport layers [89].

2.6.2 Thermal properties

Dispersing nanoparticles in a polymer can enhance both mechanical and transport properties. Nanocomposites with high thermal conductivity could be obtained by using thermally conductive nanoparticles. Carbon based nanoparticles are extremely promising, although high resistances to heat transfer from the nanoparticles to the polymer matrix could cause significant limitations [90].

2.6.3 Atomic and electronic structure of disordered carbons

Disordered carbons have sp^3 and sp^2 sites. The sp^3 sites have only sigma states while the sp^2 sites also possess sigma and pi states. It is always possible to treat sigma and pi states separately. Sigma and pi bonds have a significantly different behaviour. Sigma bonds are two centre bond orbitals between adjacent atoms. In the bond orbital approximation, [91] any property of occupied pi states such as the total energy, charge density, or polarizability can then be expressed as simply the sum of independent, short range terms for each bond. There are no long range forces in this approximation, and the electron structure depends only on short range order. pi states are different, [91] because a pi orbital usually interacts with pi states on more than one atom to form a conjugated system such as benzene. Then, one can no longer define unique bond orbitals. Conjugated bonds cannot now be expressed as the sum of independent, two centre bonds. Each bond contains contributions from adjacent bonds, and this gives rise to longer range forces and long range polarizabilities [92].

2.6.4 Mechanical Properties

Some of the most important applications of carbon nanotubes are their mechanical properties. CNTs stiff sp^2 bonds result in a Young's modulus close to that of diamond, while the relatively weak van der Waals interacts between the graphitic shells act as a form of lubrication [93]. These mechanical properties characterization involve mechanical deformation of CNTs using scanning probe microscopes [93].

2.7 Potential applications/ Uses of carbon nanotubes

2.7.1 Water purification

The efficacy and utility of adsorbents greatly depend upon the affinity of target contaminants towards the adsorbents [41]. The most important and widely used application of bulk carbon is in environmental remediation [41]. Features like large surface area and presence of surface functional groups make single sheets of carbon and their composites an attractive adsorbent candidate for water purification [41]. However, the use of graphitic materials for large scale and down to earth applications like water purification is limited. This is mainly because of the difficulty in large scale synthesis.

2.7.2 Reinforcement for polymer nanocomposites

Carbon nano composites can have enhanced thermal stability [94] and mechanical properties due to the large surface area to volume of the carbon nanotubes. They have been shown to form percolated networks in concentrations as low as 1 %·w/w for carbon nanotubes and 0.02 %·w/w for graphene [95]. The percolated networks increment properties exhibit electrical conductivity. Thermoplastic elastomer compounds based on block co-polymers have low initial modulus and durability [96].

References

1. T. A. Phan, J. S. Kim, J. S. Kim, Y. T. Jeong, *Physiochem. Eng. Aspects*. 384 (2011) 543-548.
2. B.C. Brodie, *Phios. Trans. R. Soc. London* (1859) 249-259.
3. L. Staudenmaier, V. Z. Darstellung der, *Ber. Dtsch. Chem. Ges.* 31 (1898) 1481-1499.
4. W.S. Hummers, R. E. Offenman, *S. Am. Chem. Soc.* 80 (1958) 1339.
T. A. Phan, J. S. Kim, J. S. Kim, Y. T. Jeong, *Physiochem. Eng. Aspects*. 384 (2011) 543-548.
5. P. Benito, M. Herrero, F. M. Labajos, V. Rives, C. Royo, N. Latorre, A. Monzon, *Chem. Eng. J.* 149 (2009) 455–462.
6. S. Iijima, *Nat.* 354 (1991) 56–58.
7. E. D. Dikio, F. T. Thema, C. W. Dikio, F. M. Mtunzi, *Int. J. Nanotechnol. Appl.* 4 (2) (2010) 117–124.
8. A.K. Gein, K.S Novoselov, *Nat. Mater.* 6 (2007) 183-191.
9. A. H. C. Neto, F. Guinea, N.M.R. Peres, K.S. Novoselov, A.K. Geim, *Rev. Modern Phys.* 81 (2009) 109-162.
10. K. Novoselov, A. Geim, S. Morozov, D. Jiang, Y. Zhang, S. Dubonos, I. Grigorieva, A. Firsov, *Sci.* 306 (2004) 666.
11. D.S.L. Abergel, V. Apalkov, J. Berashevich, K. Ziegler, T. Chakraborty, *Adv. Phys.* 59 (2010) 261.
12. M. J. Allen, V. C. Tung, R. B. Kaner, *Chem. Rev.* 110 (2010) 132.
13. O. V. Yazyev, *Rep. Progr. Phys.* 73 (2010) 056501.
14. A. Cresti, N. Nemeč, B. Biel, G. Niebler, F. Triozon, G. Cuniberti, S. Roche, *Nano. Res.* 1 (2008) 361.
15. C. W. J. Beenakker, *Rev. Modern. Phys.* 80 (2008) 1337.
16. S. D. Sarma, S. Adam, E. H. Hwang, E. Rossi, <http://arxiv.org/abs/1003.4731>,2010.
17. E. R. Mucciolo, C. H. Lewenkopf, *J. Phys. Condens. Mater.* 22 (2010) 273201.
18. K. I. Bolotin, K. J. Sikes, J. Hone, H. L. Stormer, P. Kim, *Phys. Rev. Lett.* 101 (2008) 096802.
19. X. Du, I. Skachko, A. Barker, E. Y. Andrei, *Nat. Nano.* 3 (2008) 491.

20. Y. M. Lin, C. Dimitrakopoulos, K. A. Jenkins, D. B. Farmer, H. Y. Chiu, A. Grill, P. Avouris, *Sci.* 327 (2010) 662.
21. T. O. Wehling, K.S. Novoselov, S. V. Morozov, E. E. Vdovin, M. I. Katsnelson, A. K. Geim, A. I. Lichtenstein, *Nano. Lett.* 8 (2008) 173.
22. J. S. Bunch, A. M. van de Zande, S. S. Verbridge, I. W. Frank, D. M. Tanenbaum, J. M. Parpia, H. G. Craighead, P. L. McEuen, *Sci.* 315 (2007) 490.
23. A. Dideykin, A. E. Aleksenskiy, D. Kirilenko, P. Brunkov, V. Goncharov, M. Baidakova, D. Sakseev, A. Y. Vul, *Diamond. Related Mater.* 20 (2011) 105-108.
24. K. S. Novoselov, A. K. Geim, S. V. Morozov, D. Jiang, M. I. Katsnelson, I. V. Grigorieva, S. V. Dubonos, A. A. Firsov, *Nat.* 438 (2005) 197.
25. K. S. Novoselov, Z. Jiang, Y. Zhang, S. V. Morozov, H. L. Stormer, U. Zeitler, J. C. Maan, G. S. Boebinger, P. Kim, A. K. Geim, *Sci* 315 (2007) 1379.
26. D. S. L. Abergel, V. Apalkov, J. Berashevich, K. Ziegler, T. Chakraborty, *Adv.Phys.* (2010) 1-17.
27. R. R. Nair, P. Blake, A. N. Grigorenko, K. S. Novoselov, T. J. Booth, T. Stauber, N. M. R. Peres, A. K. Geim, *Sci.* 320 (2008) 1308
28. P. Blake, P. D. Brimicombe, R. R. Nair, T. J. Booth, D. Jiang, F. Schedin, L. A. Ponomarenko, S. V. Morozov, H. F. Gleeson, E. W. Hill, A. K. Geim, K. S. Novoselov, *Nano. Lett.* 8 (6) (2008) 1704–1708.
29. X. Wang, L. Zhi, K. Mullen, *Nano. Lett.* 8(1) (2008) 323-327.
30. Y-M. Lin, K. A. Jenkins, A. Valdes-Garcia, J. P. Small, D. B. Farmer, P. Avouris, *Nano. Lett.* 9 (1) (2009) 422-426.
31. A. H. C. Neto, *Mater. Today.* 13 (2010) 12-17.
32. A. H. C. Neto, F. Guinea, N. M. R. Peres, *Phys. World.* 19 (2006) 33.
33. X. L. Wang, W. Q. Han, *Appl. Mater. Inter.* 2 (12) (2010) 3709-3713.
34. A. K. Geim, A. H. MacDonald, *Phys. Today.* 60 (2007) 35.
35. M. I. Katsnelson, *Mater. Today* 10 (2007) 20.
36. N. M. R. Peres, *Eur. phys. News vol.* 40. 3 (2009) 17-20.
37. A. H. C. Neto, F. Guinea, N. M. R. Peres, K. S. Novoselov, T. J. Booth, T. Stauber, *Sci.*320 (2008) 1308.
38. P. R. Wallace, *Phys. Rev.* 71 (1947) 622-632.

39. K. F. Cai, E. M€uller, C. Drařar, A. Mrotzek, *Mater. Sci. Eng. B*, 104, (2003) 45.
40. B. Wang, Y. Chang, L. Zhi, *New Carbon Mater.* 26 (1) (2011) 31-35.
41. T. S. Sreeprasad, S. M. Maliyekkal, K. P. Lisha, T. Pradeep, *J. Hazard. Mater.* 186 (2011) 921-931.
42. M. Tuzen, *Food. Chem. Toxicol.* 47 (2009) 1785-1790.
43. M. Zabihi, A. Ahmadpour, A. Haghighi Asl, *J. Hazard. Mater.* 167 (2009) 230-236.
44. S. M. Maliyekkal, K. P. Lisha, T. Pradeep, *J. Hazard. Mater.* 181 (2010) 986-995.
45. S. Babel, T. A. Kurniawan, *J. Hazard. Mater.* 97 (2003) 219-243.
46. M. Royal, M. Bhagat, R. Dhawan, *J. Hazard. Mater.* 171 (2009) 1009-1015.
47. A. Demirbas, *J. Hazard. Mater.* 167 (2009) 1-9.
48. J. M. Nabais, J. A. Gomes, Suhas, P. J. Carrott, C. Laginhas, S. Roman, *J. Hazard. Mater.* 167 (2009) 904-910.
49. M. Imamoglu, O. Tekir, *Desalination* 228 (2008) 108-113.
50. S. G. Wang, W. X. Gong, X. W. Liu, Y. W. Yao, B. Y. Gao, Q. Y. Yue, *Sep. Purif. Technol.* 58 (2007) 17-23.
51. A. K. Meena, G. K. Mishra, P. K. Rai, C. Rajagopal, P. N. Nagar, *J. Hazard. Mater.* 122 (2007) 17-23.
52. J. P. Ruparelia, S. P. Duttagupta, A. K. Chatterjee, S. Mukherji, *Desalination* 232 (2008) 145-156.
53. S. T. Yang, Y. Chang, H. Wang, G. Liu, S. Chen, Y. Wang, Y. Liu, A. Cao, *J. Colloid. Interface. Sci.* doi: 10.1016/j.jcis. 2010.07.042.
54. K. S. Novoselov, A. K. Gein, S. V. Morozov, D. Jiang, Y. Zhang, S. V. Dubonos, I. V. Grigorieva, A. A. Firsov, *Sci* 306 (2004) 666-669.
55. C. N. R. Rao, A. K. Sood, K. S. Subrahmanyam, A. Govindaraj, *Angew. Chem. Int. Ed.* 48 (2009) 7752-7777.
56. N. I. Kovtyukhova, G. A. Karpenko, A. A. Chuiko, *Russ. J. Inorg. Chem.* 37 (1992) 566-569.
57. V. Chandra, J. Park, Y. Chan, J. W. Lee, I. C. Hwang, K. S. Kim, *ACS Nano.* 4 (2010) 3979-3986.
58. W. Hu, C. Peng, W. Luo, M. Lv, X. Li, D. Li, Q. Huang, C. Fan, *ASC Nano.* 4 (2010) 4317-4823.

59. K. Zhang, V. Dwivedi, C. Chi, J. Wu, *J. Hazard. Mater.* 128 (2010) 162-168.
60. N. Savage, M. Diallo, J. Duncan, A. Street, R. Sustich (Eds.), *Nanotechnology Applications for Clean Water*, William Andrew, New York, 2008.
61. S. Zhang, X. Y. Li, J. P. Chen, *Carbon*. 48 (2010) 60-67.
62. K. Ohe, Y. Tagai, S. Nakamura, T. Oshima, Y. Baba, *J. Chem. Eng. Jpn.* 38 (2005) 671-676.
63. J. Trogolo, *Filtr. Separat.* 43 (2006) 28-29.
64. Z. Q. Wei, D. B. Wang, S. Kim, *J. Sci.* 328 (11) (2010) 1373-1375.
65. X. Wang, L. J. Zhi, N. Tsao, Z Tomovic, J Li, K. Mullen, *J. Angew Chem. Int. Ed.* 47 (16) (2008) 2990-2992.
66. M. Sung, P. Jaesung, L. Hyungwoo, *J. Adv. Mater.*, 22 (18) (2010) 2045-2049.
67. J. C. Meyer, C. O. Girit, M. F. Crommie, A. Zettl, Imaging and dynamics of light atoms and molecules on graphene, *J. Nat.* 454 (2008) 319-322.
68. X. Wang, L. J. Zhi, K. Mullen, *J. Nano Lett.* 8 (1) (2008) 323-327.
69. G. Liu, W. Stillman, S. Rumyantsev, Q. Shao, M. Shur, A. A. Balandin, *J. Appl. Phys. Lett.* 95(3) (2009) 033103.
70. Z. G. Cheng, Q. Li, Z. J. Li, Q. Zhou, Y. Fang, *J. Nano Lett.* 10 (5) (2010) 1864-1868.
71. F. Schedin, A. K. Geim, S. V. Morozov, E. W Hill, P. Blake, M. I Katsnelson, K.S. Novoselov, *J. Nat. Mater.* 6 (9) (2007) 652-655.
72. V. Dau, S. P. Surwade, S. Ammu, S. R. Agnihotra, S. Jain, K. E. Roberts, S. Park, R. S. Ruoff, S. K. Manohar, *J. Angew. Chem. Int. Ed.* 49 (12) (2010) 2154-2157.
73. J. Li, S. J. Guo, Y. M. Zhai, E. Wang, *J. Electrochem. Commun.* 11 (5) (2009) 1085-1088.
74. Y. Zhang, X. Sun, L. Zhu, H. Shen, N. Jia, *Electrochimica. Acta.* 56 (2011) 1239-1245.
75. F. Schedin, A. K. Geim, S. V. Morozov, E. W. Hill, P. Blake, M. I. Katsnelson, K. S. Novoselov, *Nat. Mater.* 6 (2007) 652-655.
76. X. Du, I. Skachko, A. Barker, E. Y. Andrei, *Nat. Nanotechnol.* 3 (2008) 491- 495.
77. K. S. Novoselov, A. K. Geim, S. V. Morozov, D. Jiang, M. I. Katsnelson, I. V. Grigorieva, S. V. Dubonos, A. A. Firsov, *Nat.* 438 (2005) 197-200.
78. I. Meric, M. Y. Han, A. F. Young, B. Ozyilmaz, P. Kim, K. Shepard, *Nat. Nanotechnol.* 3 (2008) 654.
79. U. Bach, D. Lupo, P. Comte, J. E. Moser, F. Weissortel, J. Salbeck, H. Spreitzer, M. Gratzel, *Nat.* 395 (1998) 583-585.

80. A. R. Schlatmann, D. W. Floet, A. Hilberer, F. Garten, P. J. M. Smulders, T. M. Klapwijk, G. Hadziioannou, *Appl. Phys. Lett.* 69 (1996) 1764.
81. G. Gustafsson, Y. Cao, G. M. Treacy, F. Klavetter, N. Colaneri, A. J. Heeger, *Nat.* 357 (1992) 477- 479.
82. S. Park, J. An, R. D. Piner, I. Jung, D. Yang, A. Velamakanni, S. T. Nguyen, R. S. Ruoff, *Chem. Mater.* 20 (21) (2008) 6592-6594.
83. Wang, L. Zhi, K. Mullen, *Nano. Let.* 8 (1) (2008) 323-327.
84. H. Kuzmany, A. Kukovecz, F. Simon, M. Holzweber, Ch. Kramberger, T. Pichler, *Synth. Met.* 141 (2004) 113-122.
85. S. Iijima, T. Ichihashi, *Nat. London.* 363.(1993) 603-605
86. P. Atkins, J. de Paula, *Phys. Chem.* 8th ed. Oxford University Press (2006).
87. A. Agel, A. El-Nour, R. Ammar, Al-Warthan, *Arabian J. Chem. In Press corrected proof* (2010)
88. Y. Segava, S. Miyamoto, P. Senel, T. Sassamoni, N. Tokitoh, K. Itamia, *Angew Chem.* 50 (2011) 3244-3248.
89. Z. Li, L. Zheng, V. Saini, S. Bourdo, E. Dervish, A. Biris, *J. Exper. Nano. Sci.* (2012) 1-8.
90. D. Konathan, K. N. D. Buli, D. V. Papavassilion, A. Striolo, *Molecular. Phys.* 109, 1 (2011) 97-111.
91. W. A. Harrison, *Phys. Rev.* B8 (1973) 4487.
92. C. A. Coulson, H.C. Longuet-Higgins, *Proc. R. Soc. Ser.* 191 (39) (1947) 447-
93. H. Dai, J. H. Hafner, A.G. Ringler, D. J. Colbert, R.E. Smalley, *Nat.* 384 (1996) 147-150.
94. J. Wang, X. Wang, C. Xu, M. Zhang, X. Zhang, *Polym. Int.* 60 (5) (2011) 816-822.
95. M. Sangermano, S. Marchi, L. Valentini, S.B. Bon, P. Fabbi, *Macromoleculalar. Mater. Eng.* 295 (5) (2011) 401-407.
96. T. Rati, Y. Li, *App. Sci. Manuf.* 42 (12) (2011) 1995-2002.

CHAPTER THREE: EXPERIMENTAL METHODS

CHAPTER THREE

EXPERIMENTAL METHODS

3.1 Introduction

Experimental procedures that have been conducted for the fulfillment of this research project are discussed in this chapter. Most of the techniques and experiments used for this research were done at normal condition and at the atmospheric pressure unless otherwise stated.

3.2 Chemical and Materials

All the chemicals used in this project were of reagent grade. Solvents obtained from the suppliers were of high purity and were used as they were. All reaction unless otherwise stated were performed under normal conditions. Sulphuric acid (H_2SO_4), hydrochloric acid (HCl), hydrogen peroxide (H_2O_2), potassium permanganate (KMnO_4), cobalt chloride (CoCl_2), zinc chloride (ZnCl_2), calcium carbonate (CaCO_3), aluminum oxide (Al_2O_3), magnesium oxide (MgO), sodium carbonate (Na_2CO_3), sodium hydroxide (NaOH), nitrogen gas (N_2) and acetylene ($\text{HC}\equiv\text{CH}$) were purchased from Sigma-Aldrich locally while flake graphite powder and hydrazine hydrate (H_2O_4) were imported from Germany. Filter paper qualitative advantec 90 mm was bought from Toyo Roshi Kaisha Ltd in Japan. And vacuum pump, VDE 0530/72 B/IP44 at 220 V, 0.75 Kw, 1350 1/min 50 Hz, CB =32 micro farad/400V was used.

3.3 General Experimental Procedure and Characterization Techniques

3.3.1 Synthesis of graphene oxide

Graphene oxide (GO) was prepared following the adopted Hummer's method [1]. Summarily, 2 g of natural flake graphite powder was added to 46 mls of cold ($0\text{ }^\circ\text{C}$) concentrated sulphuric acid (H_2SO_4). Then 6 g of Potassium Permanganate KMnO_4 was gradually added with continuous stirring in a cooling ice bath. The mixture was stirred at $35\text{ }^\circ\text{C}$ for 2 hours. 92 mls of distilled water was slowly added to the mixture and temperature was maintained below $100\text{ }^\circ\text{C}$ for 15 minutes. After that, 280 mls of 30 % hydrogen Peroxide (H_2O_2) solution was added to the mixture. The product was finally filtered with 500 mls of 10 % Hydrochloric acid (HCl) solution to remove metal ions then thoroughly washed with distilled water. Brownish pasty material of GO was obtained.

3.3.2 Reduction of graphene oxide

Hydrazine monohydrate, while most strong reductants have slight to very strong reactivity with water, does not, making it an attractive option for reducing aqueous dispersions of graphite oxide. GO (3.0 g) was weighed to make colloidal dispersion in distilled water with continuous stirring at temperature of 35 °C. Hydrazine hydrate (H₂O₄) that weighed 10% of the GO dispersed in water was added as a reducing agent and left for 3 hours. After this, the filtrate that turned from brown to black was filtered and a black pasty material of graphene was obtained [1].

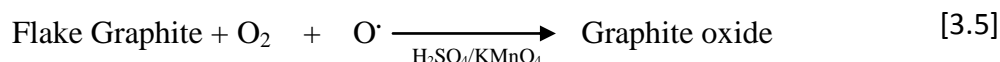
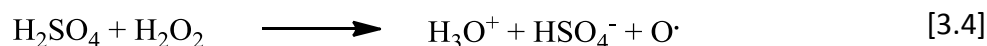
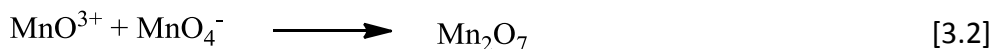
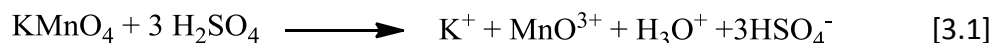
Finally the metal ions were removed by dissociation of hydrochloric acid from which the Cl⁻ reacted with Mn²⁺ and K⁺ to form manganese chloride and potassium chloride respectively and these chlorides are soluble in water hence their removal via filtration process.

3.3.3 Sample Preparation

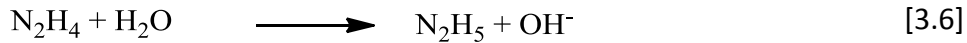
The sonicated small amounts of colloidal dispersions of GO and RGO were dropped on a silica substrate for the characterization of atomic force microscopy, optical magnification, scanning electron microscopy transmission electron microscopy and Raman while powdered samples were prepared for the characterization of attenuated total reflectance, X-ray diffractometry, liquid samples for ultraviolet-visible spectrometry, and finally pasty samples for thermogravimetric analysis.

3.4 Chemical Reactions

3.4.1 Oxidation of graphite flake



3.4.2 Reduction of graphene oxide



3.4.3 Removal of metal ions



3.5 Carbon nanotubes

3.5.1 Synthesis of catalysts

Catalyst support is an essential component for the synthesis of carbon nanotubes and in this study calcium carbonate, aluminum oxide and magnesium oxide will be used separately since they provide high surface area for catalytic chemical vapor deposition reactions (CCVD).

The solids were prepared by co-precipitation, that is mixing an aqueous solution containing chlorides of the cations (Co-Zn/Ca), (Co-Zn/Al) and (Co-Zn/Mg) in the desired amounts, with aqueous solution of Na_2CO_3 and NaOH at room temperature. 1M of NaOH was added drop wise using a burette to maintain the reaction at pH 9.5 and the molar ratios e.g. $\text{Co}^{2+}\text{-Zn}^{2+}/\text{Ca}^{2+} = 1:1:2$ were initially maintained. The slurry obtained was exposed to temperature treatment at 125 °C for 10, 30, 60 and 300 min in an oven. The precipitate was washed with distilled water and dried at 40 °C in an oven. The catalyst obtained in this reaction was not calcined and this resulted in a catalytic material as shown in Figure 3.1 below.



Figure 3.1 Picture of synthesized but not calcined catalyst.

3.5.2 Synthesis of carbon nanotubes

The following are some common techniques used to synthesize carbon nanotubes.

1. Catalytic chemical vapor deposition (CCVD)
2. Arch discharge
3. Laser ablation and
4. Nebulized spray pyrolysis (a form of CVD)

In this study the CCVD technique was used and depending on the conditions, this method produces both SWNTs and MWNTs with yields ranging from 20-100%. However, nanotubes synthesized through this technique have amorphous carbon and catalyst particles were supposed to be treated before use. The experimental setup is shown in Figure 3.3. The reactor/furnace of approximately 40 mm x 700 mm long quartz tube was heated by an electrical tube furnace with a temperature controller. Nitrogen gas was passed at the rate of 40 ml min^{-1} through the reactor for about 70 min. After stabilization of about 10 min at $700 \text{ }^\circ\text{C}$, the nitrogen gas flow was maintained at 240 ml.min^{-1} . The acetylene gas with flow rate of 90 ml.min^{-1} was passed through the reactor for an hour. It was ensured that the quartz boat be placed right at the centre of the furnace during the synthesis process. These gas flow rates were controlled by a mass flow controller (MFC). After synthesis the reactor was naturally cooled to room temperature with nitrogen flowing at a flow rate of 40 ml min^{-1} for about 3 to 4 hours. Black, soft and spongy slurry was obtained as carbon nanomaterial as shown by Figure 3.2 below.

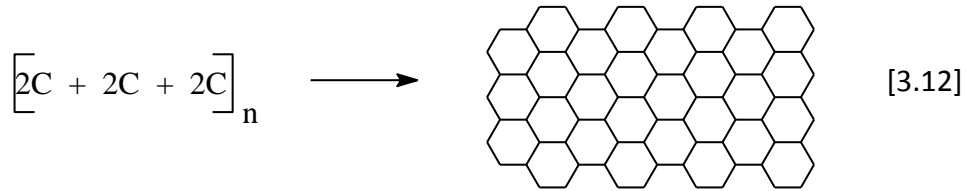
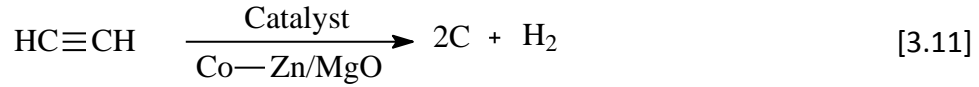


Figure 3.2 Synthesis of carbon nanomaterial.

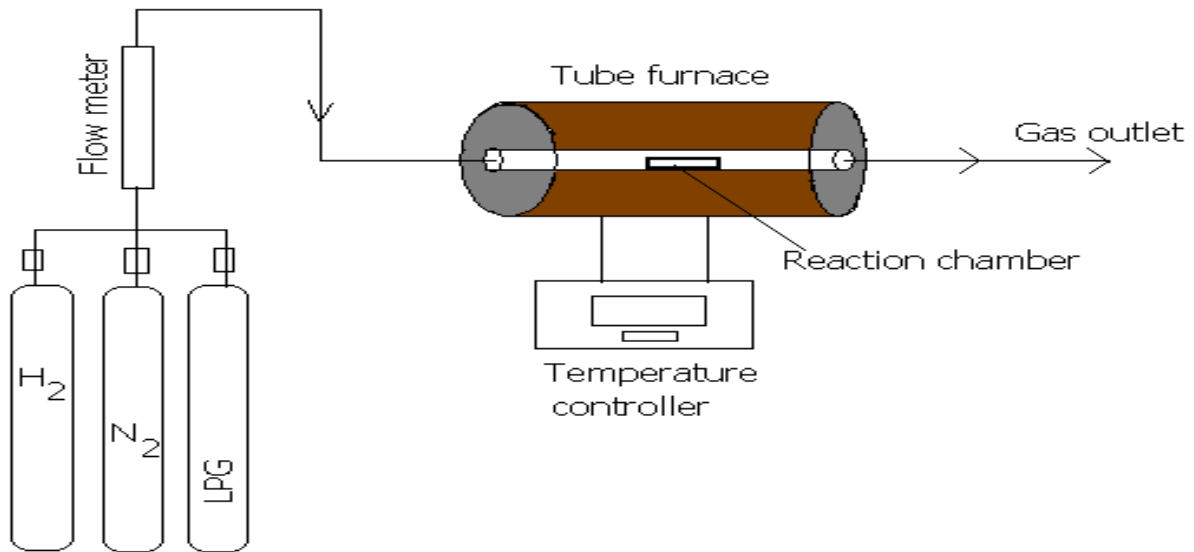


Figure 3.3 Diagram of the horizontal furnace used for synthesis of CNTs. [13]

3.6 Analytical Techniques in this study

3.6.1 X-ray Diffractometer (XRD)

Figure 3.4 below shows the X-ray diffractometer instrument which was used to determine the crystallite size structure of a sample at molecular size. It is an effective method to investigate the interlayer changes and the crystalline properties of the synthesized material. As such, X-ray scattering techniques are a family of non-destructive analytical techniques which reveal information about the crystallographic structure, chemical composition and physical properties of materials and thin films. This technique is also based on observing the scattered intensity of an X-ray beam impinging on a sample as a function of incident and scattered angle, polarization and wavelength or energy.

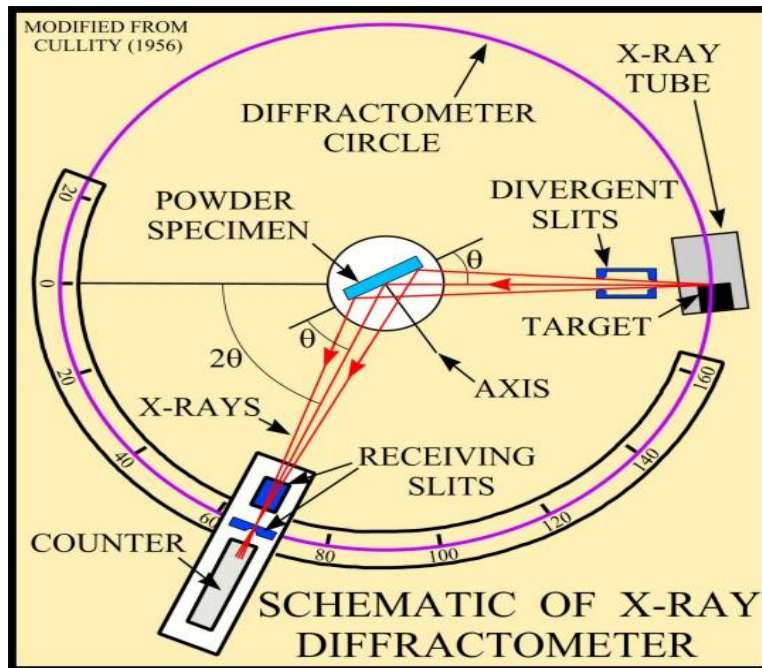


Figure 3.4 Schematic diagram of X-ray diffractometer.

Bragg's law

$$n\lambda = 2d \sin\theta \quad [3.14]$$

Where n = number of incident

λ = wavelength

d = interplanar distance

θ = angle of incidence

There are a number of sources of X-ray radiation. X-rays can be generated by an X-ray tube, a vacuum tube that uses a high voltage to accelerate the electrons released by a hot cathode to a high velocity. The velocity electrons collide with a metal target, the anode, creating the X-rays. In crystallography, like in this study a copper target is most common, with cobalt often being used when fluorescence from iron in the sample might otherwise present a problem.

3.6.2 Fourier Transform Infrared (FT-IR) Spectrophotometry

In Figure 3.5 when light interacts with matter, the photons which make up the light may be absorbed or scattered, or may not interact with the material and may pass straight through it. If the energy of an incident photon corresponds to the energy gap between the ground state and an excited state of a molecule, the photon may be absorbed and the molecule can then be promoted to a higher energy excited state. It is this change which is measured in absorption spectroscopy by the detection of the loss of that energy from the radiant light. However, it is also possible for the photon to interact with the molecule and scatter from it. In this case there is no need for the photon to have an energy which matches the difference between two energy levels of the molecule. The scattered photons can be observed by collecting light at an angle to the incident light beam.

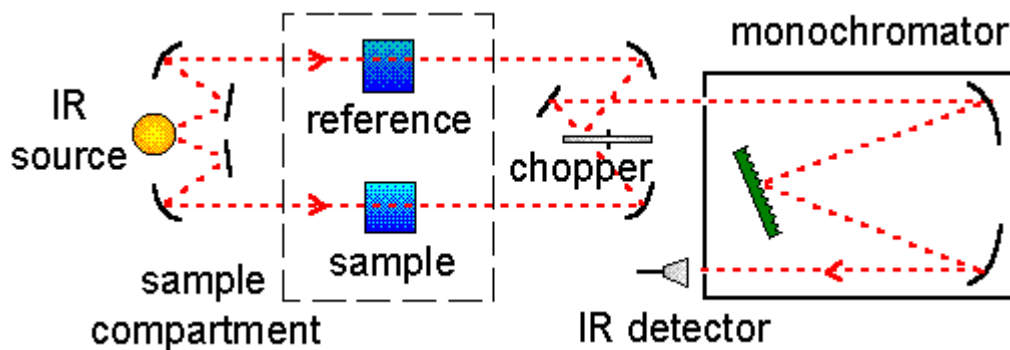


Figure 3.5 Schematic diagram of fourier transform infrared.

Infrared spectroscopy is one of the important tools used to identify functional groups that are present in a molecule or compound [2]. Infrared radiation has a low energy, under these conditions electrons cannot be excited to higher energy levels; it only causes the vibrations and rotation of molecules. The positions of atoms in a molecule are not fixed; they are subject to a number of different vibrations. Vibrations fall into the two main categories: stretching and bending. These vibrations, depending on the type of atoms, can be symmetric or asymmetric about a central point. The asymmetrical vibrations usually create a dipole with the molecule.

Molecules with these types of vibrations absorb IR radiations and are called IR active. Due to differences in bond energies, different functional groups will absorb IR radiation at different wavelength. This makes it possible to identify different functional groups present in the system as each functional group will absorb at a particular wavelength. The analysis was done on a Perkin Elmer spectrum 100 FTIR/ATR spectrometer in the $4000\text{-}500\text{ cm}^{-1}$ region. The convenience of this instrument is that no sample holder (KBr plate) is needed or a special substance such as nujol. The sample was just analysed by placing it directly on top of the detector.

3.6.3 Ultraviolet Visible (UV-visible) Spectrophotometry

UV-visible absorption spectroscopy, Figure 3.6, is used to analyse molecules that absorb ultraviolet and visible light (photons). When a molecule absorbs a photon of light, electrons in the molecule are promoted to a higher energy level. Light passes through a monochromator which selects a wavelength. This monochromatic light passes through the sample and the transmitted light is often detected by use of a photomultiplier tube or photodiode-array. By plotting absorbance units versus the wavelength, an absorption spectrum is obtained. The Beer-Lambert law is used to describe absorbance;

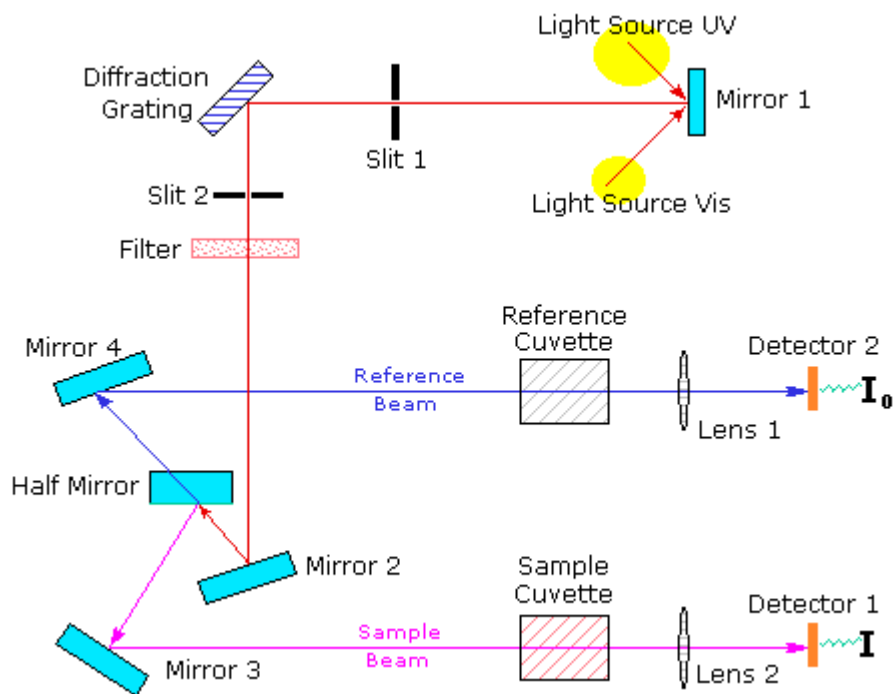


Figure 3.6 Schematic diagram of UV-visible spectrophotometer.

$$A = \epsilon bc \quad [3.14]$$

Where ϵ is the molar absorptivity ($\text{L}\cdot\text{mol}^{-1}\cdot\text{cm}^{-1}$)

b is the path length (cm)

c is the concentration of the sample.

λ_{max} is the wavelength of maximum absorption

3.6.4 Scanning Electron Microscope (SEM)

Figure 3.7 shows a schematic diagram of the scanning electron microscope (SEM) that is used for the observation of specimen surfaces. When the specimen is irradiated with a fine electron beam, secondary electrons are emitted from the specimen surface. Topography of the surface can be observed by two dimensional scanning of the electron probe over the surface and acquisition of an image from the detected secondary electrons.

The specimen is observed at a high magnification in an electron microscope. A specimen stage, which stably supports the specimen and moves smoothly, is required. The specimen stage for SEM can perform the following movements: horizontal (X, Y), vertical (Z), specimen tilting (T), and rotation (R). The X and Y are used for the selection of a field view; (Z) movement provides the change of image resolution and the depth of focus.

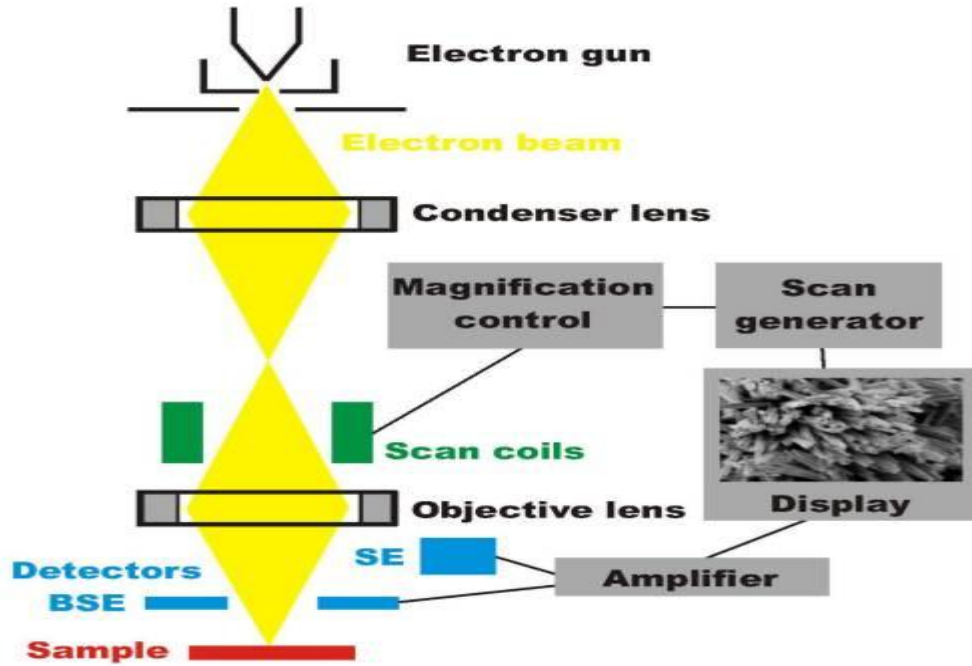


Figure 3.7 Schematic diagram of scanning electron microscope.

3.6.5 Transmission Electron Microscope (TEM)

One of the typical characters of nanophase materials is the small sizes. Although, some structural can be revealed by x-ray and neutron diffraction, direct imaging of nano particles is only possible using the transmission electron microscopy and scanning electron microscopy. TEM is unique because it can provide a real space image on the atom distribution in the nanocrystal and its surface [3]. Today's TEM, Figure 3.8, is a versatile tool that provides not only atomic resolution lattice images, but also chemical information at a spatial resolution of 1 nm or better, allowing direct identification of the chemistry of a single nanocrystals. With a finely focused electron probe, the structural characterization of a single nanoparticle can be fully characterized [3].

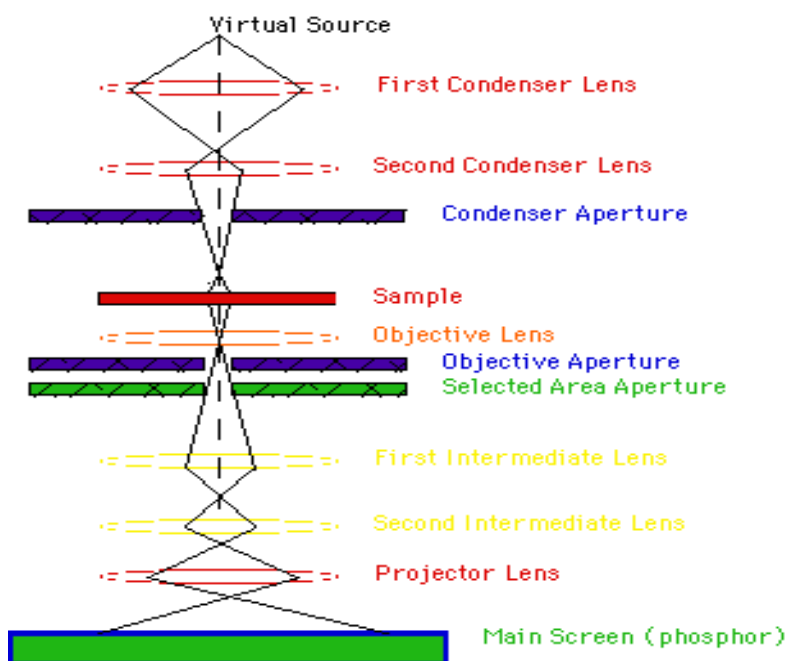


Figure 3.8 Schematic diagram of transmission electron microscope.

Images in TEM are usually dominated by three types of contrast. First, diffraction contrast [4] which are produced due to a local distribution in the orientation of the crystal (by dislocation, for example) so that the diffracted intensity of the incident electron beam is perturbed, leading to contrast observed in bright-field image [4].

3.6.6 Raman Microscope

Since the mid-1990s, surface-enhanced Raman scattering (SERS) has greatly advanced and gained wider application and renewal interest than in the previous two decades [5-13]. There have been several new and creative developments, e.g., SERS of single molecules, nanostructures and transition metals, tip-enhanced Raman scattering (TERS), surface-enhanced hyper-Raman scattering (SEHRS), ultraviolet-excited SERS (UV-SERS), surface enhanced resonance Raman scattering (SERRS) [12].

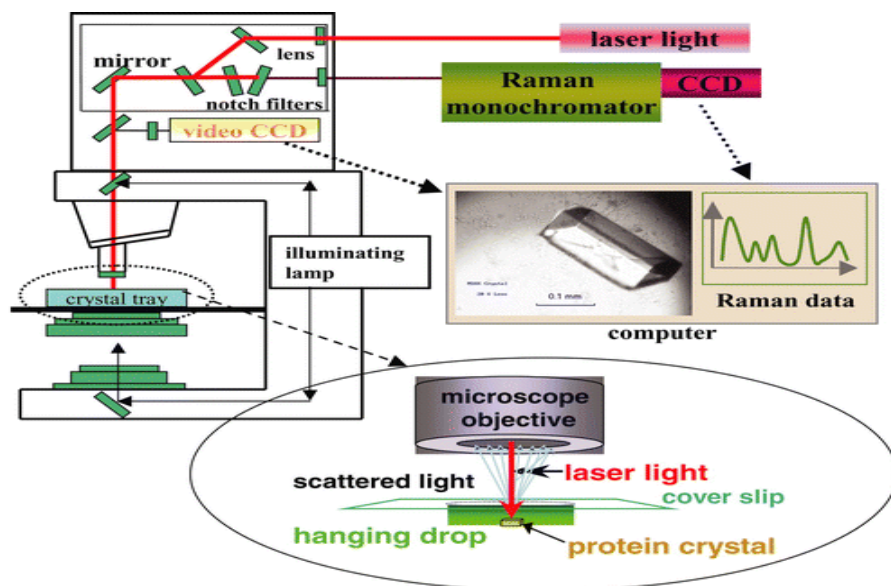


Figure 3.9 Schematic diagram of conventional Raman spectroscopy.

The main spectroscopy employed to detect vibrations in molecules are based on the process of Raman scattering shown in figure 3.9. This technique is widely used to provide information on chemical structures and physical forms, to identify substances from the characteristic spectral patterns (fingerprinting) and to determine quantitatively or semi-quantitatively the amount of a substance in a sample [6-9]. Samples can be examined in a whole range of physical states, for example, as solids, liquids or vapours and in hot or cold states, in bulk, as microscopic particles or as surface layers [7-11].

The technique is very wide ranging and provides solutions to a host of interesting and challenging analytical problems. Raman scattering is less widely used than infrared absorption, largely due to problems with sample degradation and fluorescence. However, recent advances in instrument technology have simplified the equipment and reduced the problems substantially. These advances, together with the ability of Raman spectroscopy to examine aqueous solutions and samples inside glass containers and samples without any preparation have led to a rapid growth in the application of this technique. In practice, modern Raman spectroscopy is simple. Variable instrument parameters are few, spectral manipulation is minimal and a simple interpretation of the data may be sufficient.

After the analysis of a sample, Raman produces two significant peaks, that is, the D band which is associated with the order/disorder of the system and the G band which is an indicator of the stacking structure. These peaks are dominant vibrational modes observed in the graphitic structures. The ratio of the intensities of the two bands explains the following:

1. D/G is often used as a means of determining the number of layers in a graphene sample and its overall stacking.
2. Increase in D/G ratio indicates a high degree of exfoliation/disorder.
3. Decrease in D/G ratio indicates good order.

3.6.7 Atomic Force Microscope (AFM)

Figure 3.10 shows schematic diagram of AFM that gives significant information about surface features with unprecedented clarity [14]. The AFM can examine any sufficiently rigid surface either in air or with the specimen immersed in a liquid [15]. Recently developed instruments can allow temperature control of the sample, can be equipped with a closed chamber for environmental control, and can be mounted on an inverted microscope for simultaneous imaging through advanced optical techniques.

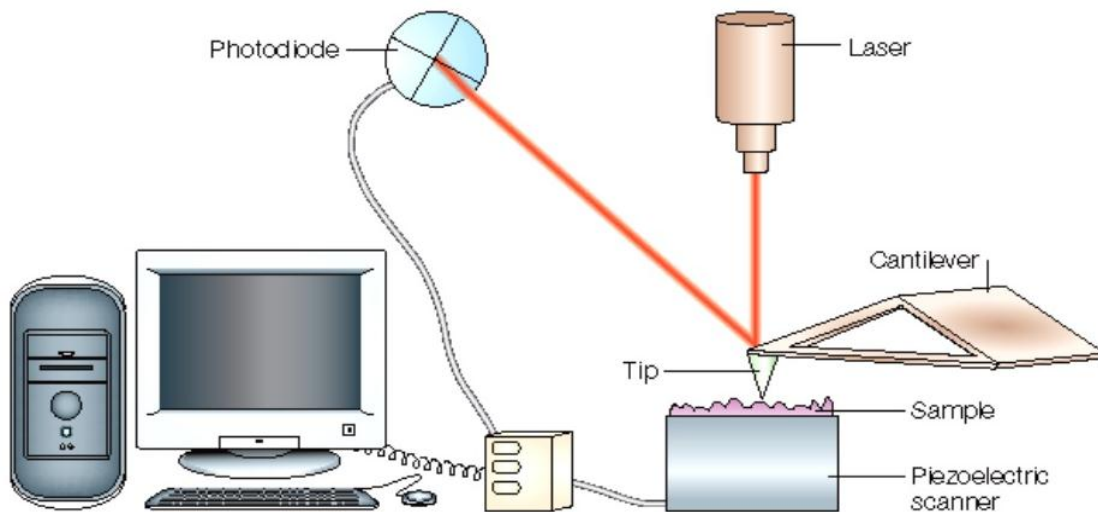


Figure 3.10 Schematic diagram of atomic force microscope.

Compared with transmission electron microscopes, 3D AFM images are obtained without expensive sample preparation and yield far more complete information than the 2D profiles available from cross sectioned samples. The tip, which is mounted at the end of a small cantilever, is the heart of the instrument because it is brought in closest contact with the sample and gives rise to the image through its force interactions with the surface. When the first AFM was made, a very small diamond fragment was carefully glued to one end of a tiny piece of gold foil. The tip cantilever assembly typically is fabricated from silicon or silicon nitride and, using technology similar to that applied to integrated circuit fabrication, allows a good uniformity of characteristics and reproducibility of results [14-15].

The AFM can provide much more information than just taking images of the surface of the sample [16]. The instrument can be used to record the amount of force felt by the cantilever as the probe tip is brought close to a sample surface, eventually indent the surface and then pulled away. By doing this, the long range attractive or repulsive forces between the probe tip and the sample surface can be studied [17]. Local chemical and mechanical properties like adhesion and elasticity may be investigated, and even the bonding forces between molecules may be directly measured [16-18]. By acquiring a series of force curves, one at each point of a square grid, it is possible to acquire a so called force vs. volume map that will allow the user to compute images representing local mechanical properties of the sample observed [19].

3.6.8 Optical Microscope

The term optical spectroscopy can be attributed to any kind of optical photon interactions with matter. Two most general classes of such interactions are absorption and emission. Consequently, one can distinguish between absorption spectroscopy and emission spectroscopy. In the former case we will speak about absorption spectra and in the latter the emission spectra will be the subject of measurements [20]. Advantages of the optical spectroscopy methods are their non-destructive nature and possibility to monitor the studied object without physical contact to it. This makes them popular in applications such as environment monitoring and technological process control [21-24].

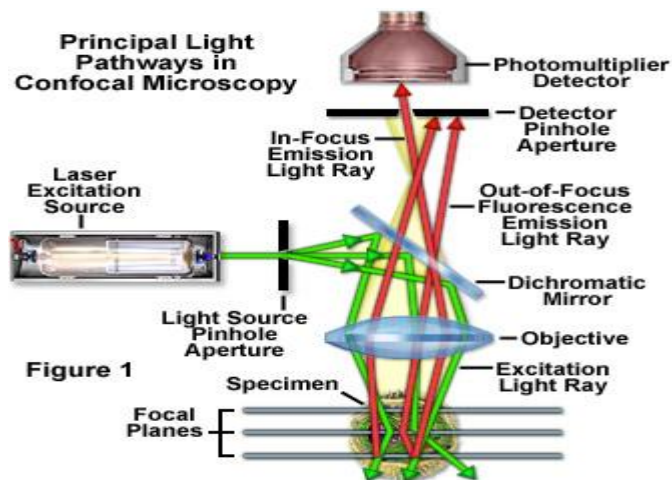


Figure 1
Figure 3.11 Schematic diagram of optical microscope.

Originally the studies were related to the wavelength dependences of these processes, but as new methods and directions of research were developed the scope of optical spectroscopy has enlarged [22-23]. One of the important directions of such development today is time resolved spectroscopy, where optical methods provide superior time resolution not achievable by any other methods available [21]. There are also specialized areas of optical spectroscopy such as single molecule spectroscopy and non-linear optical spectroscopy, which have also been under active development during the past decade [21]. Naturally, the reason for the great attention paid to the optical spectroscopy techniques in recent fundamental research is new exciting knowledge gained. To mention few there are chemical reaction dynamics at single bond level, called femtochemistry and single molecule spectroscopy. Furthermore, non-destructive spectroscopy methods have found numerous applications in monitoring different processes in industry and environmental technologies [22-24].

Optical properties of surfaces are determined to a great extent by structure and morphology [20]. The term structure implies the geometrical arrangement of atoms in the crystal lattice. It reflects the detailed microscopic picture of a surface under equilibrium conditions. In contrast, morphology characterizes the macroscopic shape of a surface. These two distinct features of surfaces manifest themselves under different conditions which are determined by the spatial resolution of the surface probe. When the surface is irradiated by X-rays whose wavelength is comparable with inter atomic distance in a crystal, the microscopic structure is probed. The same

is true for fast particle beams. For example, Helium (He) atoms with a kinetic energy of 20 meV have a de Broglie wavelength of 1 Å and hence represent a surface probe with microscopic resolution. For the optical spectral range the typical wavelengths are essentially longer, of the order of several hundred nanometers. Correspondingly, light sources probe the surface morphology rather than the surface structure [20].

3.6.9 Thermogravimetric Analyser (TGA)

Thermogravimetric analysis (TGA) is an instrumental technique used to study the change in the sample weight with respect to change in temperature. The changes are often associated with the weight loss resulting from the dehydration and decomposition of the sample with increase in temperature. The weight loss can also arise from the formation of physical and chemical bonds that may lead to the release of volatile compounds. [5]

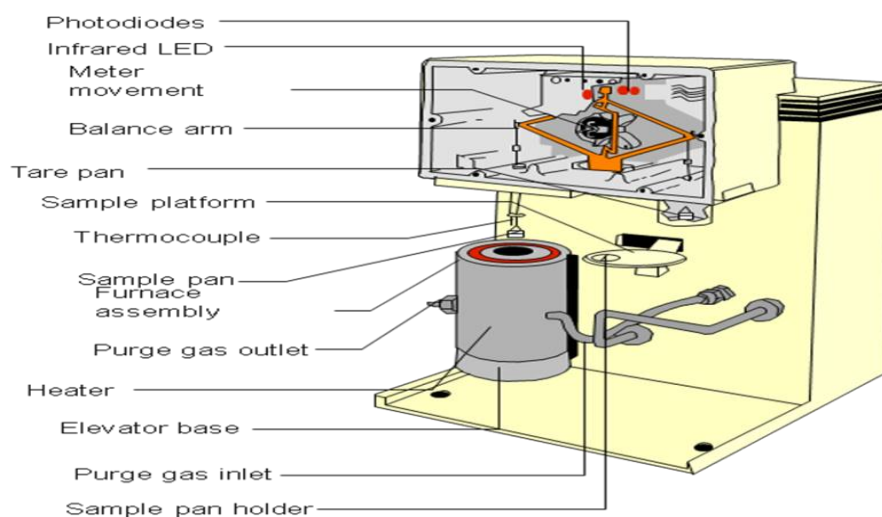


Figure 3.12 Scheme of a thermogravimetric analyser

Figure 3.1.2 shows the schematic diagram of a thermo gravimetric analyser. TGA comprises of an automatic balance onto which the sample is loaded. The pan containing the sample is encapsulated by a furnace as shown above, which is heated from room temperature to about 1000 °C at a heating rate of 5-10 °C per minute. The sample is continuously weighed while being heated to higher temperatures and the mass loss is recorded as function of temperature. The analysis was done on STA 6000 simultaneous thermal analyser from Perkin Elmer.

References

1. C. Hou, Q. Zhang, M. Zhu, Y. Li, H. Wang, *Carbon*. 49 (2011) 47-53.
2. M. S. Ahmad, B. Mirza, M. Hussain, M. Hanif, S. Ali, M. J. Walsh, F. L. Martin, *Biophysics*. (2008) 1-19.
3. P. Buseck, J. M. Cowley, L. Eyring eds, *New York, London, Amsterdam, Oxford University Press*, 1988.
4. P. B. Hirsch, A. Howie, R. B. Nicholson, D. W. Pashley, M. J. Whelan, *New York, Roberts E. Krieger Publishing Company*, 1977.
5. Z. Q. Tian, Special issue on SERS, *J. Raman Spectrosc.* 36 (2005) 125.
6. A. Campion, P. Kambhampati, *Surf. Sci.* 427 (1999) 115-125.
7. J. K. Kneipp, H. Kneipp, I. Itzkan, R. R. Dasari, M. S. Feld, *Chem. Rev.* 99 (1999) 2957-2975.
8. M. Moskovits, L. L. Tay, J. Yang, T. Haslett, *Springer, Berlin, Heidelberg, New York* (2002) 215–226.
9. K. L. Kelly, E. Coronado, L. L. Zhao, G. C. Schatz, *J. Phys. Chem. B* 107 (2003) 668-677.
10. J. Jiang, K. Bosnick, M. Maillard, L. Brus, *J. Phys. Chem. B* 107 (2003) 9964.
11. T. R. Jensen, M. D. Malinsky, C. L. Haynes, R. P. Van Duyne, *J. Phys. Chem. B* 104 (2000) 10549-10556
12. D. T. Chiu, *Ana. Chem.* 22 (9) (2003).
13. Z. Q. Tian, B. Ren, J. F. Li, Z. L. Yang, *Ann. Rev. Phys. Chem.* 55 (2007) 122-125.
14. T. R. Albercht, S. Akamine, T. E. Carver, C. F. Quate, *J. Vac. Sci. Technol. A*(8) (1990) 3386-3396.
15. M. Tortonese, *IEEE I. Engl. Med. Biol. Mag.* 16 (1997) 28-33.
16. H-J. Butt, *Biophys. J.* 60 (1991) 1438-1444.
17. A. Vinckier, G. Semenza, *FEBS. Lett.* 430 (1998) 12-16.
18. J. L. Hutter, J. Bechhoefer, *J. Vacuum. Sci. technol.* B 12 (1994) 2251-2253.
19. J. P. Cleveland, S. Manne, D. Bocek, P. K. Hansma, *Rev. Sci. Instrum.* 64 (1993) 403-405.
20. V. G. Bordo, H-G. Rubahn, *Optics and Spectroscopy at surfaces and interfaces*, (2005).

21. J. J. O’Gallagher, R. Winston, R. Gee, VI (R. Winston, Ed.) 60, *Proceedings of the SPIE*. 4446 (2001) 60.
22. J. J. O’Gallagher, R. Winston, A. Lewandowski, *Proceedings of the 11th Annual ASME Solar Energy Conference, 195–200, San Diego, CA* (1989).
23. J. J. O’Gallagher, R. Winston, A. Lewandowski, *Proceedings of the 1993 ISES Solar World Congress, Budapest, Hungary* (1993).
24. J. J. O’Gallagher, R. Winston, R. Diver, A. Lewandowski, *Proceedings of the 1997 ASES Annual Conference, Washington, D.C.* (1997).

CHAPTER FOUR: RESULTS AND DISCUSSION

CHAPTER FOUR

RESULTS AND DISCUSSION

4.1 Introduction

In this chapter, results obtained in the characterization of graphene oxide, graphene and carbon nanotubes are presented, interpreted and discussed. The adopted Hummer's method was used to synthesize graphene oxide (GO) from flake graphite powder which was then reduced to graphene [1]. Catalytic chemical vapor deposition (CCVD) method was used for the synthesis of CNTs with acetylene used as carbon source.

4.2 Synthesis of graphene oxide, graphene and carbon nanotubes.

Graphene oxide, graphene and carbon nanotubes were synthesized according to the methods mentioned above. On completion of the synthesis, hydrophilic GO and hydrophobic RGO and CNTs samples were obtained respectively. The characterizations of the as-prepared samples were done on a variety of analytical techniques.

4.3 Physico-chemical measurements

The structural characterization of GO, RGO carbon nano material were carried out by powder X-ray diffraction (XRD) analysis performed on a Bruker- D 8 advance, GER x-ray diffractometer using Cu K α with a wavelength of 1.54 nm radiation. The operating voltage and current were 40 kV and 300 mA respectively. Attenuated Total Reflectance (ATR) FT-IR spectra were recorded on a Perkin elmer spectrum 100 spectrometer in the 4000-500 cm⁻¹ region. Ultra-violet visible absorbance measurements were carried out on CE 2021, 2000 series UV-vis spectrophotometer. The surface measurements were recorded with a JEOL 7500F field emission scanning electron microscope (FE-SEM). The Transmittance electron microscope (TEM) images were obtained on Fei Tecnai G2-20 operated at 200 kV using an energy filter of 20 eV. Raman spectra were carried out using a Horiba Jobin Yvon HR 800 model DU 420A-OE with power of 20 mWatts at a wavelength of 514.5 nm with an argon ion laser from 100 to 4000 cm⁻¹ space. The imaging of the material was carried out by using an Atomic force microscope (Nanoman V AFM) in tapping mode to determine the thickness and morphology of the as prepared samples.

For the images to be taken, samples were initially sonicated and dispersed in water solution and spray coated on a freshly ethanol cleaned silicon substrate surface by using a fine atomizer. The Ultra violet visible (CE 2021, 2000 series) was also used to further confirm the oxidation and reduction of graphite and graphene oxide. Magnified Optical Microscope M-service 470 majmf with 2000 magnification was used. Thermogravimetric and Derivative gravimetric analysis were recorded on Perkin Elmer STA 6000 Simultaneous thermal analyzer.

4.4 Graphene and Graphene oxide characterization

4.4.1 X-ray Diffraction Spectroscopy

X-ray diffractometer instrument is used to determine the crystallinity structure of a sample at molecular size. It is an effective method to investigate the interlayer changes and the crystalline properties of the synthesized material. Therefore, GO and RGO have been carefully characterized by X-ray diffraction (XRD)

Figure 4.1 shows XRD patterns of GO and expandable graphite. The diffractogram shows a very intense and narrow peak centred at $2\theta = 11.8^\circ$, corresponding to the (002) inter-planar spacing of 7.49 Å. The most intense peak for expandable graphite at $2\theta = 26.4^\circ$, corresponding to a *d*-spacing of 3.37 Å is very minimal in GO sample. The basal spacing increases in the course of oxidation due to the expansion of the layer planes caused by the accommodation of various oxygen species.

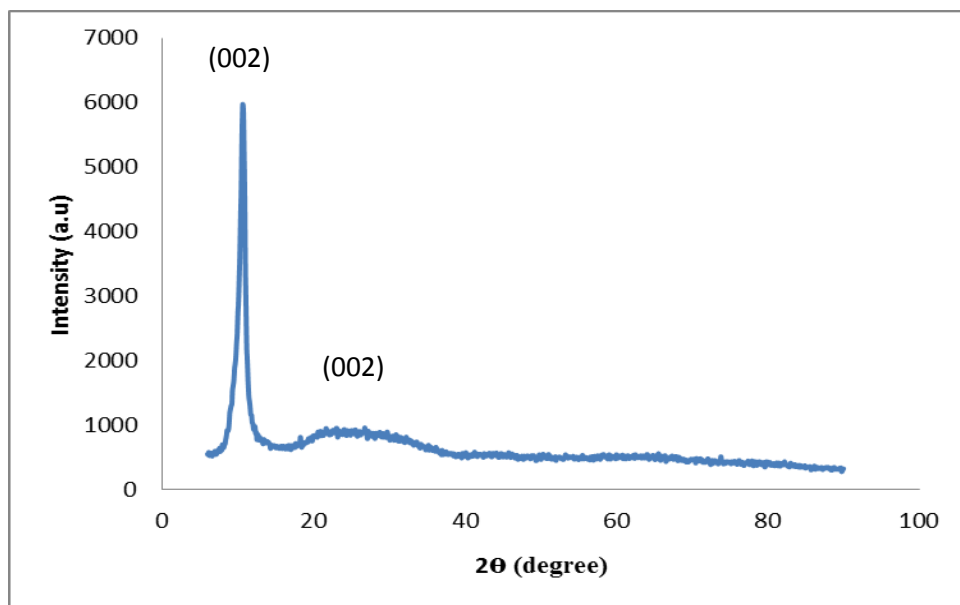


Figure 4.1 XRD patterns of graphene oxide.

Unlike Figure 4.1, Figure 4.2 below shows XRD patterns of RGO with a more pronounced peak at $2\theta = 26.4^\circ$ corresponding to a d-spacing of 3.37 \AA confirming that truly the removal of oxygen species took place during the reduction process hence reduced graphene oxide. So, XRD confirms that the completion of the oxidation reaction as the layer distances of the starting expandable graphite and the end products.

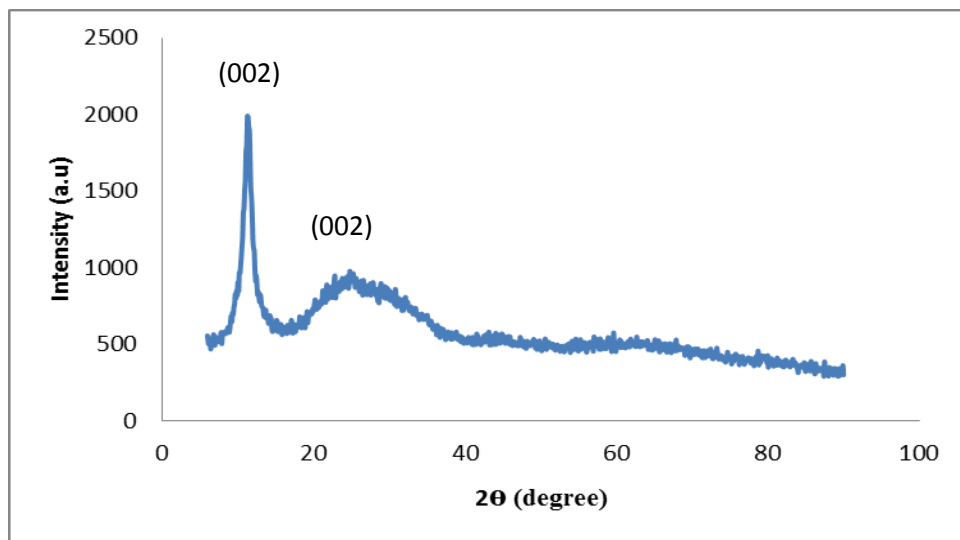


Figure 4.2 XRD patterns of reduced graphene oxide.

4.4.2 Fourier Transform Infrared Spectroscopy (FTIR-ATR)

Infrared spectroscopy is one of the most important tools used to identify functional groups that are present in a molecule or compound. Figure 4.3 compares the FTIR spectrometry of graphene oxide and reduced graphene oxide.

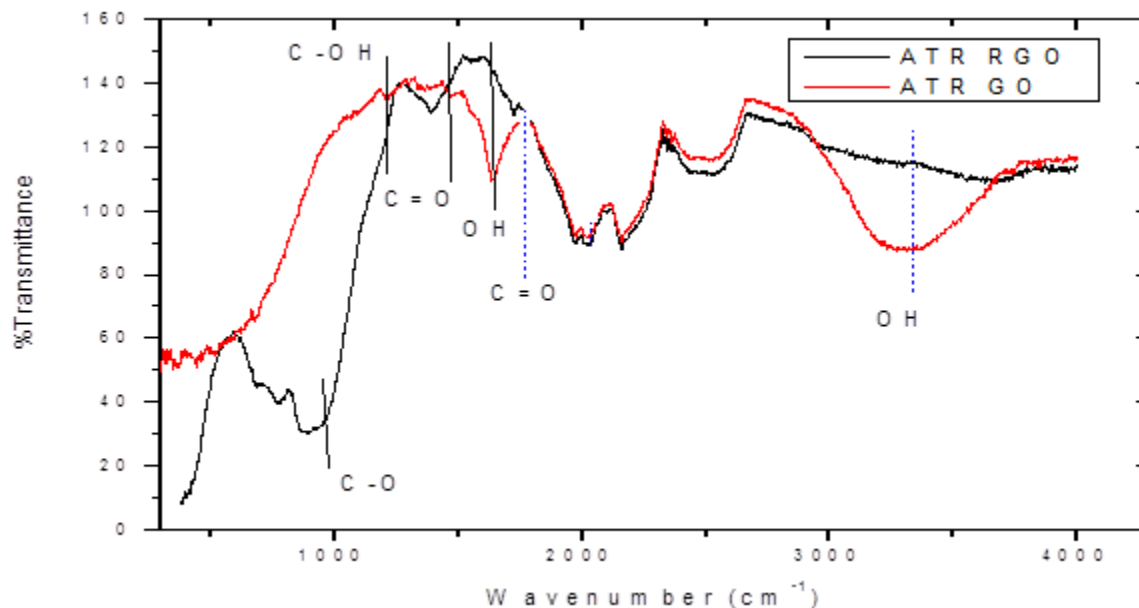


Figure 4.3 FTIR (ATR) patterns of graphene oxide and reduced graphene oxide.

From the structure of graphene oxide and reduced graphene oxide the following essential functional groups like OH: hydroxyl, COOH: carbonyl (for carboxylic acid) and C=O: carbonyl can be identified. OH exhibits a broad band of medium to strong intensity occurring at 400-2400 cm^{-1} , C=O: Carbonyl (for carboxylic acid) shows a strong broad band at 1725-1700 cm^{-1} , -O gives an absorption band of strong to medium intensity at 1300-1000 cm^{-1} and at 3500 to 3100 cm^{-1} and band with medium to strong intensity at 1640-1550 cm^{-1} . The FT-IR spectrum of GO illustrated in Figure 4.3, also confirms the successful oxidation of graphite. The characteristic vibrations are the broad and intense peak of O-H groups centred at 3420 cm^{-1} .

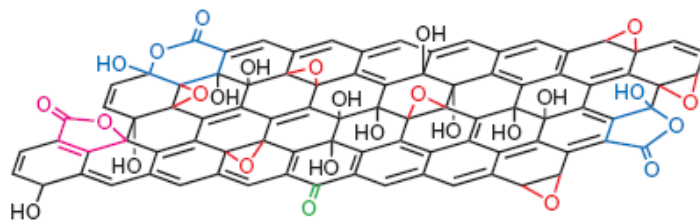


Figure 4.4 The structure model of the graphite oxide species [2].

No clear distinction seems possible between C-OH and H₂O peaks. According to our perusal of the literature, no special attempts have been exercised for the removal of the physically adsorbed water during IR measurements. The relatively strong peak at 1720 cm⁻¹ is most often related to the C=O stretching of COOH groups situated at the edges of the oxidized graphene (structure model as illustrated in Fig 4.4. The peak at 1630 cm⁻¹ was attributed either to oxygen surface compounds, like cyclic ethers, or to ring vibrations throughout the carbon skeleton, but the HOH bending vibrations also appear in a very close range of wavenumbers. The C-OH stretching peak at 1260 cm⁻¹ characterizes the spectrum of carbonyl groups, and the C-O stretching peak at 1070 cm⁻¹ characterizes the spectrum of epoxy groups on the surface of the oxidized graphene. GO consists of carbon, oxygen, and hydrogen. The atomic composition of a specific sample was found to vary with the synthetic methods and conditions (time and temperature oxidation) and the origin and grain size of the graphite specimen [3].

4.4.3 Ultra violet–visible Spectroscopy

Figure 4.5 shows the Ultra-violet visible spectra of graphene and graphene oxide with absorption peaks at 230 nm that is red shifted to 270 nm indicating that the electronic conjugation was revived upon reduction of graphene oxide to graphene. This red shift is due to electronic configuration in graphene in the reduction of graphene oxide. The absorption peak at 230 nm is attributed to π - π^* transition of aromatic C-C ring.

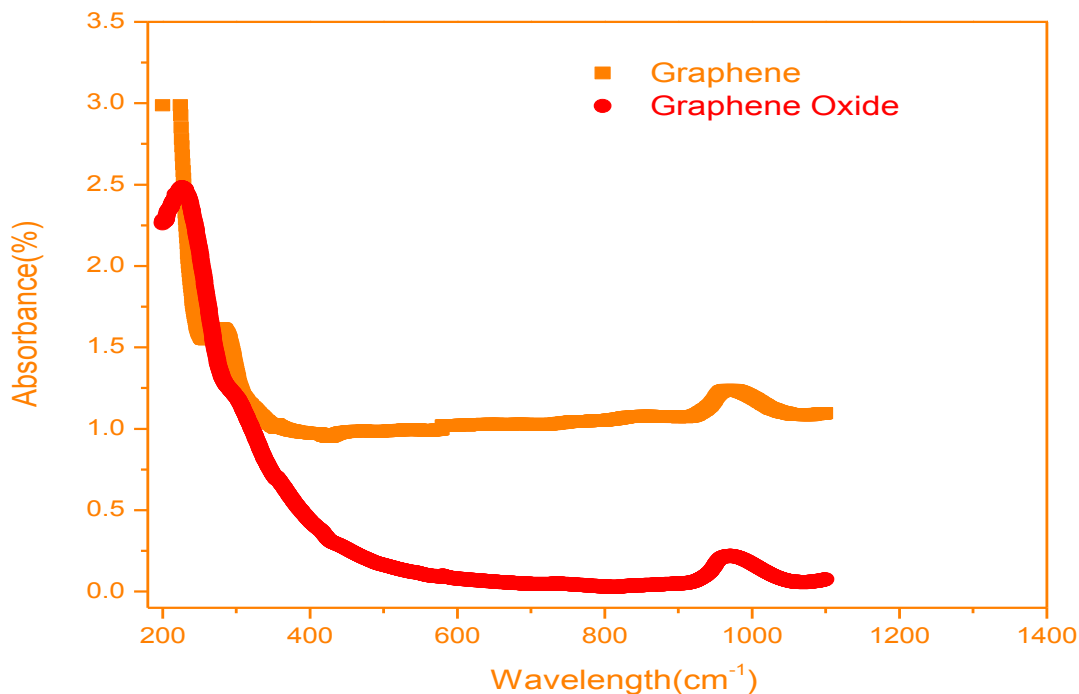


Figure 4.5 Uv-vis spectra of graphene and graphene oxide.

4.4.4 Scanning Electron Microscopy

The morphology of graphene oxide and reduced graphene oxide as shown in Figure 4.6. It can be seen that the GO image looks lighter while the RGO image looks darker. This could be attributed to the fact that as the oxygen functional species are removed during reduction process, the separated GO sheets during intercalation now stick together and result in more thickly or decrease in interlayer spacing of single sheets. This further confirms the reduction of GO into RGO. According to some reports [4-5] when the chemical conversion of graphite oxide to graphene, holes and defects are easily produced on the carbon grid. It is possible that these holes are a result of removal of oxygen functional group species during the reduction process. It is also possible that the nanocomposites can grow around these holes and defects and are inclined to insert into graphene sheets [6]. And in addition, the rigid particles may also easily sink into the supported materials [7].

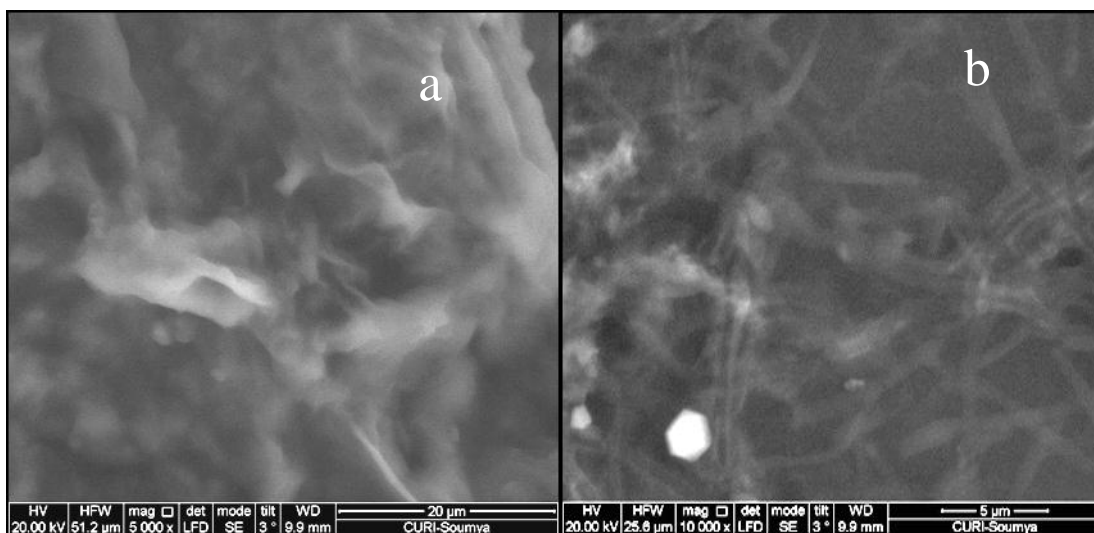


Figure 4.6 SEM images of (a) GO and (b) RGO.

4.4.5 Transmission Electron Microscopy

The morphology and structure of the graphene oxide and reduced graphene oxide were observed by TEM analysis. Figure 4.7 (a) shows large GO sheets that were observed on the top of the copper grid. The most transparent and featureless regions seen are likely to be monolayer of GO. Different from bulk GO sheets, the RGO are no longer totally flat and smooth but always exhibit some corrugation, where they resemble crumpled silk veil waves. Especially, any particular area of the particle shows considerable folding (Figure 4.7 (b)). As reported previously [8], this phenomenon is caused by the thermodynamic stability of the 2D membrane results from microscopic crumpling via bending or buckling. This phenomenon also supports that the coarse aggregates be exfoliated completely. When the modification process completed, a very significant morphology change can be observed.

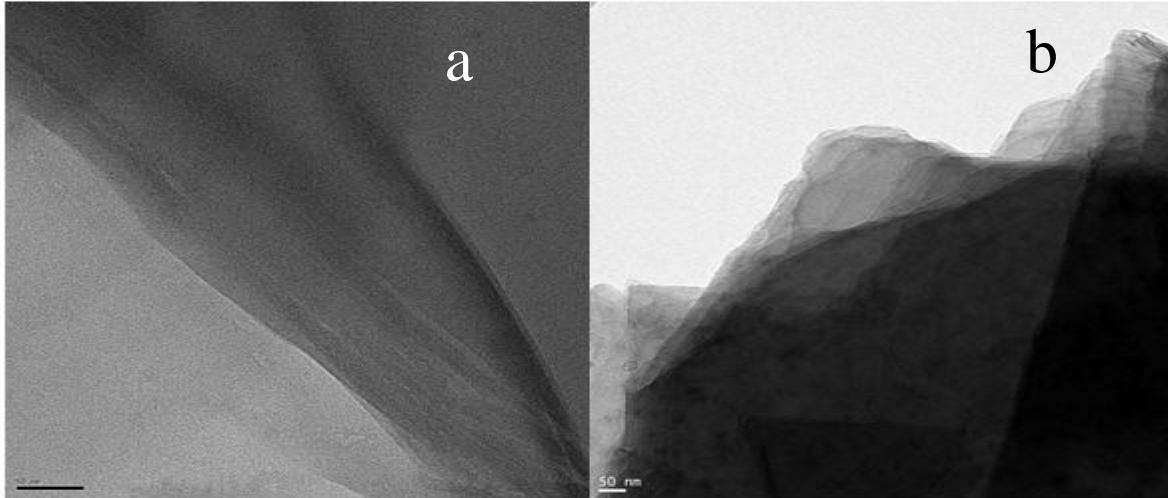


Figure 4.7 TEM images of (a) GO and (b) RGO.

4.4.6 Raman Spectroscopy

It is well known that Raman scattering is very sensitive to the microstructure of nanocrystalline materials [3]. Figures 4.8 and 4.9 above show the Raman spectra of GO and RGO respectively. Comparing GO with RGO, the D- and G- band of graphene shift from 1355 and 1605 cm^{-1} to 1340 and 1586 cm^{-1} respectively. Lambert [9] and Stankovic *et al* [10] confirmed that this relative intensity of D/G increased after hydrothermal reaction simultaneously, this further confirms that graphene oxide was reduced to graphene.

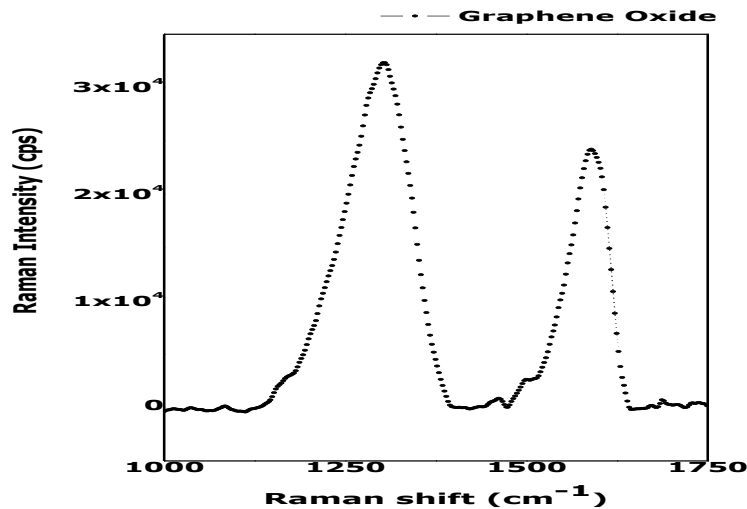


Figure 4.8 Raman spectrum of graphene oxide.

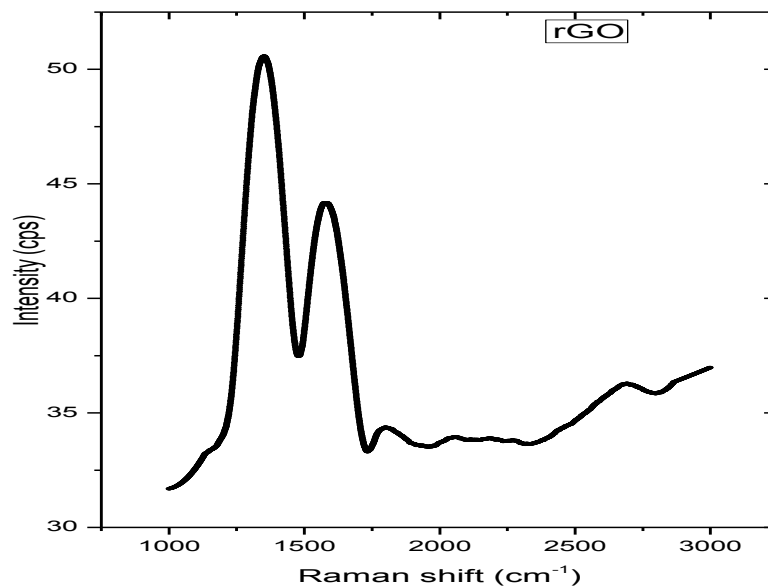


Figure 4.9 Raman spectrum of reduced graphene oxide.

The absence of the 2D band around 2726 cm^{-1} after oxidation indicates that all graphite layers have been oxidized while the formation of D band after oxidation process was an evidence for success of the reaction process. Two peaks around 1500 cm^{-1} (D and G band) are essentially identical to the characteristic peaks of graphene oxide. Therefore, oxidized expandable graphite (EG) is the same material as graphene oxide (GO) made from graphite.

4.4.7 Atomic Force Microscopy

The level of exfoliation was evaluated by AFM as indicated by Figures 4.10 and 4.11 that show a three dimensional AFM topography of graphene oxide and reduced graphene respectively. The GO sheets are expected to be thicker due to the presence of covalently bonded oxygen and the displacement of sp^3 hybridized carbon atoms slightly above and below the original graphene plane as opposed to RGO which is thinner due to removal of oxygen species. The images also in 3D view confirm the formation of rippled graphene layers and effect of reactions in each step. The height difference between arrows is 1 nm in GO and 1.2 nm in RGO indicating a single

graphene oxide sheet due to intercalating of oxygen into the graphite gallery. This further confirms the reduction of graphene oxide into graphene.

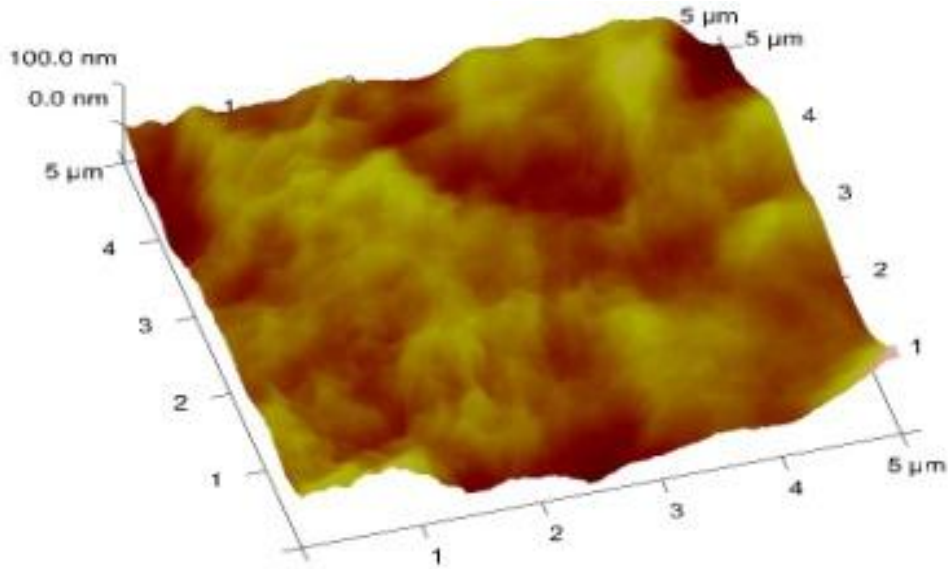


Figure 4.10 AFM topography of graphene oxide in 3D.

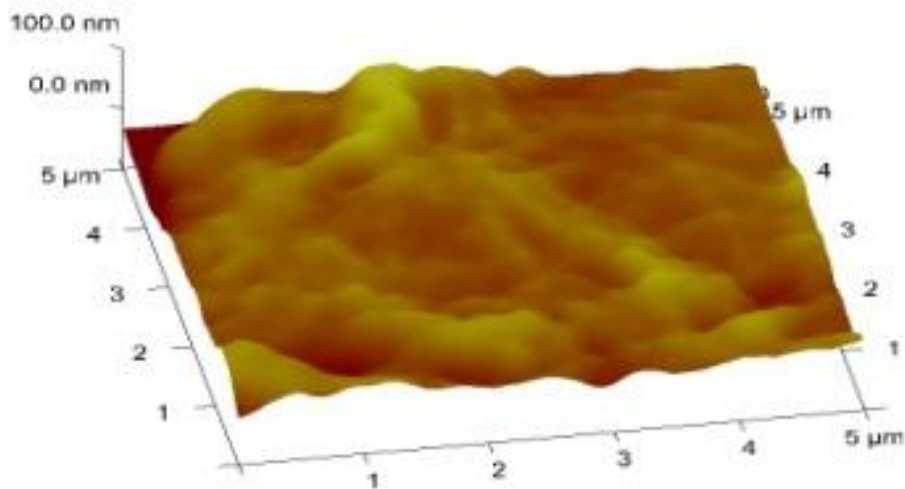


Figure 4.11 AFM topography of reduced graphene oxide in 3D

4.4.8 Optical Microscopy

Figure 4.12 (a) and (b) show the optical images of graphene oxide and reduced graphene oxide respectively. The optical image in Figure 4.1 (a) shows the graphene oxide which is brownish in colour and (b) shows blackish material that indicate the agglomerated graphene dispersions and some shiny like spots which reveal pasty graphene product.

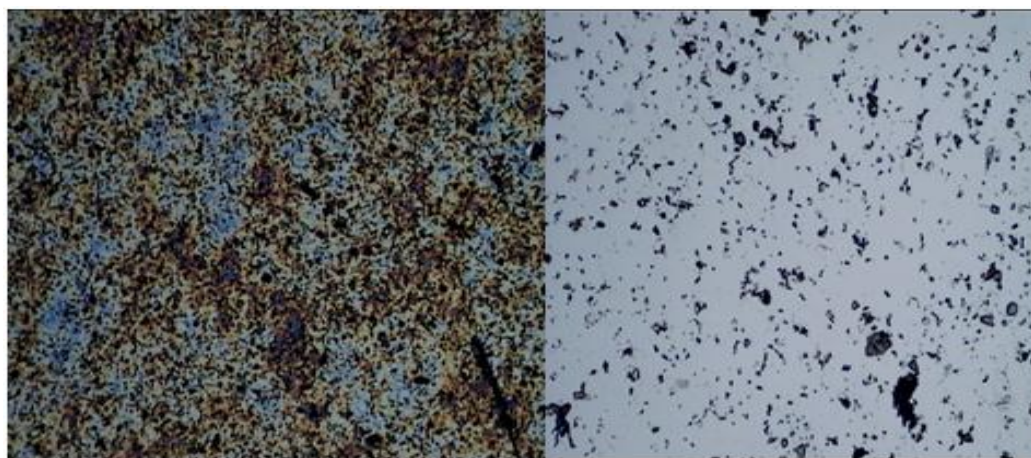


Figure 4.12 Optical (a) graphene oxide and (b) reduced graphene oxide.



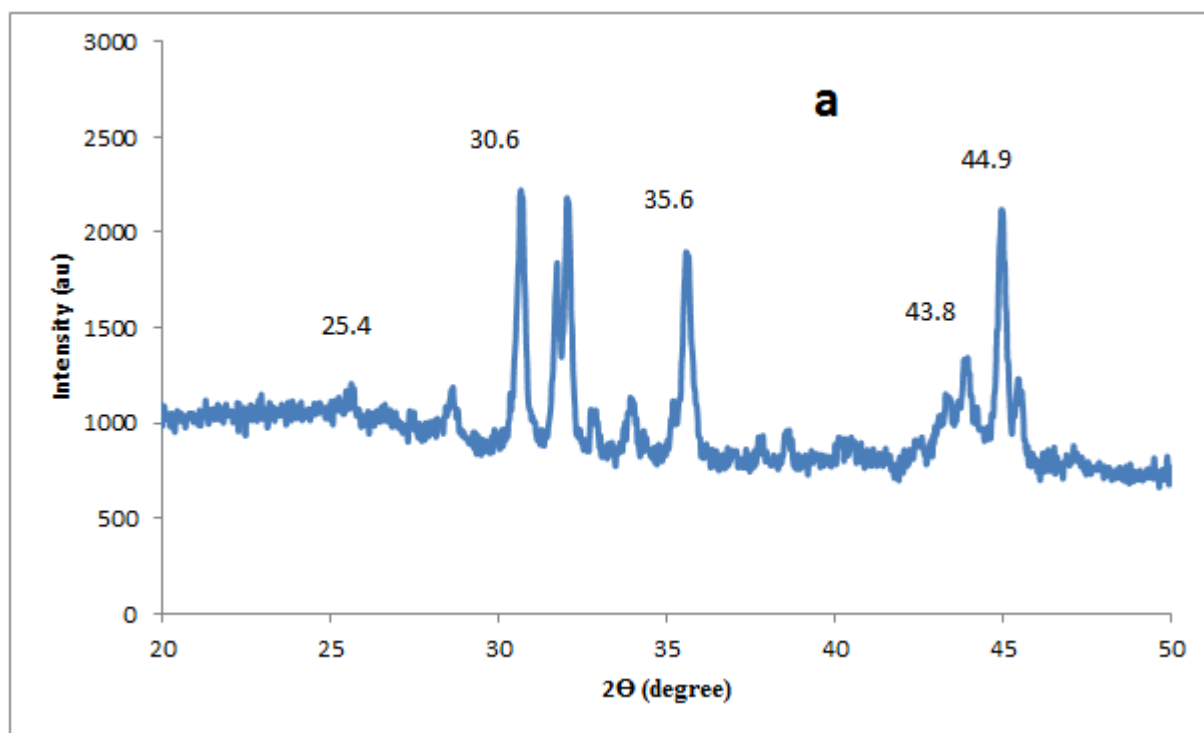
Figure 4.13 Pictures of brownish graphene oxide (GO) and blackish reduced graphene oxide (RGO)

Figure 2.13 above supports the optical images above since the brownish colour indicates the success of oxidation process while blackish colour confirms the success of the reduction process.

4.5 Carbon Nanotubes Characterization

4.5.1 X-Ray Diffraction Microscopy

The XRD patterns of carbon nanotubes synthesized with Co/Sn, Co/Sr and Co/Zn catalysts supported on Al_2O_3 , CaCO_3 and MgO are therefore, presented in figures. 4.13 to 4.15.



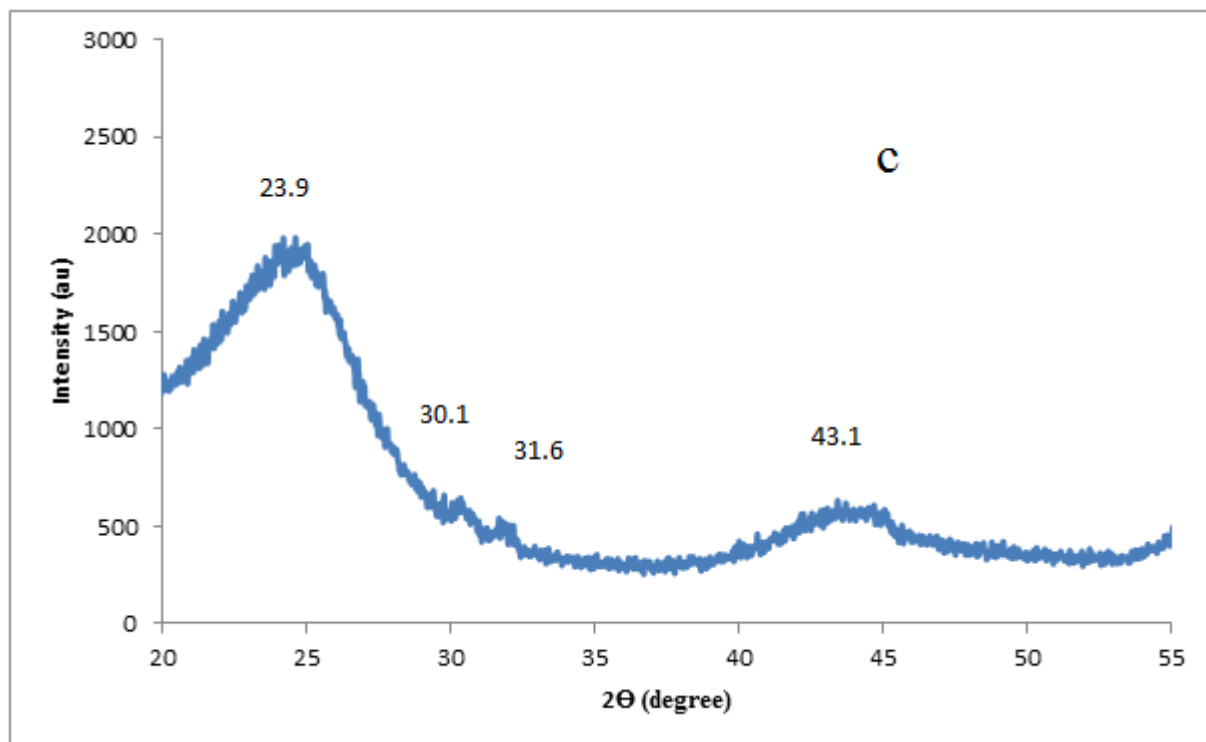
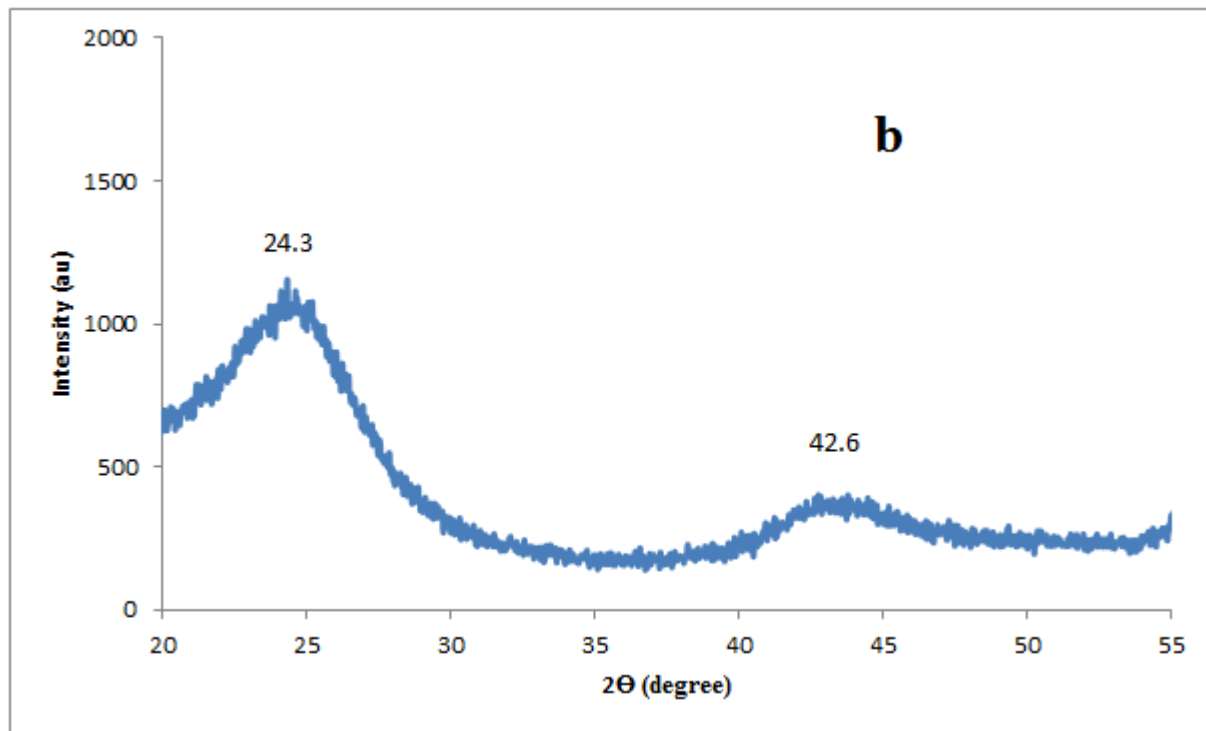
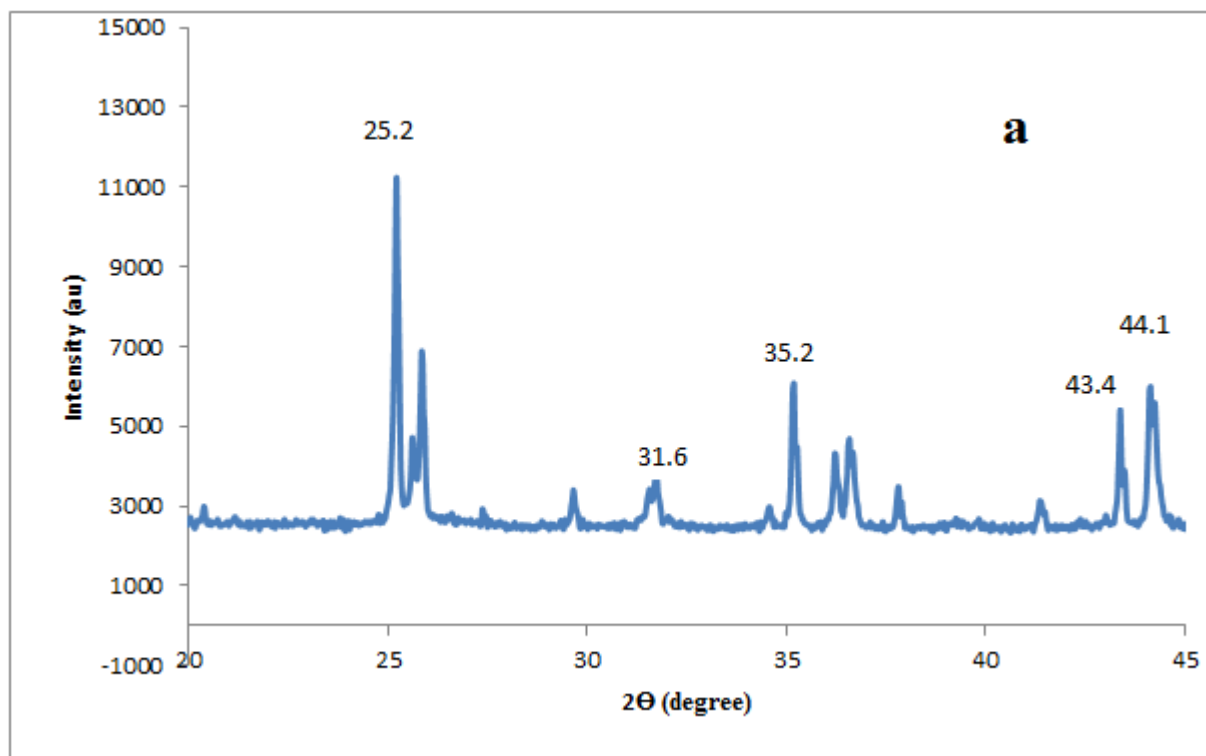


Figure 4.13 XRD patterns of carbon nanomaterial synthesized with Co-Sn catalysts supported on (a) Al₂O₃ (b) CaCO₃ (c) MgO.

Figure 4.13 (a) shows a small peak intensity at $2\theta = 25.4^\circ$ which is just above the range of the characteristic lattice structure peak. It also shows a peak at 43.8° which is a lattice characteristic peak. (b) & (c) have two characteristic peaks at $2\theta = 24.3^\circ$ and 42.6° , and 23.9° and 43.1° respectively.



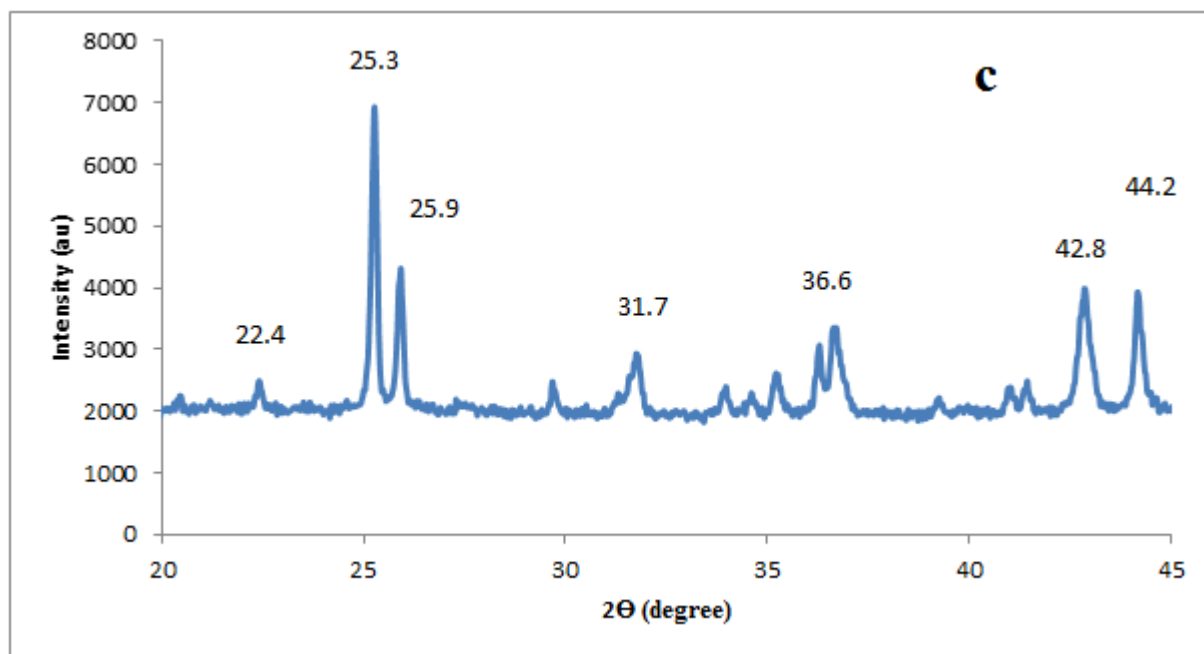
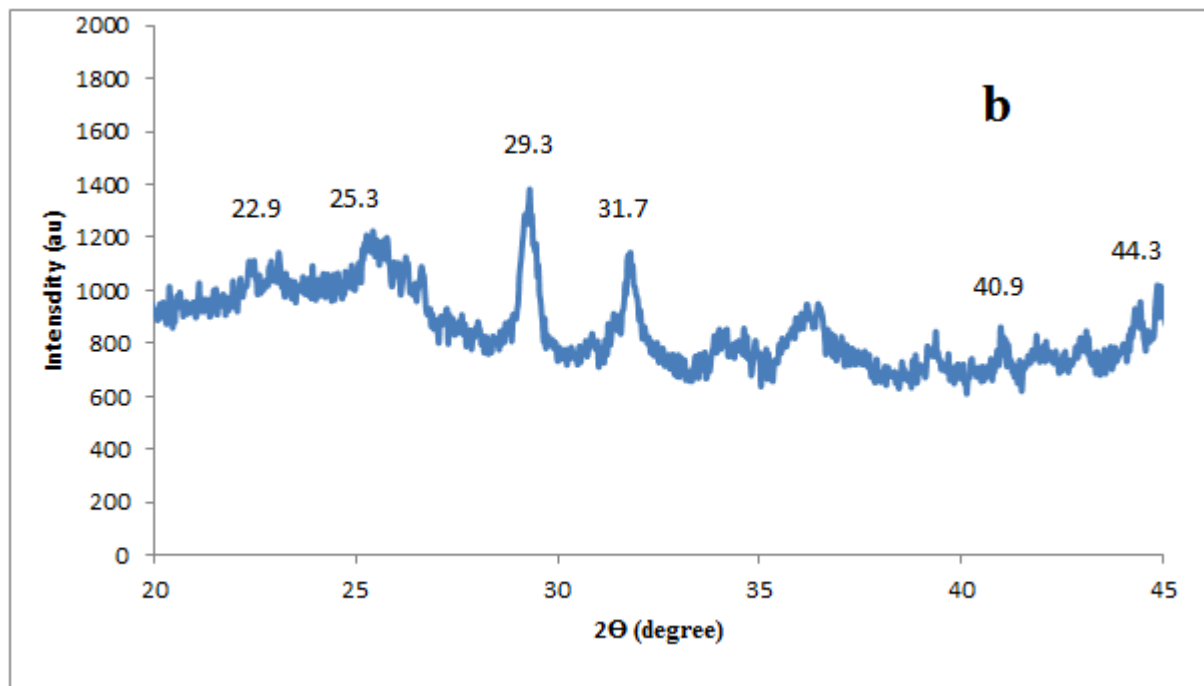
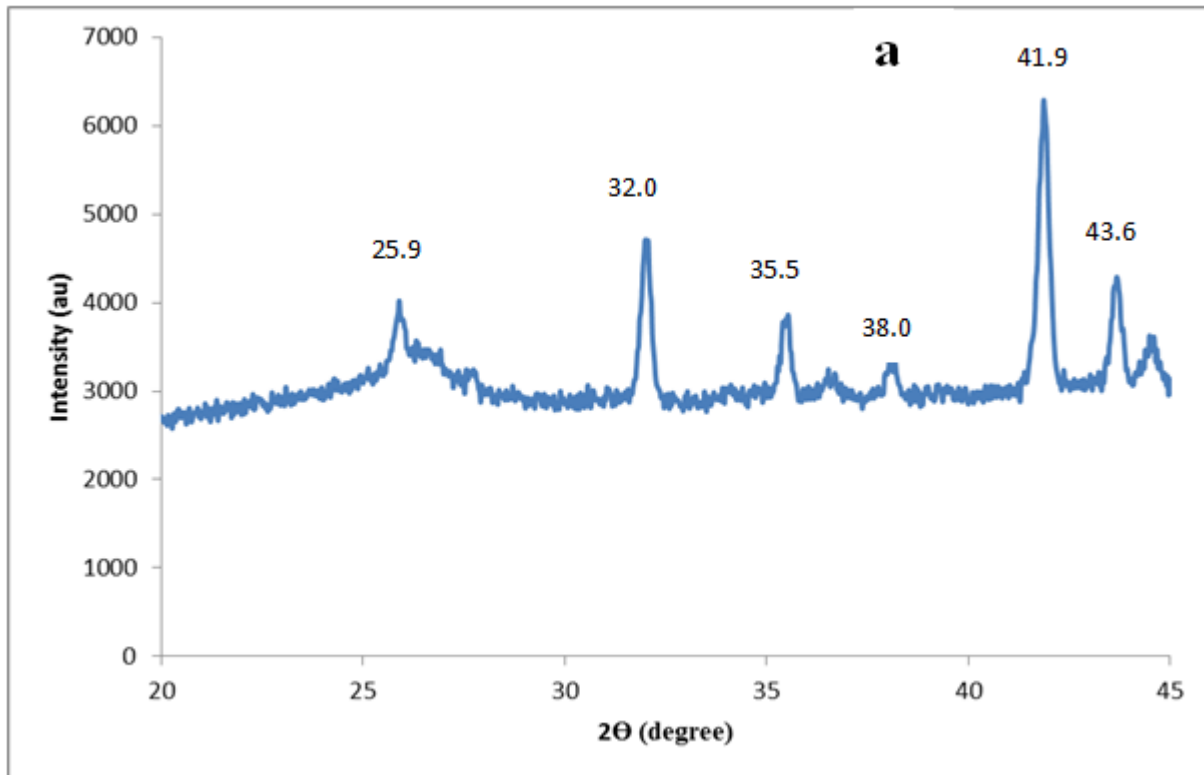


Figure 4.14 XRD patterns of carbon nanomaterial synthesized with Co-Sr catalysts supported on (a) Al_2O_3 (b) CaCO_3 (c) MgO .

Figure 4.14 (a) shows intense peak at $2\theta = 25.2^\circ$ which is just above the range of the characteristic lattice structure peak. It also shows a pronounced peak at 43.4° which is a lattice characteristic peak. (b) shows a small peaks at $\theta = 22.9^\circ$ and $2\theta = 40.9^\circ$. While (c) shows a small characteristic peak at $2\theta = 22.4^\circ$ & 25.3° and intense peaks 42.8° & 44.2° .



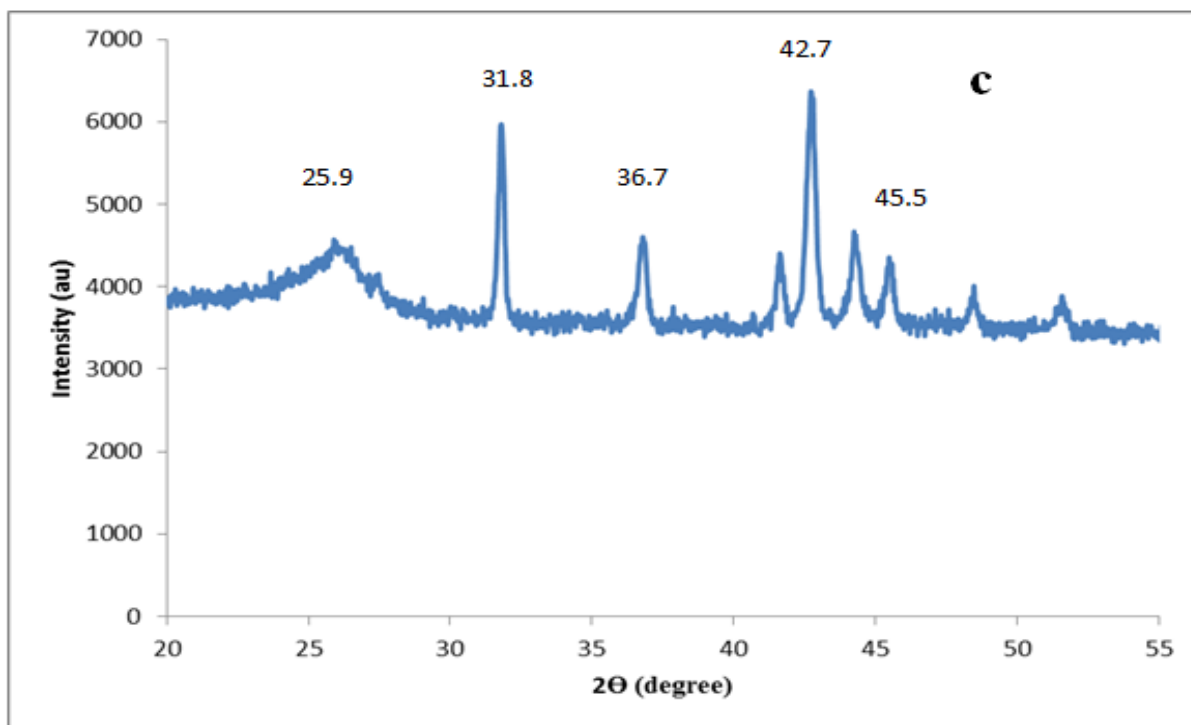
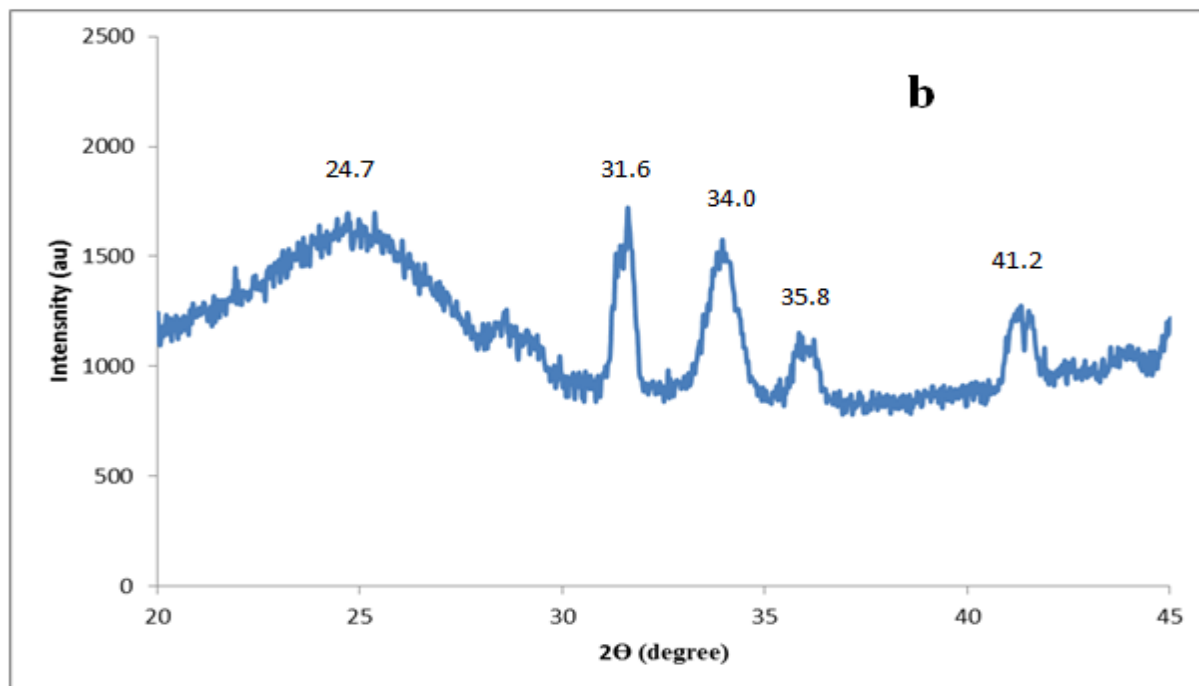


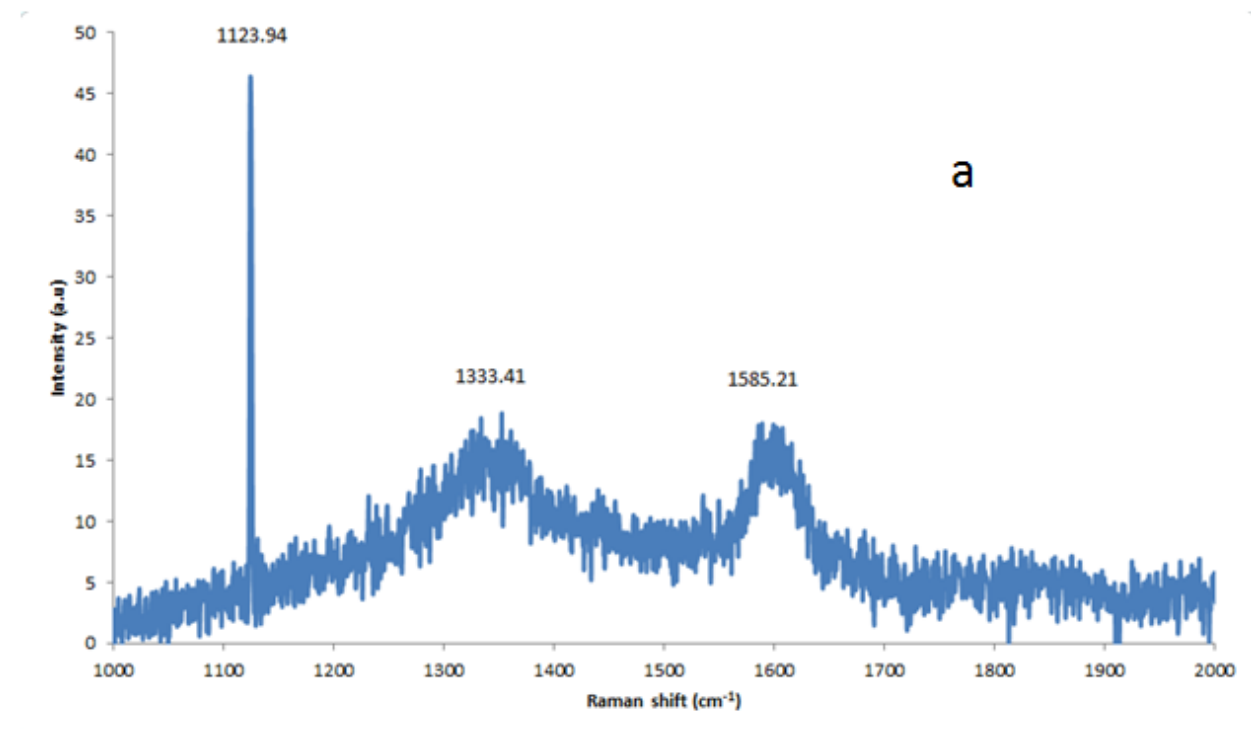
Figure 4.15 XRD patterns of carbon nanomaterial synthesized with Co-Zn catalysts supported on (a) Al_2O_3 (b) CaCO_3 (c) MgO .

Figure 4.15 (a) shows small and broad peak at $2\theta = 25.9^\circ$ which is just above the range of the characteristic lattice structure peak. It also shows a pronounced peak at $2\theta = 41.9^\circ$ & 43.6° which are lattice characteristic peak. (b) also shows a small and broad peak at $2\theta = 24.7^\circ$ and a small at $2\theta = 41.2^\circ$. While (c) shows both intense and sharp characteristic peaks at $2\theta = 25.9^\circ$ & 42.7° .

4.5.2 Raman Spectroscopy

The Raman spectra below show the vibrational density of states (VDOS) of graphite. The graphite VDOS extends beyond its T point Raman frequency up to a band limit of 1620 cm^{-1} due to the upwards phonon dispersion away from T peak [11].

Raman spectral analysis for carbon nanotubes synthesis are therefore, presented in Figure. 4.16 to 4.18. The Raman spectra are for three different catalysts employed in this research. The aim is to determine the effect of the metals Co/Sn, Co/Sr and Co/Zn supported on Al_2O_3 , CaCO_3 and MgO in the synthesis of carbon nanotubes.



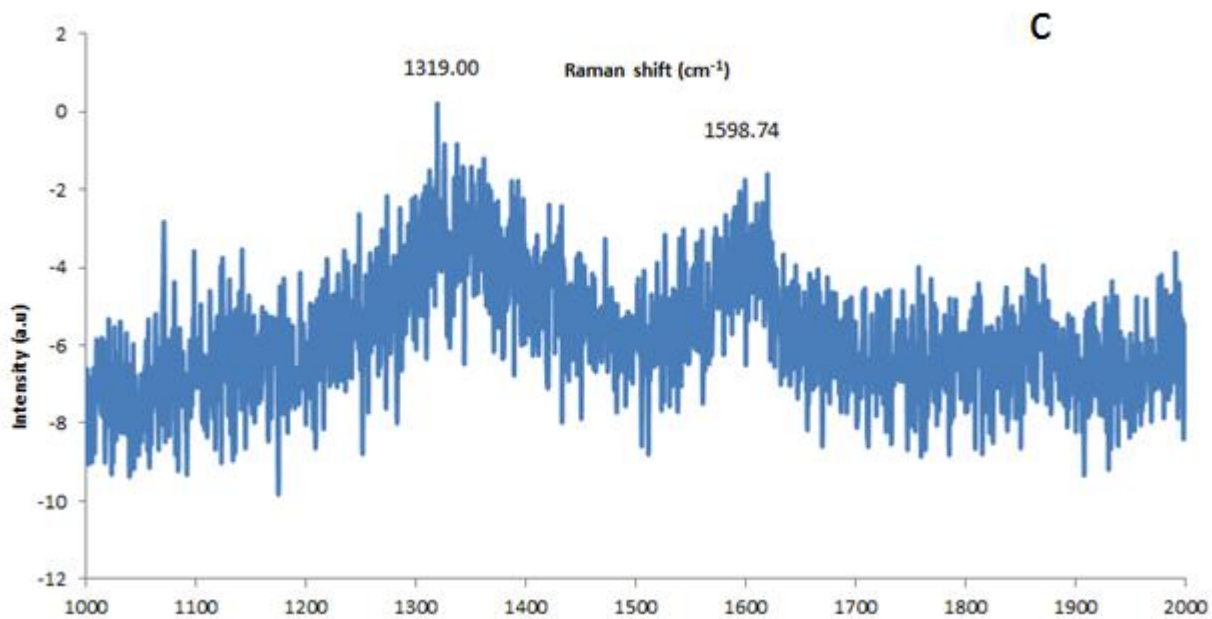
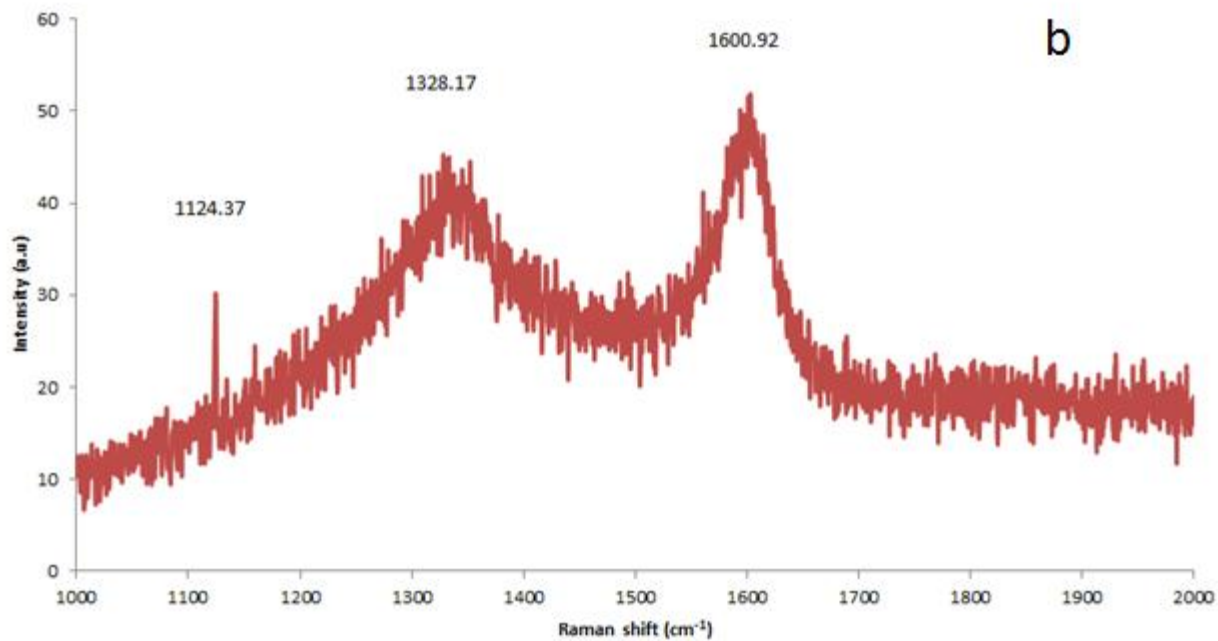
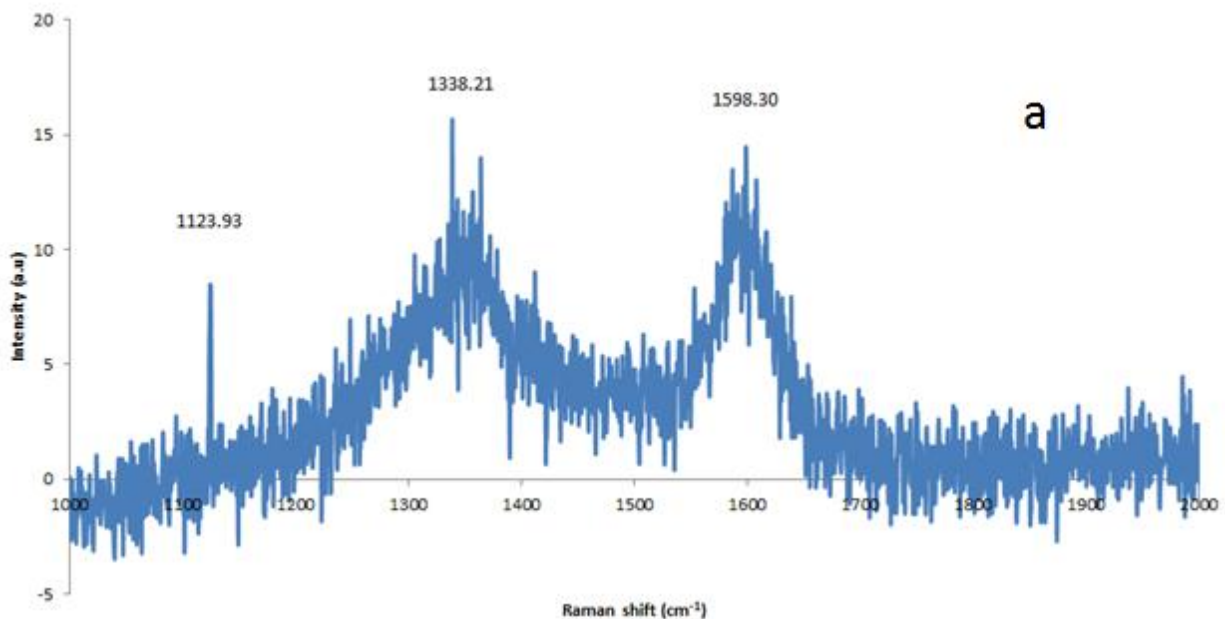


Figure 4.16 Raman spectra of carbon nanomaterial synthesized with Co-Sn catalyst supported on (a) Al₂O₃ (b) CaCO₃ and (c) MgO.

Figure 4.16 (a) shows the peak height and intensity of the T, D and G bands for the Raman spectra with the characteristic peaks at 1123.94, 1333.41 and 1585.21 respectively. The (I_D/I_G) ratio is 0.84.

Figure 4.16 (b) shows the peak height and intensity of the T, D and G bands for the Raman spectra with the characteristic peaks at 1124.37, 1328.17 and 1600.92 respectively and (I_D/I_G) ratio is 0.83. However, it must be noted that the intensity of T-peak is not as intense as in (a) and the intensity of the G-peak is more intense than the D-peak unlike in (a) where the D- and G-peaks have the same peak intensities. Figure 4.16 (c) shows the peak height and intensity of the D and G bands for the Raman spectra with the characteristic peaks at 1319.00 and 1598.74 respectively and (I_D/I_G) ratio is 0.83. This spectrum does not have a T-peak and the D-peak is more intense than the G-peak.



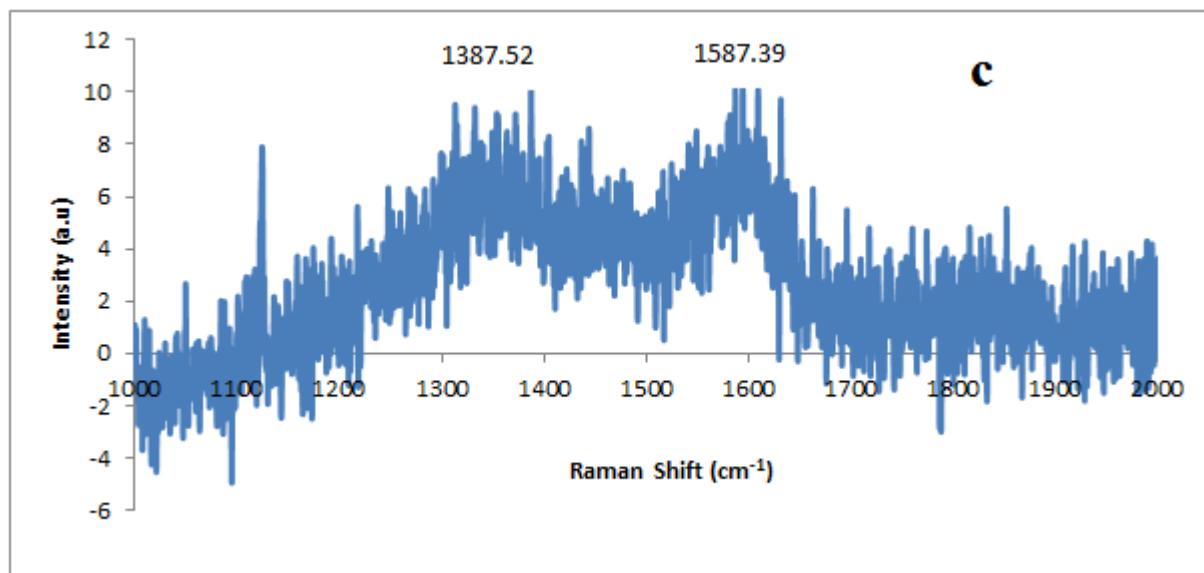
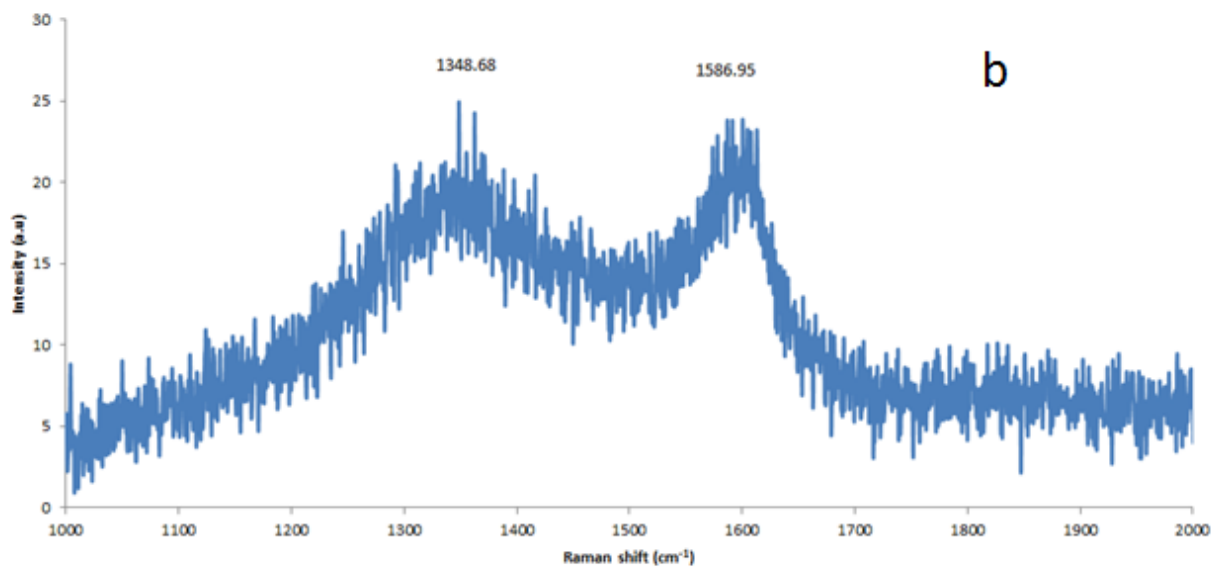
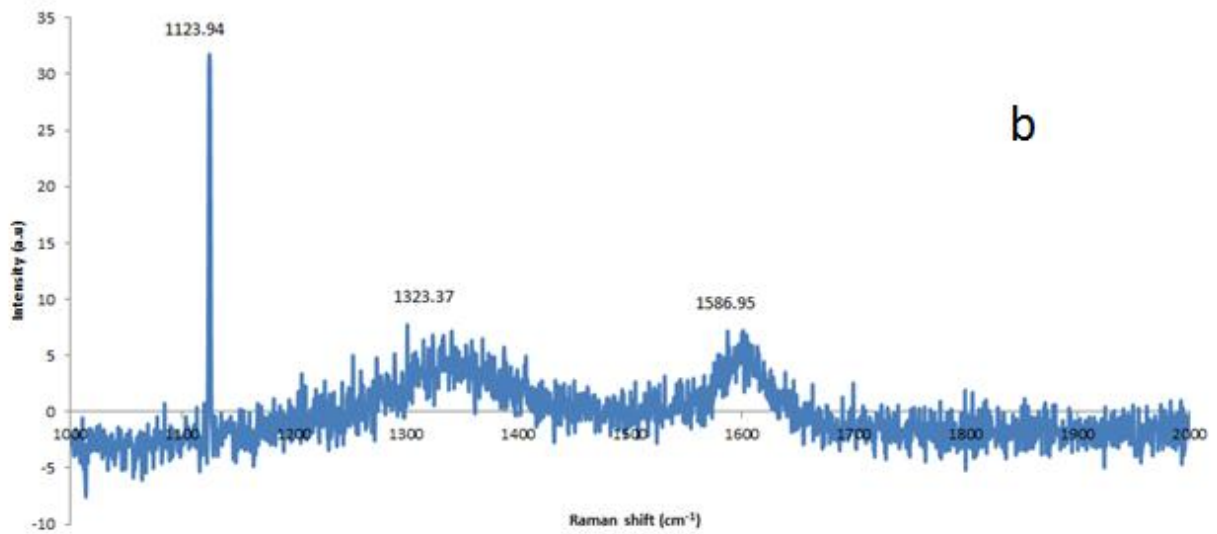
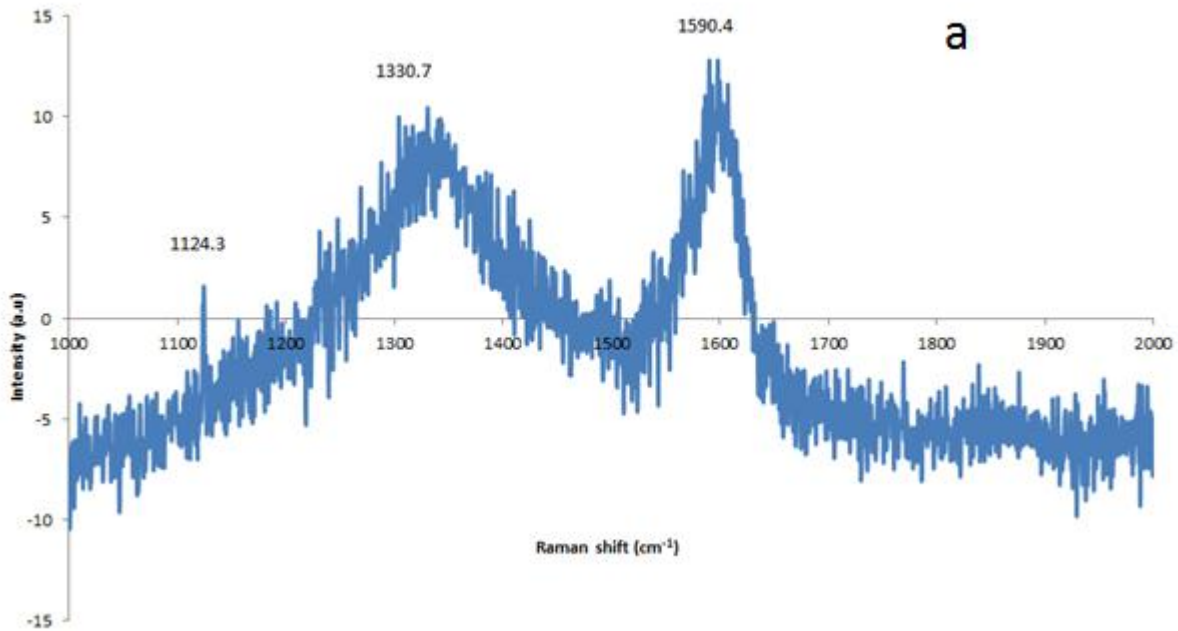


Figure 4.17 Raman spectra of carbon nanomaterial synthesized with Co-Sr catalyst supported on (a) Al₂O₃ (b) CaCO₃ and (c) MgO.

Figure 4.17 (a) shows the peak height and intensity of the T, D and G bands for the Raman spectra with the characteristics peaks at 1123.93 1333.21 and 1598.30 respectively and (I_D/I_G) ratio is 0.84. The intensity of the T-peak is very small. Figure 4.17 (b) shows the peak height and intensity of the D and G bands for the Raman spectra with the characteristics peaks at 1348.68

and 1586.95 respectively and (I_D/I_G) ratio is 0.85. There is no T-peak observed. Figure 4.17 (c) shows the peak height and intensity of the T, D and G bands for the Raman spectra with the characteristics peaks at 1124.37 1387.52 and 1587.39 respectively and (I_D/I_G) ratio is 0.87. The intensity of the T-peak is very small.



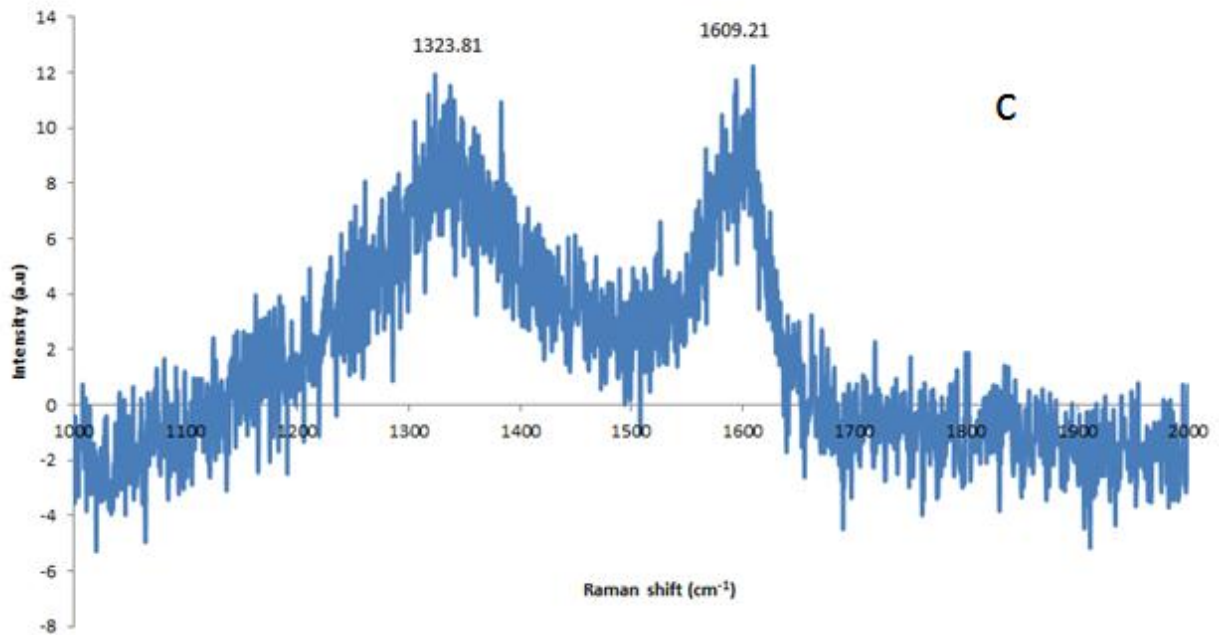


Figure 4.18 Raman spectra of carbon nanomaterial synthesized with Co-Zn catalyst supported on (a) Al_2O_3 (b) CaCO_3 and (c) MgO .

Figure 4.18 (a) shows the peak height and intensity of the T, D and G bands for the Raman spectra with the characteristic peaks at 1124.30, 1330.70 and 1590.40 respectively and (I_D/I_G) ratio is 0.84. The intensity of the T-peak is very small. Figure 4.18 (b) shows the peak height and intensity of the T, D and G bands for the Raman spectra with the characteristic peaks at 1123.94, 1323.37 and 1586.95 respectively and (I_D/I_G) ratio is 0.83 and with an intense T-peak. Figure 4.18 (c) shows the peak height and intensity of the D and G bands for the Raman spectra with the characteristic peaks at 1323.81 and 1609.21 respectively and (I_D/I_G) ratio is 0.83. There is no T peak in this spectrum.

Table 4.1: T, D and G band, their peak heights, intensities and the ratios of D and G band for carbon nanomaterials synthesized with various catalyst and support materials.

Sample	D-band (cm ⁻¹)	Intensity (a.u)	G-band (cm ⁻¹)	Intensity (a.u)	T-band (cm ⁻¹)	Intensity (a.u)	Ratio (I _D /I _G)
Co-Sn/Al	1333.41	18.00	1585.21	17.8	1123.94	46.35	0.84
Co-Sn/Ca	1328.17	45.20	1600.92	51.38	1124.37	30.17	0.83
Co-Sn/Mg	1319.00	0.20	1598.74	-1.77	-	-	0.83
Co-Sr/Al	1338.21	15.60	1598.30	14.43	1123.93	8.48	0.84
Co-Sr/Ca	1348.68	24.94	1586.95	23.83	1124.37	7.51	0.85
Co-Sr/Mg	1387.52	10.16	1587.39	10.21	-	-	0.87
Co-Zn/Al	1330.79	8.67	1590.44	12.73	1124.37	1.59	0.84
Co-Zn/Ca	1323.37	6.01	1586.95	7.13	1123.94	31.77	0.83
Co-Zn/Mg	1323.81	11.93	1609.21	12.22	-	-	0.82

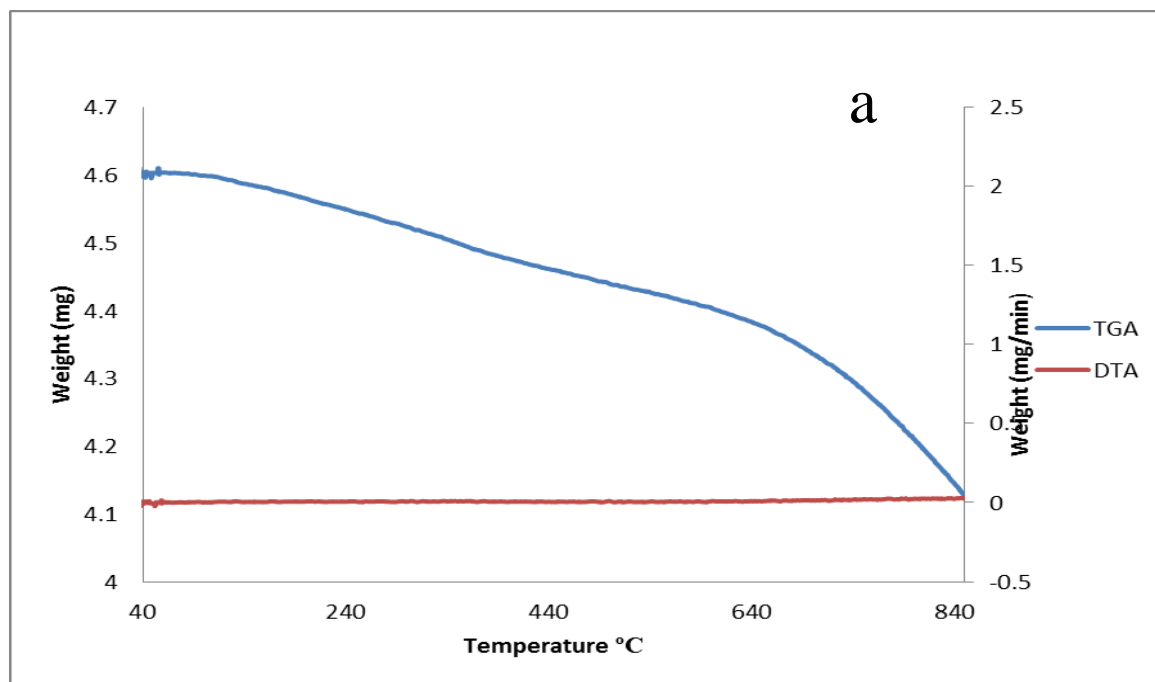
Table 4.1 summarises the Raman spectra of the carbon nanomaterial synthesized using different catalyst. From this table it is shown that the D- band of disordered graphitic carbon in carbon nanomaterial and G- band which indicates the presence of crystalline graphitic carbon in carbon nanomaterial have same peaks hence they have the same ratios. However, the intensities of the D and G bands are different for different catalysts. The vibrational density of states (VDOS) of D- and G- bands extends within their Raman frequency of 1332 – 1360 cm⁻¹ respectively. The T- band that originates from sp³ bonded carbon and sensitive to small changes in sp³ content [12] resonates significantly in the Co-Sn/Al, Co-Sn/Ca Co-Zn/Ca and minutely in the Co-Sr/Al, Co-Sr/Ca and Co-Zn/Al. It is noted that there is no any T peak which resonates where MgO is used as support material.

It is also indicated that the intensity of both the D- and G- peaks where MgO was used as support are averagely quite minimum followed by Al₂O₃ and the biggest being CaCO₃. The D- and G- bands in this spectra have not produced any overtone that resonates at 2600 cm⁻¹ which is an indication of low quality of carbon nanomaterial produced.

4.5.3 Thermogravimetric analysis

The thermogravimetric analysis provides a measure of the reaction kinetics associated with structural decomposition, oxidation, corrosion and moisture adsorption/desorption and gas evolution. There are three weight loss regions. 1st region ranges from 65 °C to 160 °C which is a characteristic for the loss of water, 2nd region ranges from 480 °C to 530 °C which is for cyanide decomposition and the last 3rd region which ranges from 624 °C is decomposition of sample impurities. And the TGA and DTA curves of the weight loss are in most instances used to investigate the presence of carbon nanotubes.

The aim of this synthesis is therefore, to determine the thermal stability of the metals Co/Sn, Co/Sr and Co/Zn supported on Al₂O₃, CaCO₃ and MgO in the synthesis of carbon nanotubes. The TGA and DTA analysis are therefore, presented in Figures 4.19 to 4.21.



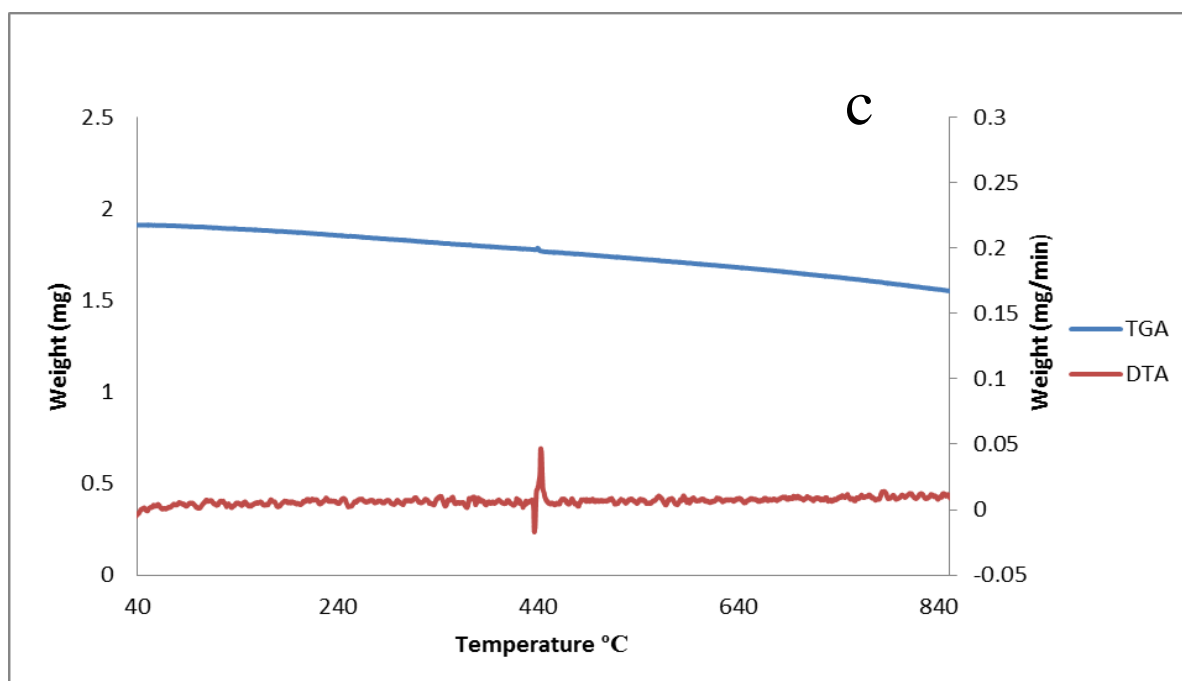
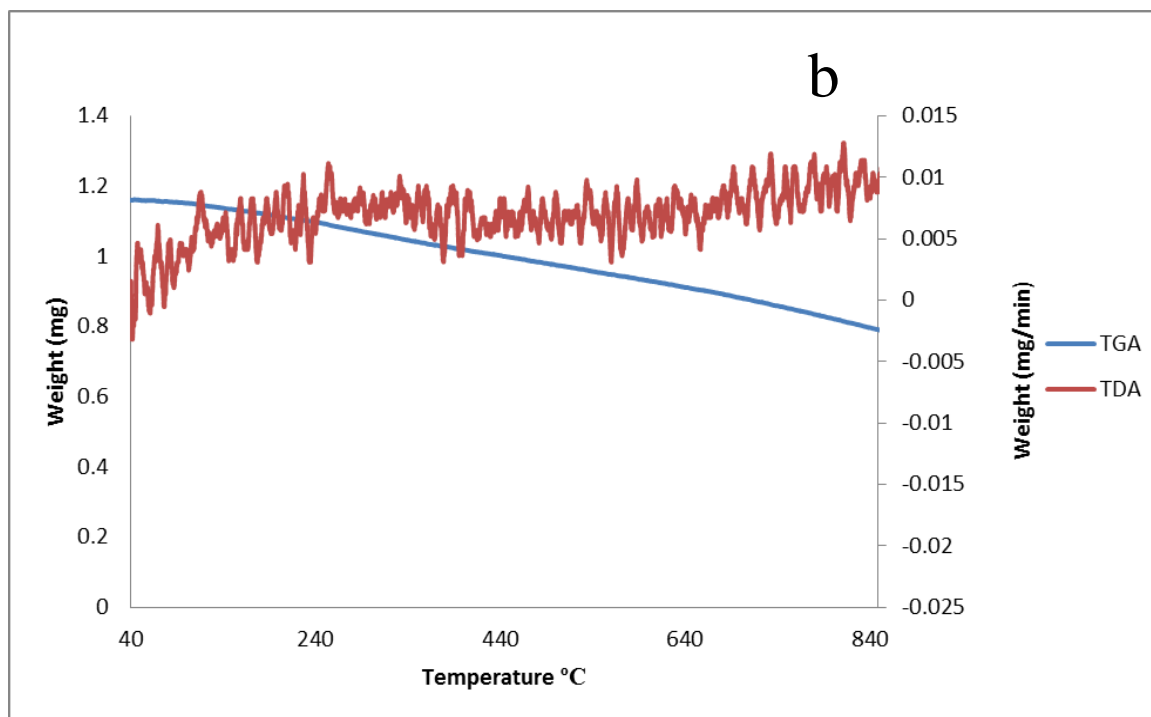
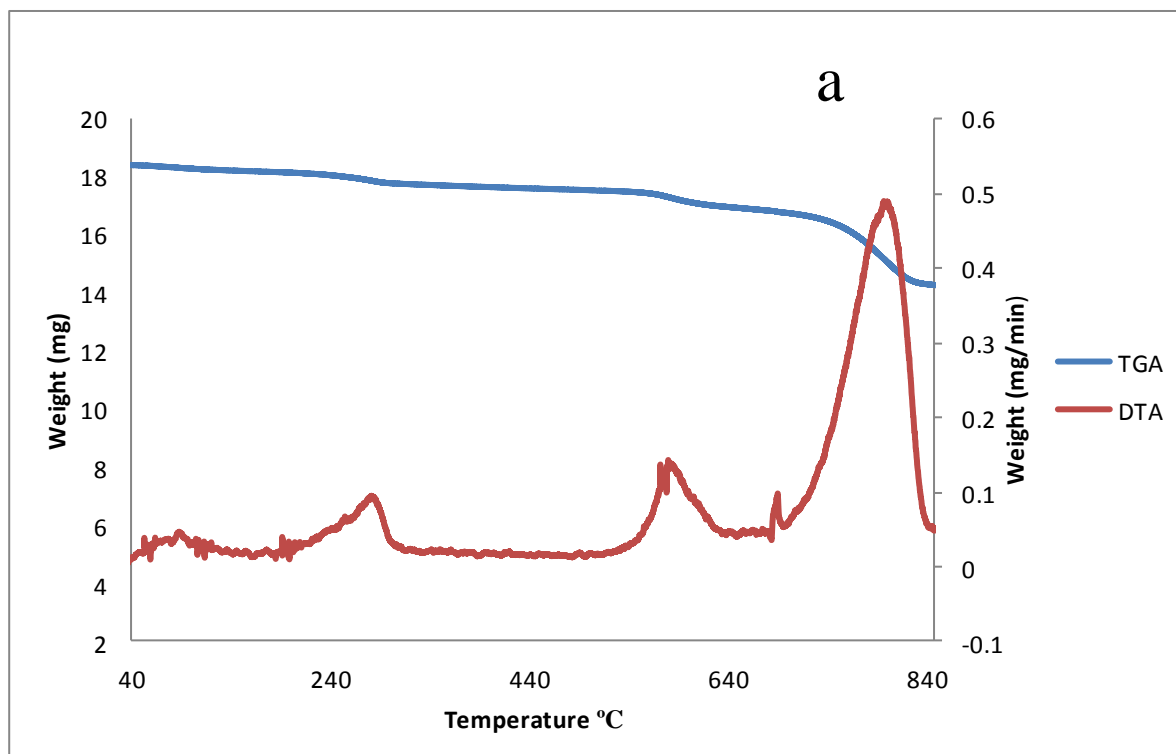


Figure 4.19 Thermogravimetric and derivative thermogravimetric analysis of carbon nanomaterial obtained from Co-Sn catalyst supported on (a) Al₂O₃ (b) CaCO₃ and (c) MgO.

Figure 4.19 (a) & (b) show no sign of decomposition while (c) shows decomposition at 440 °C just 20 °C below the second region of cyanide decomposition which starts at 480 °C. However, (a) has significant weight loss from 4.6 mg to 4.1 mg as compared to (b) & (c) which have quite minimal weight losses.



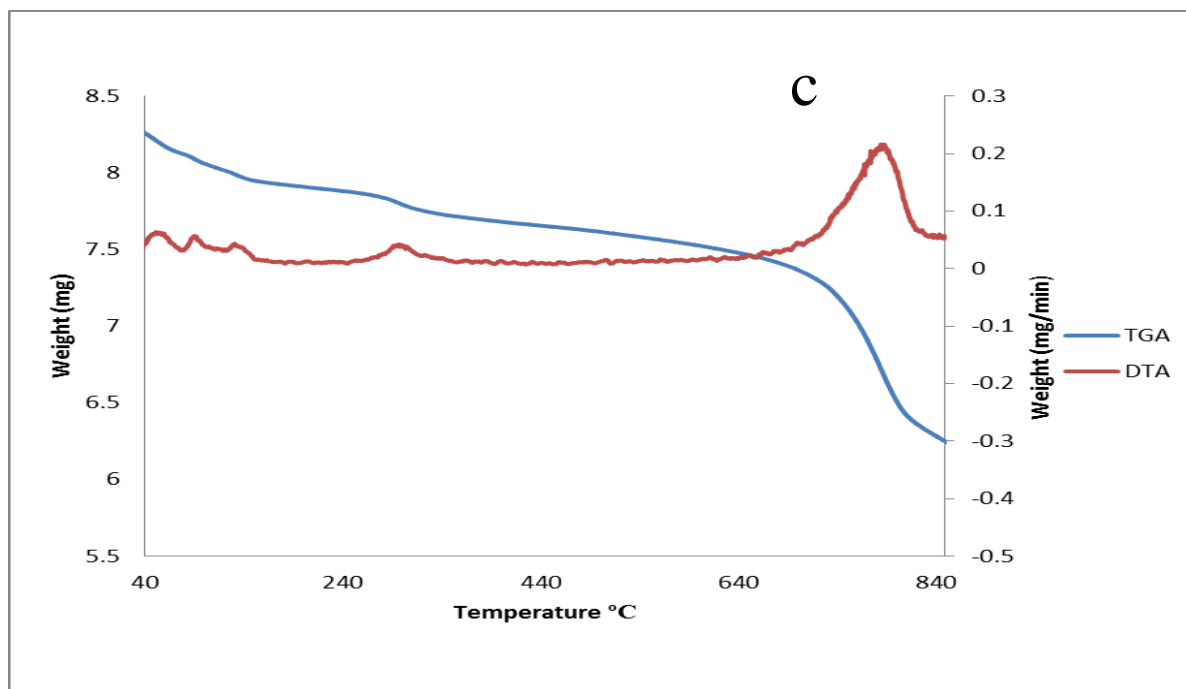
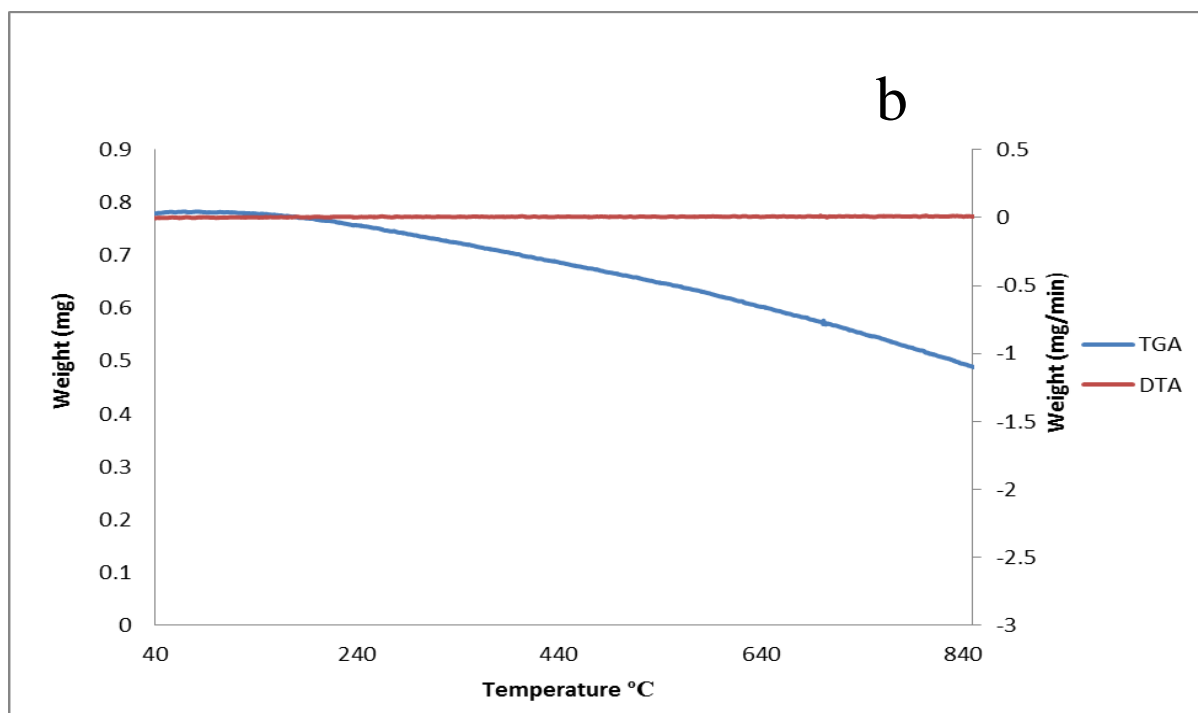
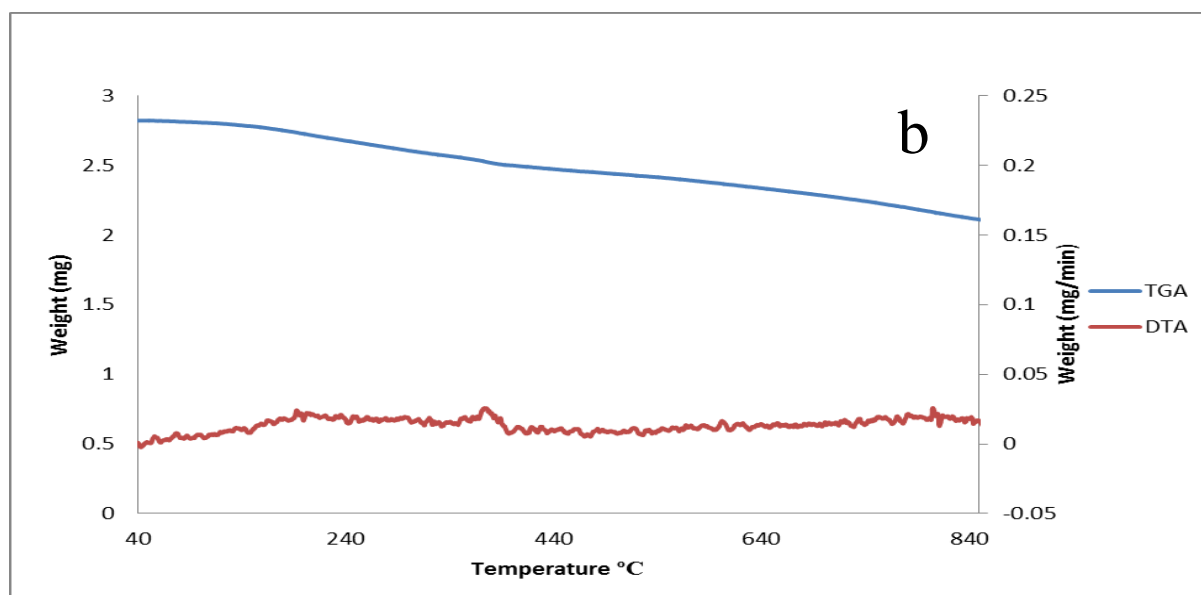
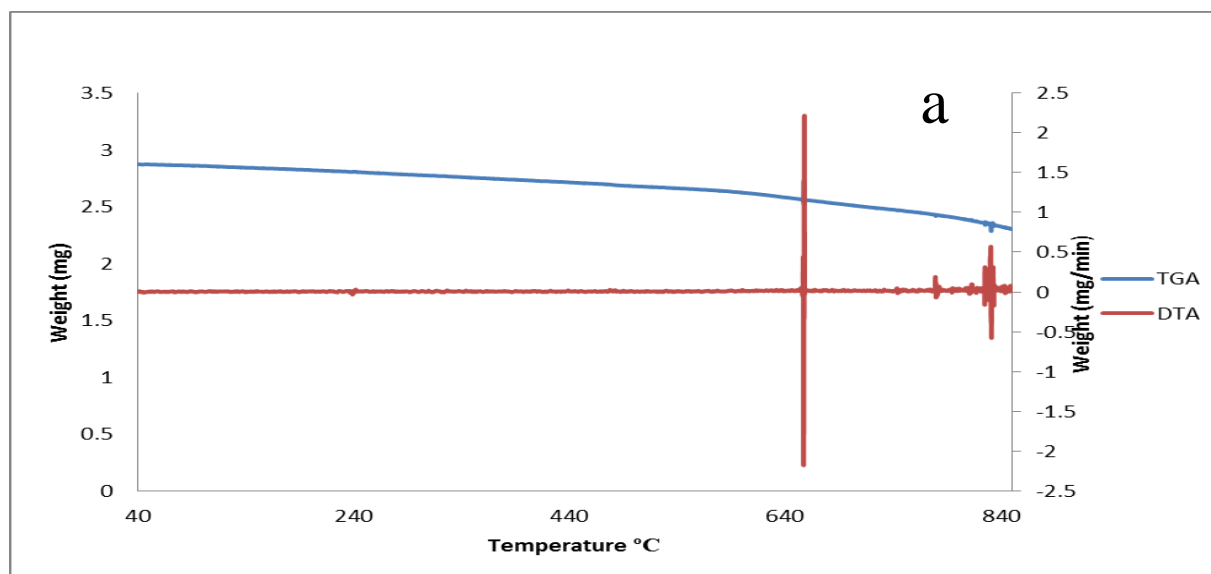


Figure 4.20 Thermogravimetric and derivative thermogravimetric analysis of carbon nanomaterial obtained from Co-Sr catalyst supported on (a) Al_2O_3 (b) CaCO_3 and (c) MgO .

Figure 4.20 (a) shows decomposition at 240 °C and 520 °C which is attributed to water loss and cyanide decomposition respectively. It further shows decomposition at 680 °C and 700 °C attributed to sample impurities in the third region. (b) does not show any decomposition at all while (c) shows decomposition at 250 °C and 800 °C attributed to water loss and sample impurities. Figure 4.20 (c) though does not have that significant weight loss, it is evident when compared with (a) & (b) which had very small weight losses.



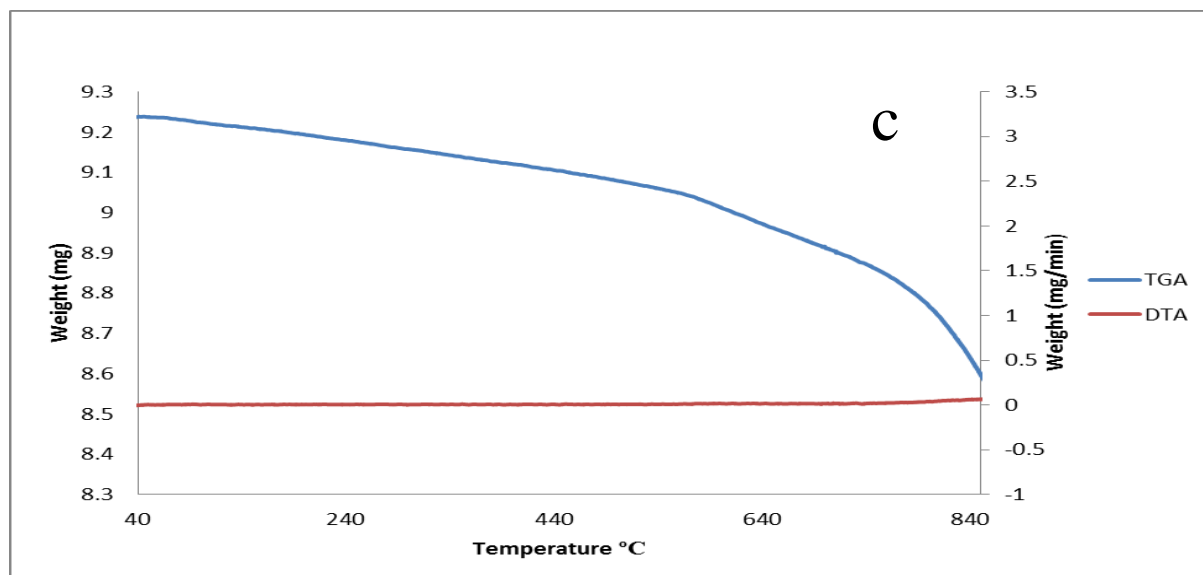


Figure 4.21 Thermogravimetric and derivative thermogravimetric analysis of carbon nanomaterial obtained from Co-Zn catalyst supported on (a) Al_2O_3 (b) CaCO_3 and (c) MgO .

Figure 4.21 (a) & (c) do not show any decomposition but (b) has slight decomposition at 380 °C. The Co-Zn/Mg which is (c) has significant weight loss while (a) & (b) don't have weight loss.

4.5.4 Scanning Electron Microscopy

The quality of carbon nano material and growth is determined by many parameters such as the flow rate gas used, supporting material, catalyst temperature at each particular time and the position of the quartz boat in a reactor. The SEM images for carbon nanomaterial synthesized with Co-Sn, Co-Sr and Co-Zn catalysts supported on Al_2O_3 , CaCO_3 & MgO are presented in Figures 4.22 to 4.24.

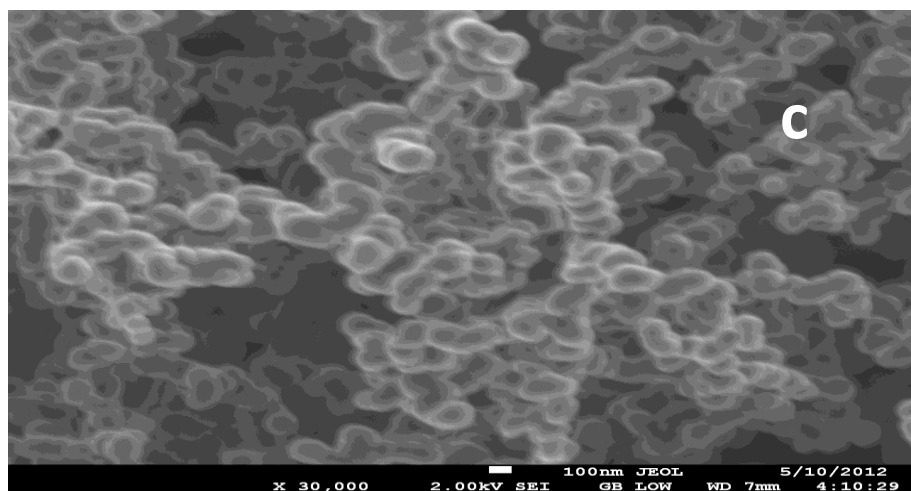
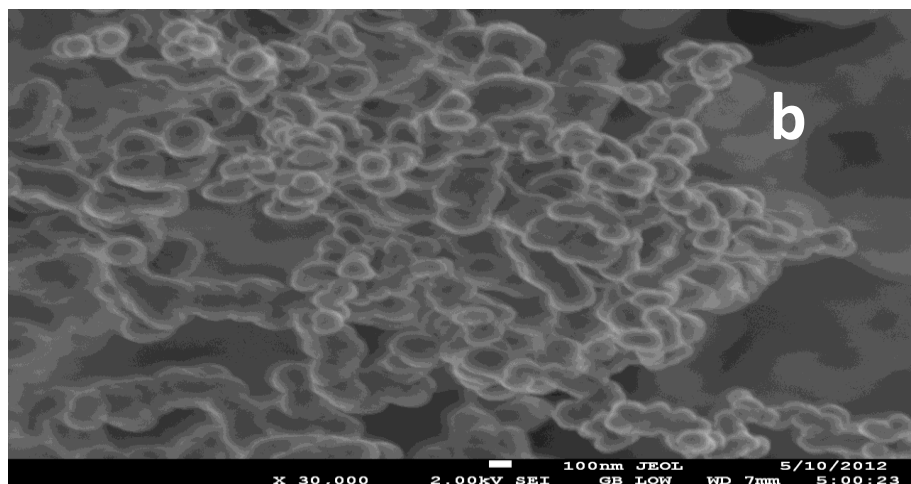
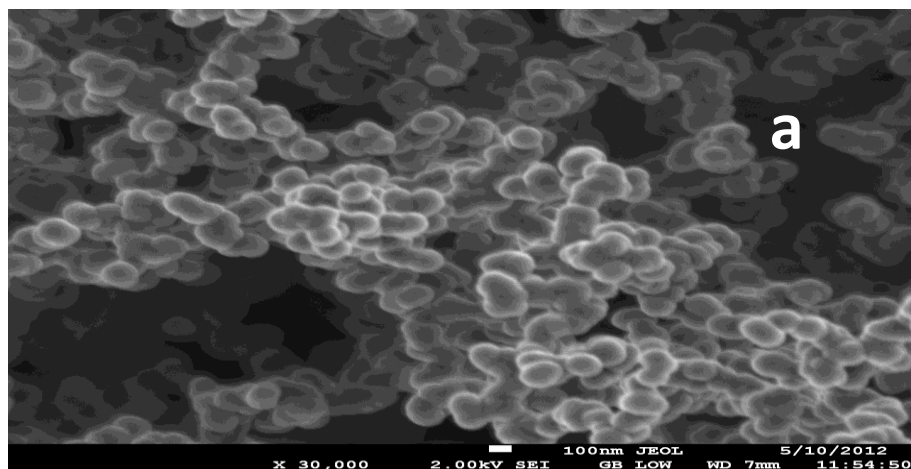
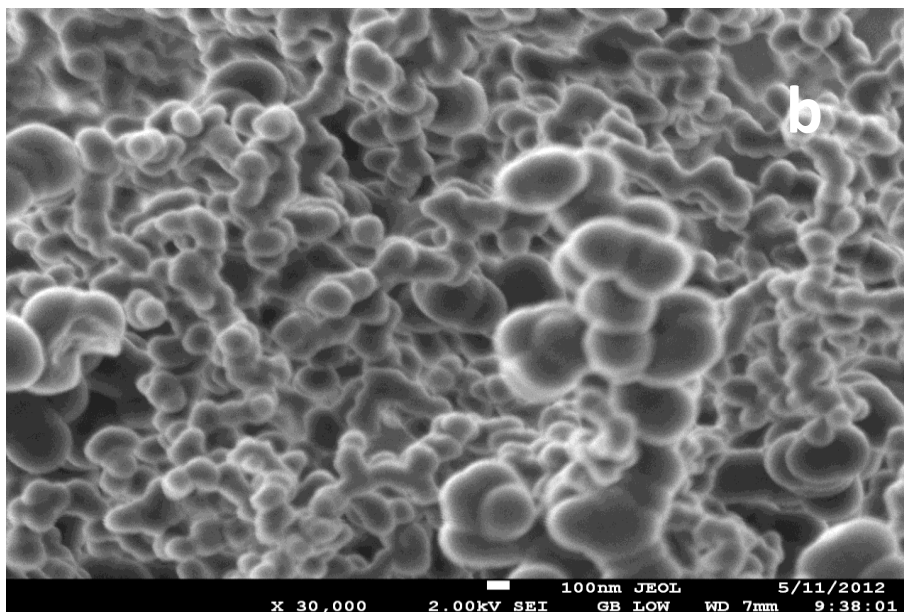
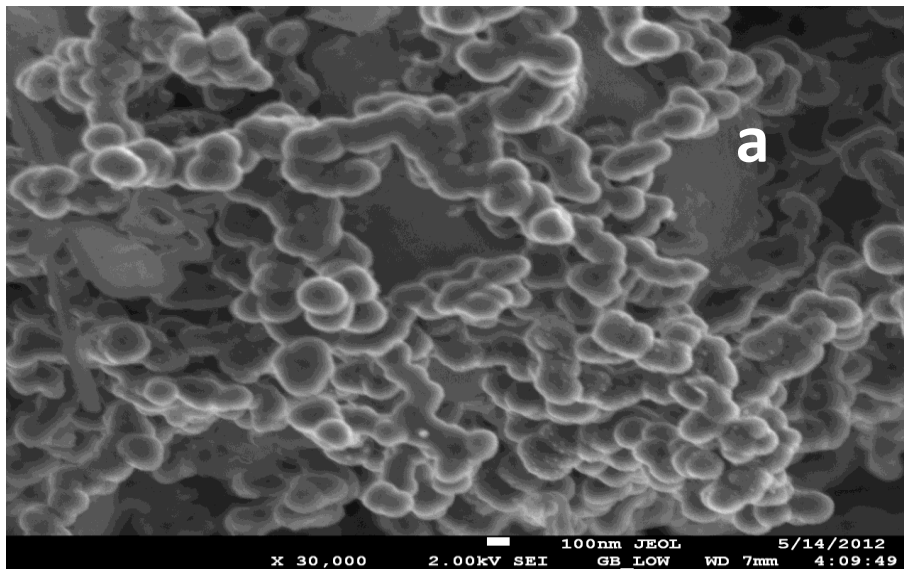


Figure 4.22 SEM images for carbon nanomaterial synthesized with Co-Sn catalysts supported on (a) Al_2O_3 (b) CaCO_3 (c) MgO .

Figure 4.22 presents the scanning electron microscopy images for carbon nanomaterial synthesized with Co-Sn catalyst supported on (a) Al_2O_3 , (b) CaCO_3 and (c) MgO respectively. Images show that CNTs were not formed as expected instead only nanospheres are evidenced. This could be attributed to many factors. Some being that there was no constant flow of gases or the catalyst was not a good one on these supporting materials synthesis. It could also be that there was no constant flow of acetylene.



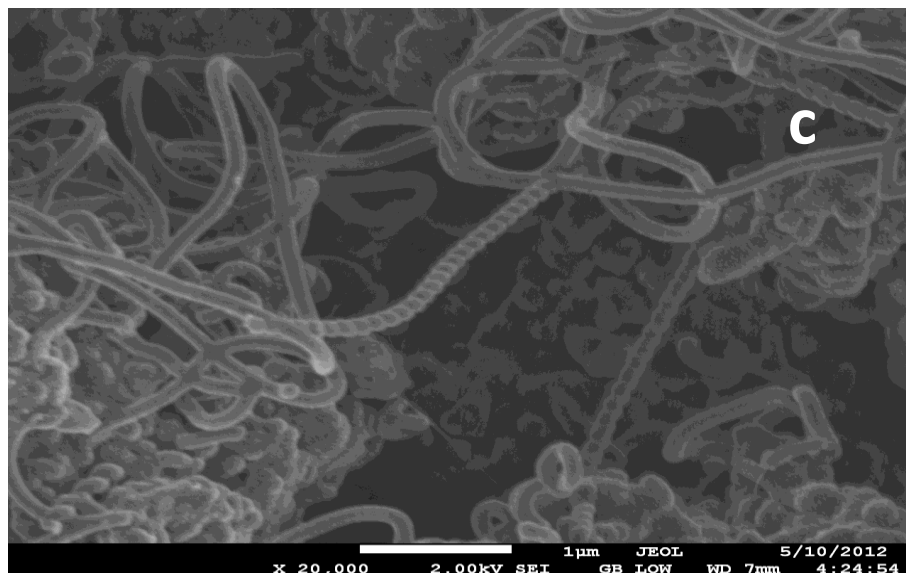
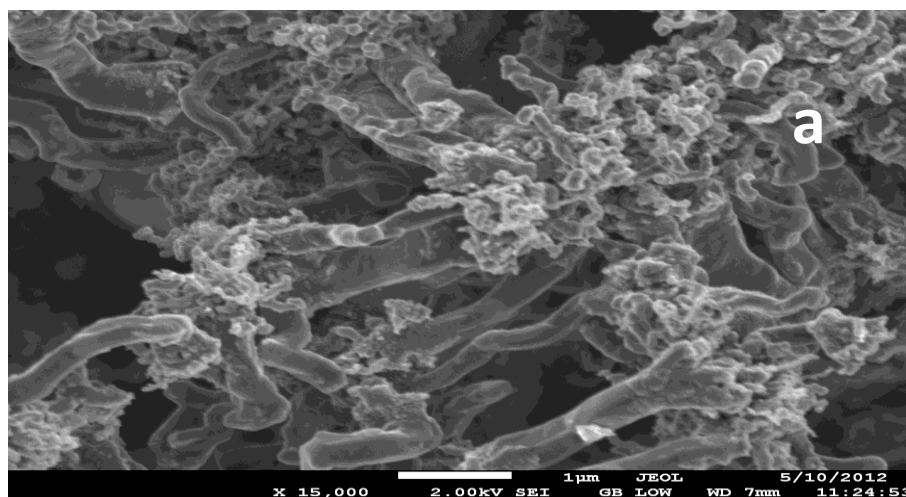


Figure 4.23 SEM images for carbon nanomaterial synthesized with Co-Sr catalysts supported on (a) Al_2O_3 (b) CaCO_3 (c) MgO .

Figure 4.23 presents the scanning electron microscopy images for carbon nanomaterial synthesized with Co-Sr catalyst supported on (a) Al_2O_3 , (b) CaCO_3 and (c) MgO respectively. Images show that where (a) Al_2O_3 and (b) CaCO_3 were used as supporting material CNTs were not formed but only nanospheres were produced. However, as the catalyst was kept constant, MgO proved to be a very good supporting material for this synthesis as evidenced by these distinguishable CNTs as shown in Figure 4.2.3 (c). It is observed that one of the nanotubes is segmented.



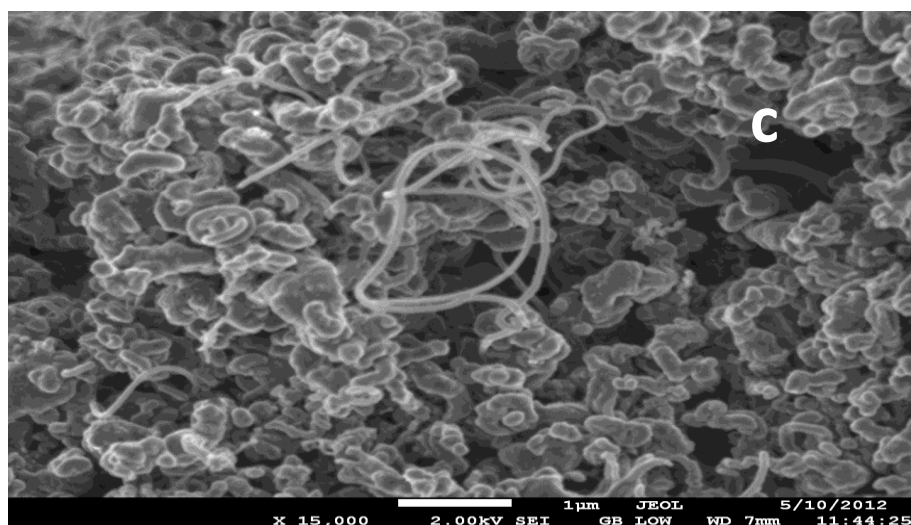
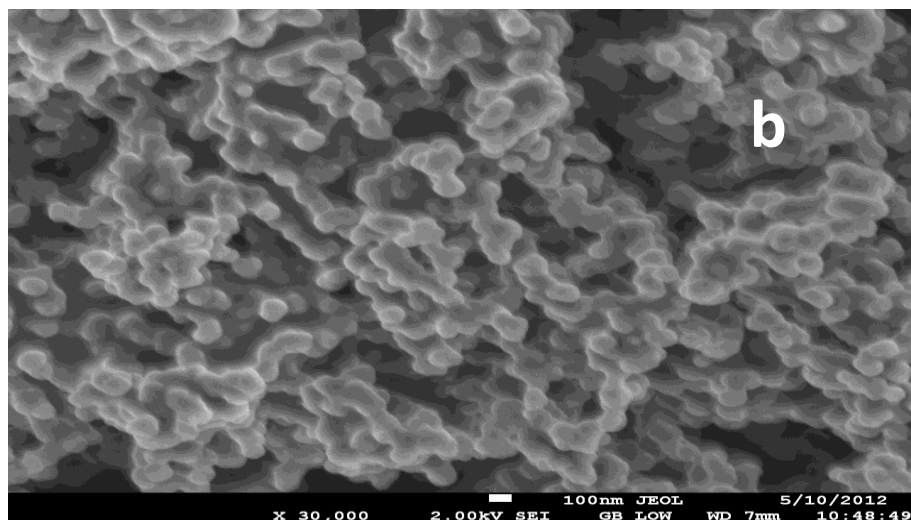
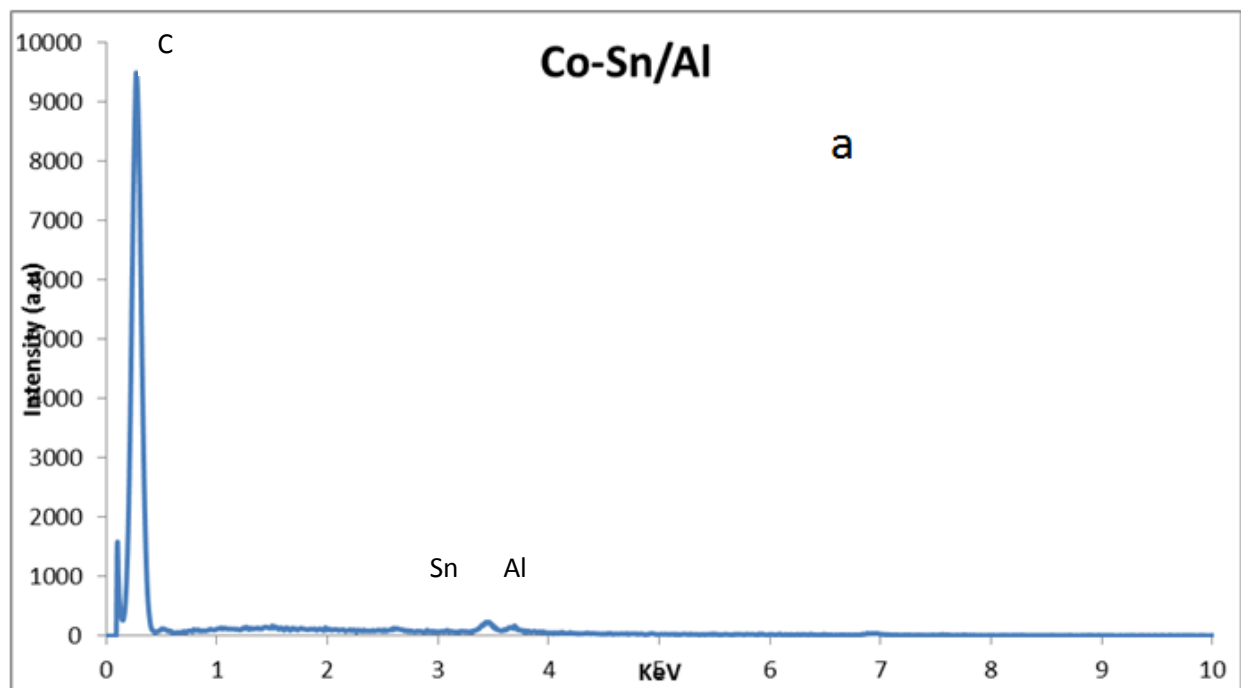


Figure 4.24 SEM images for carbon nanomaterial synthesized with Co-Zn catalysts supported on (a) Al_2O_3 (b) CaCO_3 (c) MgO .

Figure 4.24 presents the scanning electron microscopy images for carbon nanomaterial synthesized with Co-Zn catalyst supported on (a) Al_2O_3 , (b) CaCO_3 and (c) MgO respectively. Image (a) shows that where (a) Al_2O_3 was used as supporting material CNTs were produced though with a lot of amorphous carbon that resulted in very thick and short CNTs and image (b) for CaCO_3 only shows that spheres were produced. However, MgO still persists be a very good support material for this synthesis with Co-Zn as catalyst as shown in Figure 4.24 (c).

4.5.5 Energy Dispersive Spectroscopy

EDS is an analytical technique used for elemental analysis or chemical characterization of a sample. It indicates the presence of elements or atoms in a reaction confirming the success of that particular synthesis. The EDS analysis for CNTs synthesized with Co-Sn, Co-Sr and Co-Zn catalysts supported on Al_2O_3 , CaCO_3 & MgO are presented in figures 4.25 to 4.27.



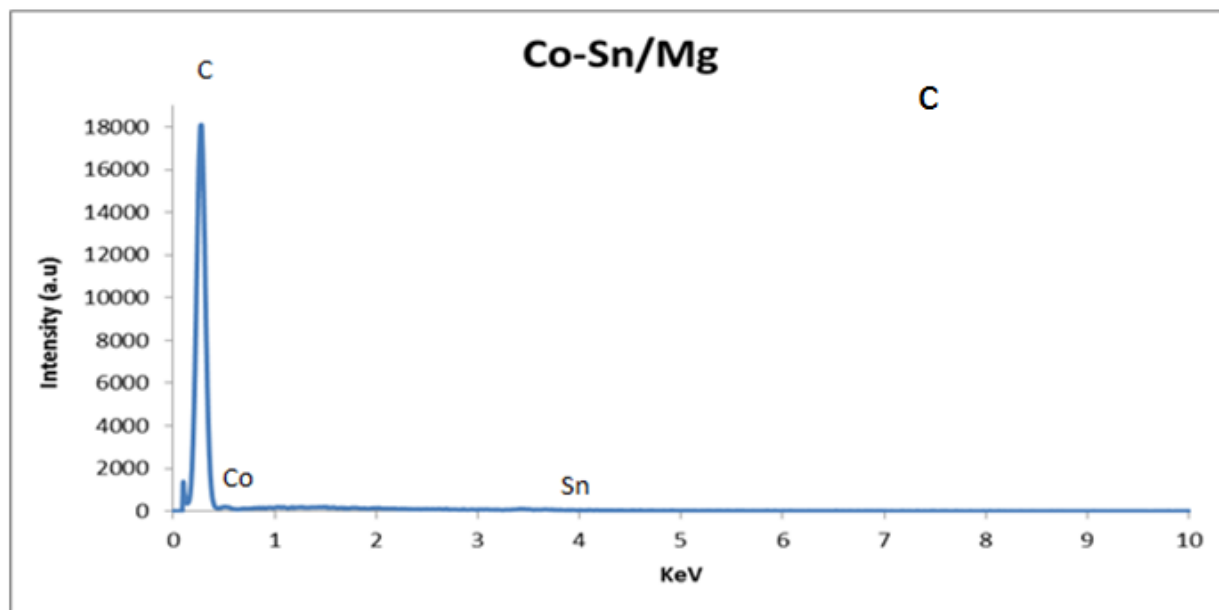
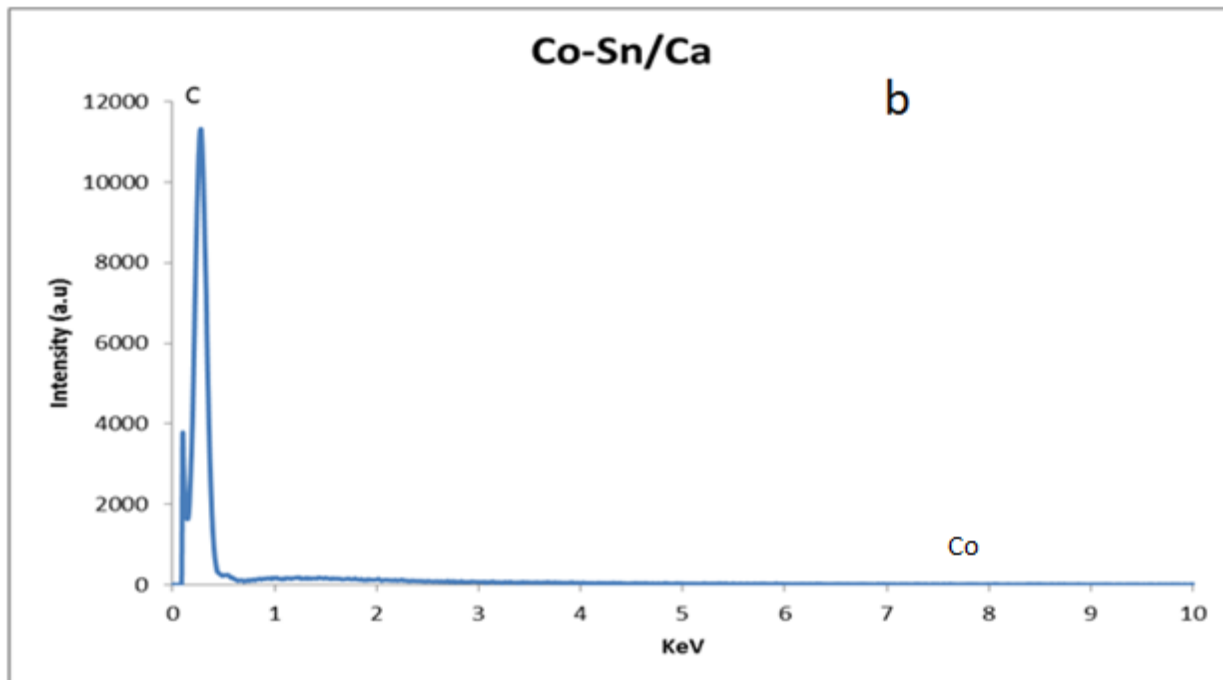
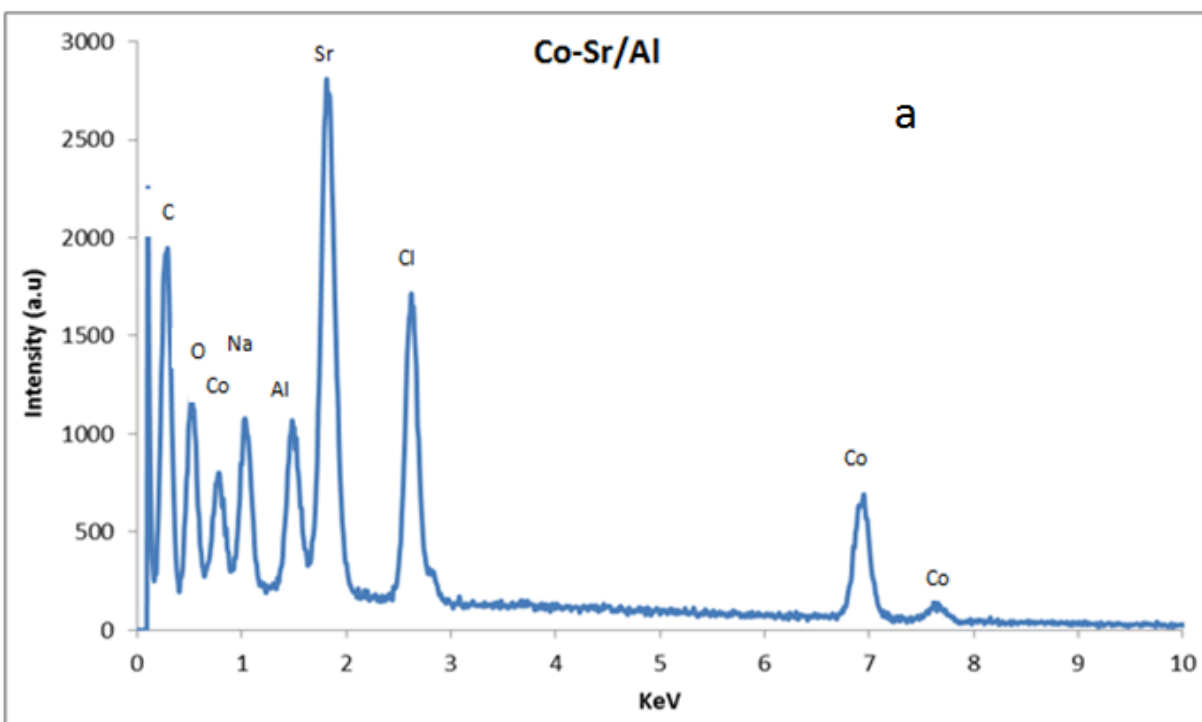


Figure 4.25 Energy dispersive spectroscopy analysis of carbon nanomaterial obtained from Co-Sn catalyst supported on (a) Al₂O₃ (b) CaCO₃ and (c) MgO.

Figure 4.25 (a) above shows the EDS analysis of CNTs obtained from Co-Sn catalyst and Al_2O_3 as support material. (a) Indicates C atom intensity as carbon source was acetylene. (a) Co and Sn peaks are insignificant indicating that they have been consumed in the reaction.

Figure 4.25 (b) does not show the catalytic activity on CaCO_3 support material at all. And figure (c) where MgO was used as supporting material shows minute presence of elements involved. It can then be concluded that Co-Sn is proving to be not an ideal catalyst especially for these respective supporting materials.



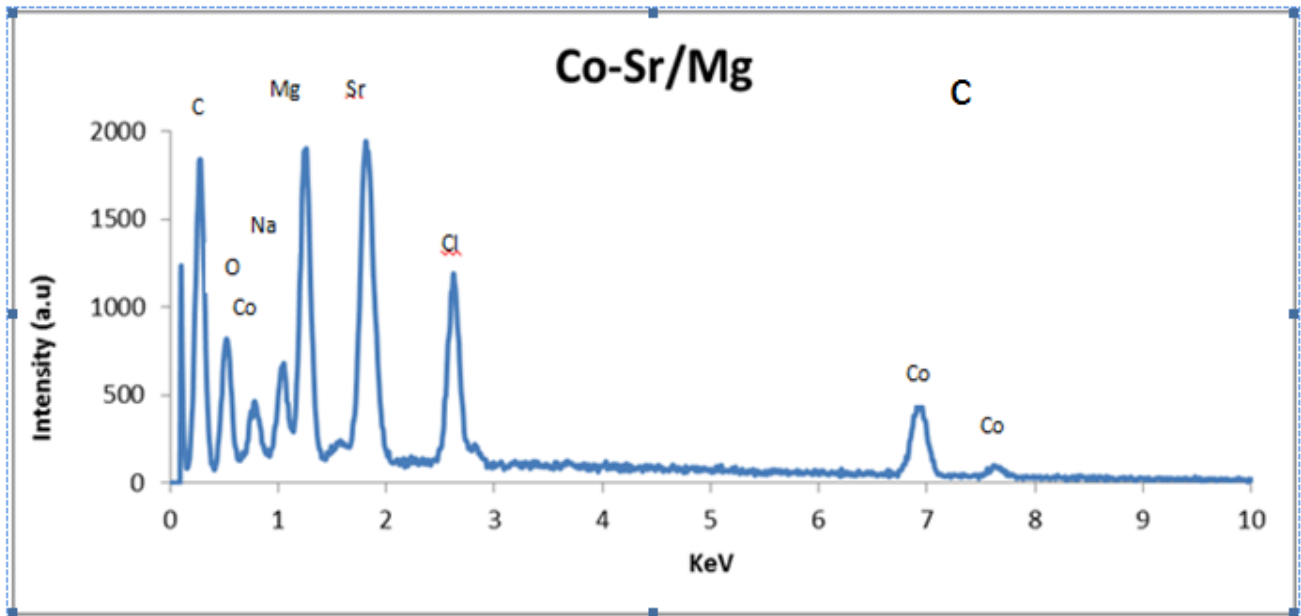
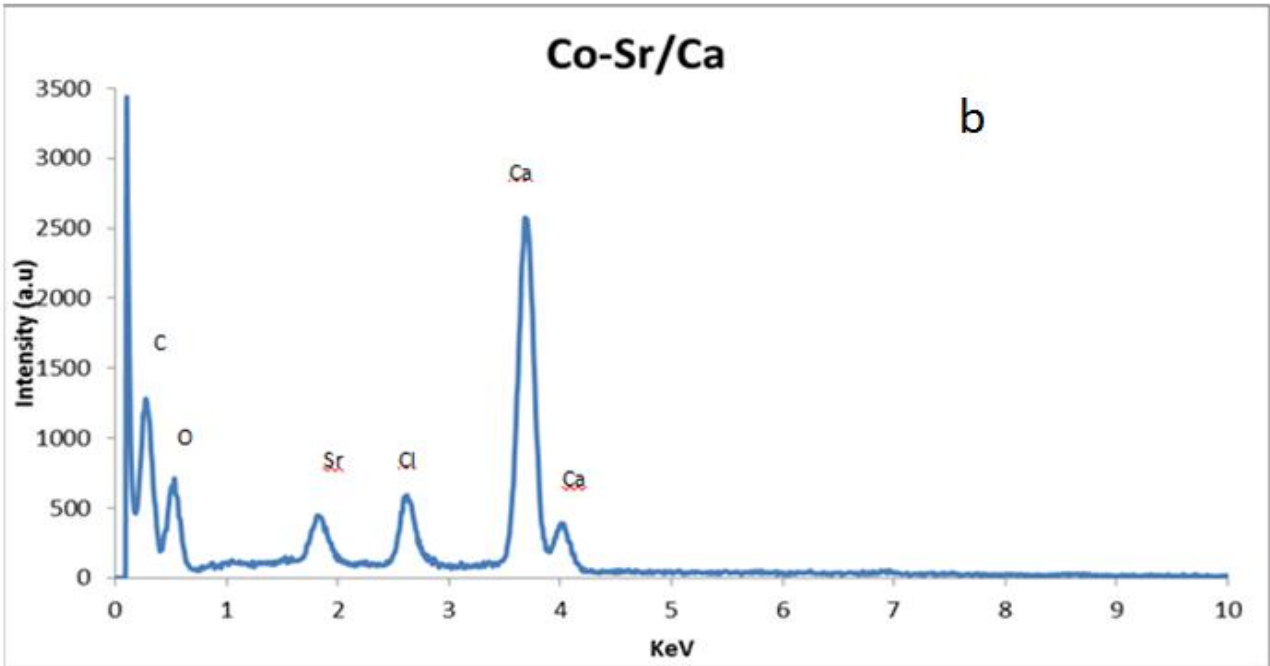
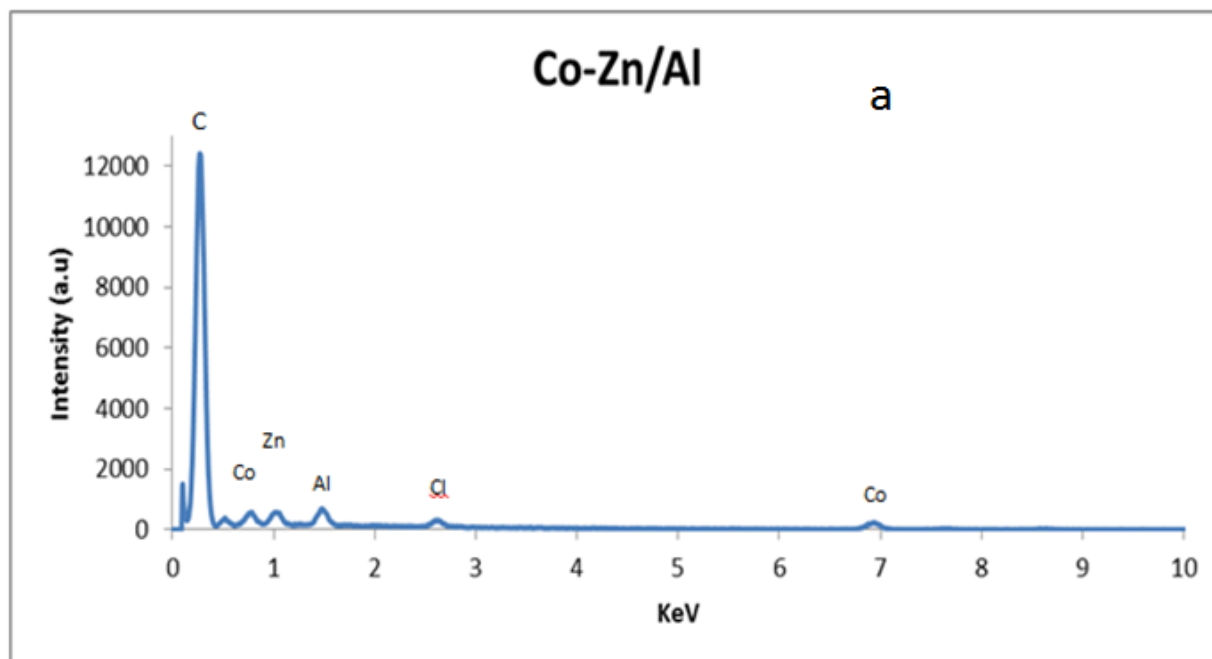


Figure 4.26 Energy dispersive spectroscopy analysis of carbon nanomaterial obtained from Co-Sr catalyst supported on (a) Al₂O₃ (b) CaCO₃ and (c) MgO.

Figure 4.26 (a) above shows the EDS analysis of CNTs obtained from Co-Sr catalyst on Al_2O_3 as support material. (a) Indicates C atom intensity as carbon source was acetylene. The C, O, Na, Al, Sr, and Cl peaks are significant and Sr being the most pronounced. Sr seems to be a good catalyst as compared with Co in relation to their peak intensities. Na is evident and could be from some external impurities while Cl is a result of chlorides from CoCl_2 which were not completely reacted during the catalyst synthesis. Al has a significant peak that to some extent is big enough to recognize it as a good support material in this synthesis.

Figure 4.26 (b) where CaCO_3 was used as support material shows consumption of Co and Sr as compared with (a) but pronounced Ca peak. And figure (c) where MgO was used as supporting material shows intense peaks of Sr and Mg but quite small Co peak

Here Co-Sr is proving to be ideal catalysts expect that Co seems to limit Sr catalytic performance. Figure 4.26 (c) where MgO is a support material seems to be the best as compared with (a) & (b). This is evidenced by Sr & Mg peaks however, Co has small peak intensity.



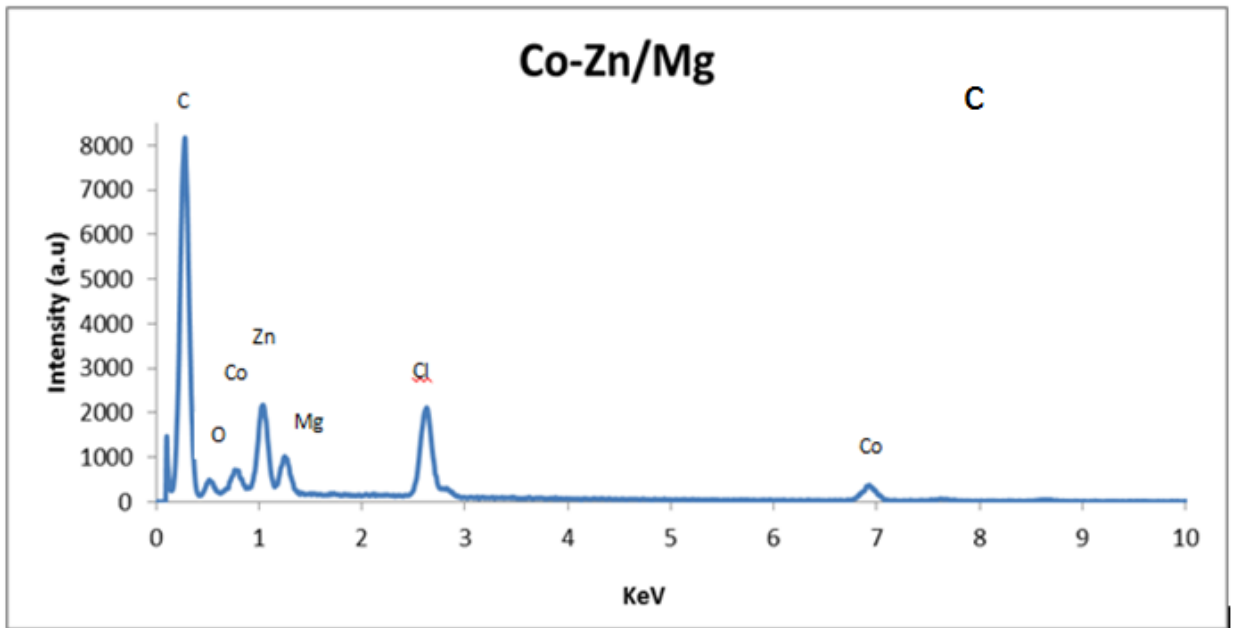
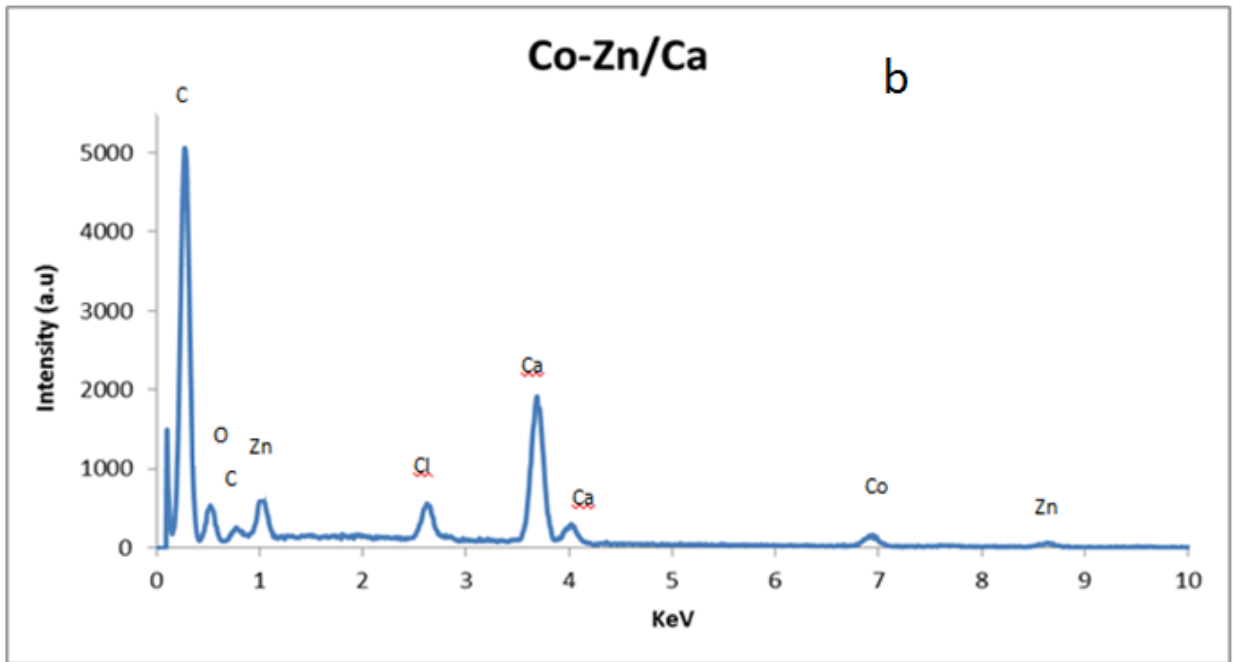


Figure 4.27 Energy dispersive spectroscopy analysis of carbon nanomaterial obtained from Co-Zn catalyst supported on (a) Al_2O_3 (b) CaCO_3 and (c) MgO .

Figure 4.27 (a) above shows the EDS analysis of CNTs obtained from Co-Zn catalyst and Al_2O_3 as support material. (a) Indicates C atom intensity as carbon source was acetylene. From the elemental observation (a) where Al_2O_3 was used as support was the worse followed by (b) where CaCO_3 was used lastly (c) where MgO has a slight improvement.

Ideally, catalyst should not be involved in a reaction but only to speed up reaction. However, in some instances it was observed that some catalysts were involved in catalytic activity. In conclusion from the EDS elemental analysis it can be observed that proved to be a bad catalyst followed by Zn the Sr being the best. Similarly, MgO has been proved to be the best support material as compared with Al_2O_3 & CaCO_3 .

4.5.6 Transmission Electron Microscopy (TEM)

TEM is a versatile tool that provides not only atomic resolution lattice images, but also chemical information at a spatial resolution has been used for the analysis of carbon nanomaterial.

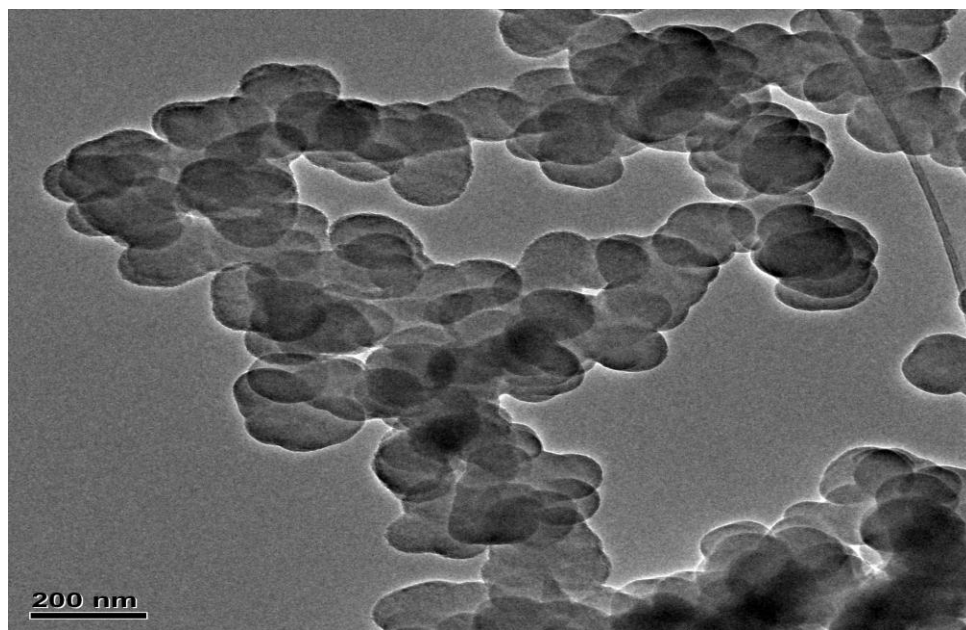


Figure 4.28 TEM image for Co-Sn/Ca

Figure 4.28 depicts TEM image for Co-Sn/Ca and it shows that carbon nanotubes were not synthesized but only carbon spheres.

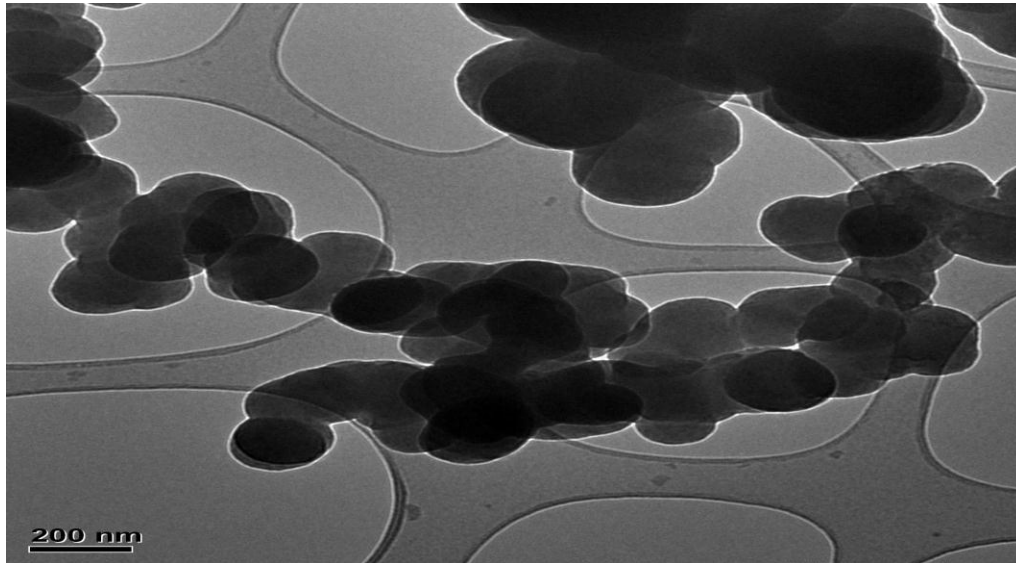


Figure 4.29 TEM image for Co-Sr/Ca

Figure 4.29 depicts TEM image for Co-Sr/Ca and it shows that carbon nanotubes were not synthesized but only carbon spheres were produced.

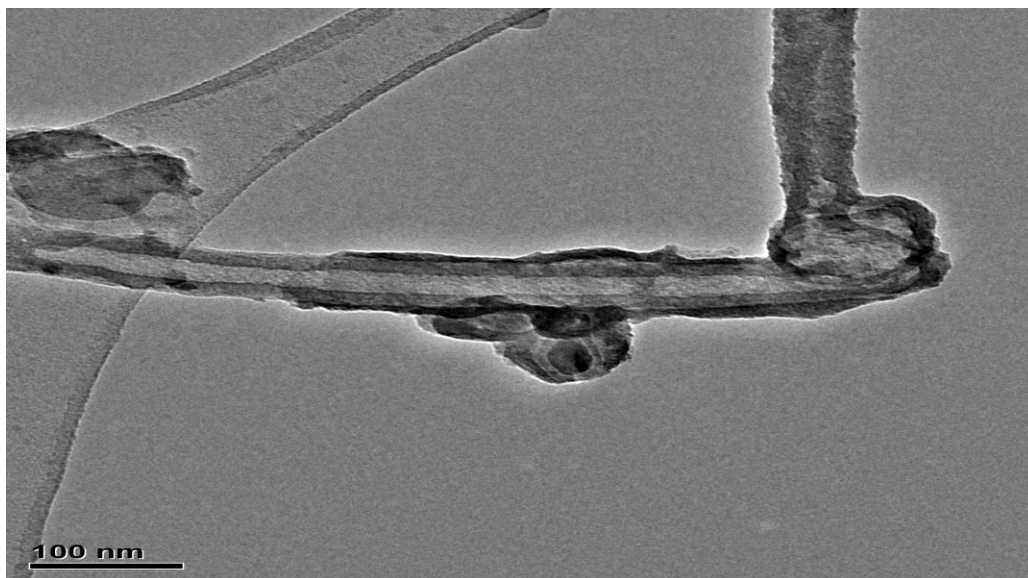


Figure 4.30 TEM image for Co-Sr/Mg

Figure 4.30 depicts TEM image for Co-Sr/Mg and it shows that carbon nanotubes were synthesized. This image further confirms that these are carbon nanotubes but not carbon fibers.

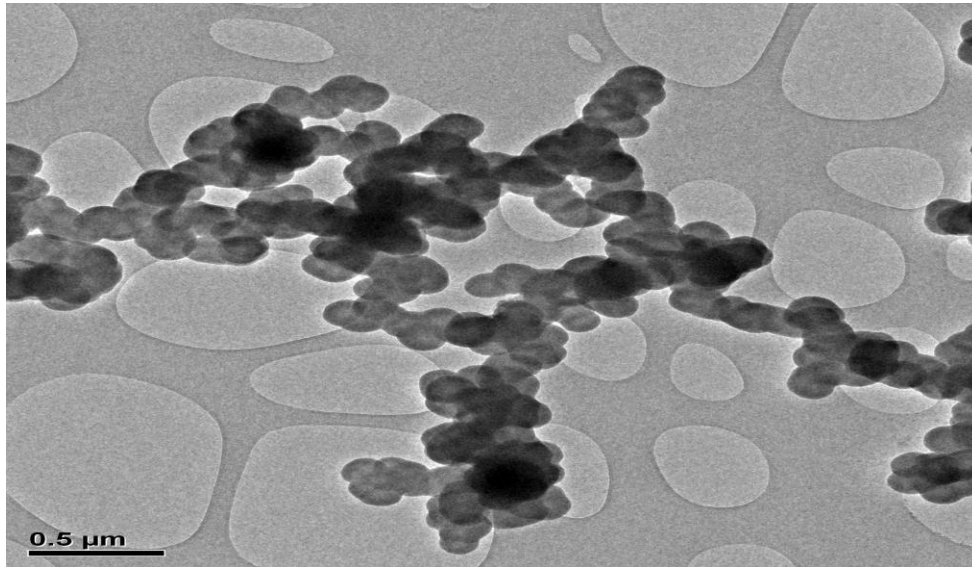


Figure 4.31 TEM image for Co-Zn/Ca

Figure 4.31 depicts TEM image for Co-Sr/Mg and it shows that carbon nanotubes were not synthesized. This image further confirms only carbon spheres were produced

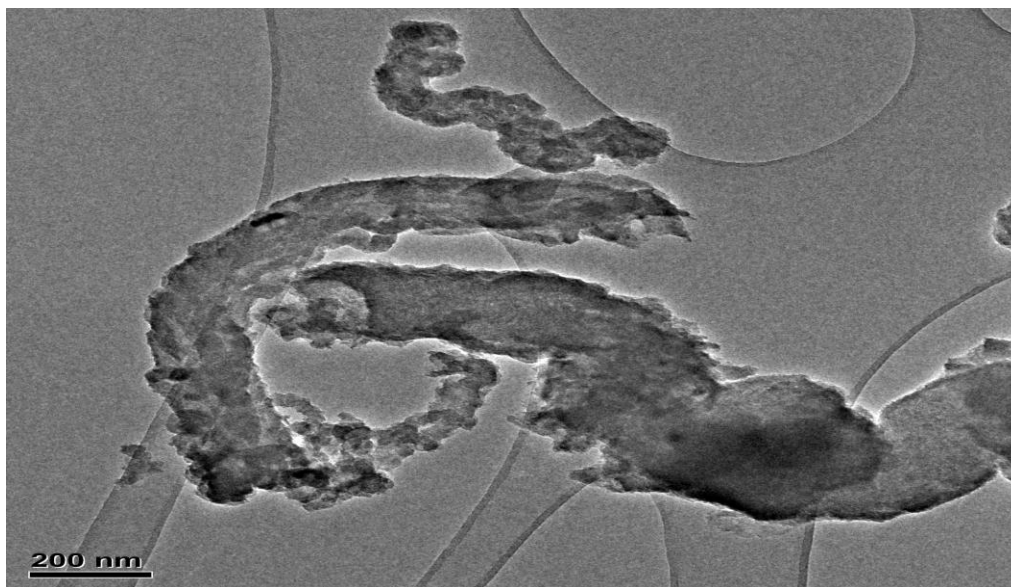


Figure 4.32 TEM image for Co-Zn/Mg

Figure 4.32 depicts TEM image for Co-Zn/Mg and it shows that short, thick and not elongated carbon nanotubes were synthesized. This image further shows some defects on nanomaterial.

The TEM results have shown that Co-Sr/Mg has produced carbon nanomaterial of better quality than Co-Zn/Mg while Co-Sn/Ca, and Co-Zn/Ca did not produce carbon nanotubes at all.

4.5.6 Heavy Metals Extraction Analysis

Pb(NO₃)₂ (10 ml of 0.01M) was mixed with 2.0 g of as prepared nanomaterial, that is graphene, graphene oxide and carbon material and left for three hours at room temperature then filtered through a filter paper. The initial solution and filtrate were then reacted with potassium iodide.

Table 4.2 showing pH for Pb(NO₃)₂ before and after filtered through graphene oxide.

Sample (0.01M)	pH before filtered	pH after filtered
Pb(NO ₃) ₂	4.0	6.7

Table 4.3 showing pH for Pb(NO₃)₂ before and after filtered through reduced graphene oxide.

Sample (0.01M)	pH before filtered	pH after filtered
Pb(NO ₃) ₂	4.0	4.2

Table 4.4 showing pH for Pb(NO₃)₂ before and after filtered through carbon nanotubes.

Sample (0.01M)	pH before filtered	pH after filtered
Pb(NO ₃) ₂	4.0	4.0

Table 4.2 shows that Pb(NO₃)₂ that has been filtered through GO has a significant pH change while Figures 4.3 & 4.4 show that pH results for lead nitrate that has been filtered through RGO and CNTs remain the same.



Figure 4.28 images of 0.01M $\text{Pb}(\text{NO}_3)_2$ reacted with 0.01M of KI (a) before and (b) after filtered through GO.

Figure 4.28 (a) shows that when potassium iodide is reacted with lead nitrate a yellow precipitate forms. But Figure 4.28 (b) shows that when potassium iodide was reacted with lead nitrate that was stirred and filtered through graphene oxide, the yellow colour was very mild with very little precipitation.

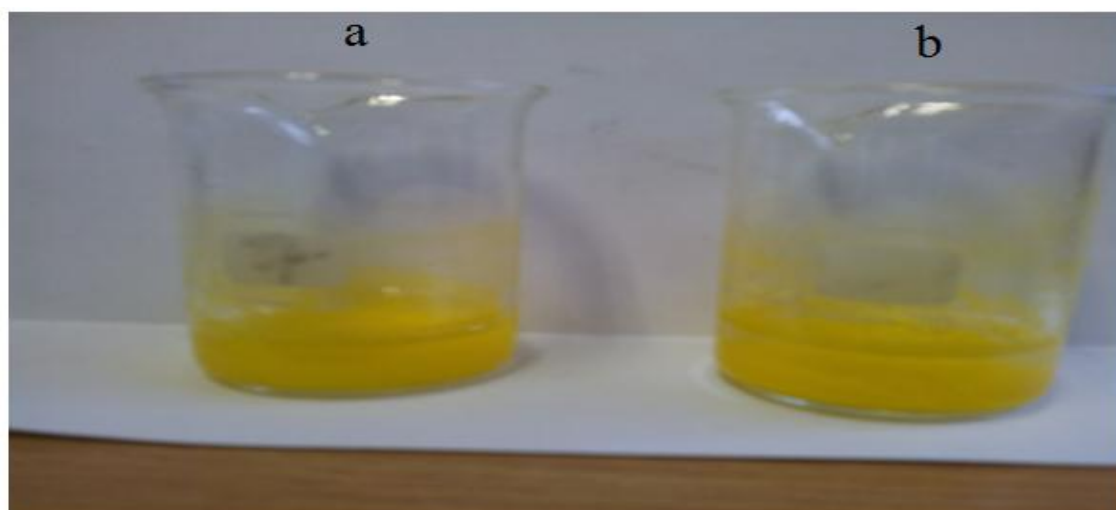


Figure 4.29 Images of 0.01M $\text{Pb}(\text{NO}_3)_2$ reacted with 0.01M of KI (a) before and (b) after filtered through RGO.

Figure 4.29 (a) shows that when potassium iodide is reacted with lead nitrate a yellow precipitate forms. But figure 4.29 (b) still shows that when potassium iodide was reacted with lead nitrate that was stirred and filtered through RGO, the yellow colour was still there with same intense precipitation.



Figure 4.30 Images of 0.01M $\text{Pb}(\text{NO}_3)_2$ reacted with 0.01M of KI (a) before and (b) after filtered through CNTs.

Figure 4.30 (a) shows that when potassium iodide is reacted with lead nitrate a yellow precipitate forms. But figure 4.30 (b) still shows that when Potassium iodide was reacted with lead nitrate that was stirred and filtered through CNTs, the yellow colour was still there with same intense precipitation.

The observation could be evidenced by the fact that graphene and carbon nanotubes do not have functional groups attached to them hence they are hydrophobic while GO has functional groups attached to it and that makes it hydrophilic. The readily attached functional groups could be attributed to the adsorption process.

References

1. C. Hou, Q. Zhang, M. Zhu, Y. Li, H. Wang, *Carbon*. 49 (2011) 47-53.
2. http://www.google.co.za/search?q=structure+model+of+the+graphite+oxide+species&hl=en&rlz=1W1ADRA_enZA473&prmd=imvns&source=lnms&tbm=isch&ei=UeTET5_VMcSdOtf13e8J&sa=X&oi=mode_link&ct=mode&cd=2&ved=0CD8Q_AUoAQ&biw=1440&bih=665, 12, March, 2012.
3. T. Nakajima, A. Mabuchi, R. Higawara, *Carbon*. 26 (1988) 357-361.
4. K. N. Kudin, B. Ozbas, H. C. Schniepp, R. K. Prud'homme, I. A. Aksay, R. Car, *Nano. Lett.* 8 (2008) 36-41.
5. M. J. McAllister, J. L. Li, D. H. Adamson, H. C. Schniepp, A. A. Abdala, J. Liu, M. Herrera-Alonso, D. L. Milius, R. Car, I. A. Aksay, *Chem. Mater.* 19 (2007) 4396-4404.
6. Y. Yu, L. L. Ma, W. Y. Huang, F. P. Du, J. C. Yu, J. G. Yu, *Carbon*. 43 (34) (2005) 670-673.
7. S. Pan, X. Liu, X. Wang, *Mater. Charact.* 62 (2011) 1094-1101.
8. J. C. Meyer, A. K. Geim, M. I. Katsnelson, T. J. Booth, *Nat.* 446 (2007) 60-63.
9. T. N. Lambert, C. A. Chavez, B. Hernandez-Sanchez, P. Lu, N. S. Bell, A. Ambrosini, *J. Phys. Chem. C* 113 (2009) 19812-19823.
10. S. Stankovich, D. A. Dikin, R. D. Piner, K. A. Kohlhaas, A. Kleinhammes, Y. Jia, Y. Wu, S. T. Nguyen, R. S. Ruoff, *Carbon*. 45 (2007) 1558-1565.
11. D. S. Knight, W. B. White, *J. Mater. Res.* 4 (1989) 385.
12. J. Wasyluk, T. S. Perova, D. W. Lau, M.B. Taylor, D. G. McCulloch, J. Stopford, *Diamond. Relat. Mater.* 19 (2010) 514-519.

CHAPTER FIVE: CONCLUSION AND RECOMMENDATION

CHAPTER FIVE

CONCLUSION AND RECOMMENDATION

5.1 Introduction

The objectives of this research were to synthesize graphene oxide from flake graphite powder and reduce it to graphene. To synthesize carbon nanotubes using different catalysts and supporting materials and study structural and morphological properties using XRD, FTIR, UV-Vis, SEM, EDS, TEM, Raman, AFM, TGA & DTA and optical spectroscopy and finally to remove heavy metals from water.

5.2 Graphene and graphene oxide

5.2.1 Structured analysis

- The XRD diffractogram shows a very intense and narrow peak centred at $2\theta = 11.8^\circ$, corresponding to the (002) inter-planar spacing of 7.49 \AA which confirms oxidation. The basal spacing increases in the course of oxidation due to the expansion of the layer planes caused by the accommodation of various oxygen species.
- The most intense peak for expandable graphite at $2\theta = 26.4^\circ$, corresponding to a d-spacing of 3.37 \AA is present in RGO sample. The basal spacing decreases in the course of reduction due to the shrinking of the layer planes caused by the removal of various oxygen species.
- XRD results indicated reduction of the average number of graphene layers steadily from raw graphite to graphene nanosheets by one-step chemical procedure.
- The relatively strong FTIR peak at 1720 cm^{-1} is most often related to the C=O stretching of COOH groups situated at the edges of the oxidized graphenes.
- The peak at 1630 cm^{-1} was attributed either to oxygen surface compounds, like cyclic ethers, or to ring vibrations throughout the carbon skeleton
- The HOH bending vibrations also appear in a very close range of wavenumbers. The C-OH stretching peak at 1260 cm^{-1} characterizes the spectrum of carbonyl groups, and the C-O stretching peak at 1070 cm^{-1} characterizes the spectrum of epoxy groups on the

surface of the oxidized graphene. Elemental analysis also supports that the situation of oxidation.

- Ultra-violet visible spectra with absorption peak at 230 nm that is red shifted to 270 nm indicating that the electronic conjugation was revived upon reduction of graphene oxide.
- Raman spectra indicated that there is a linearly decrease in graphene with respect to the decrease in G intensity.
- Formation of D band after oxidation process is evident from the success of the reaction procedure.
- The formation of the 2D band indicates good quality material
- After heat treatment and reduction processes, quasi-defect graphene sheets were formed as I_G/I_D ratio decrease after chemical layer number decreases.

5.2.2 Morphological Analysis

- The TEM RGO sheets are no longer totally flat and smooth but always exhibit some corrugation, where they resemble crumpled silk veil waves. This is evidenced by some areas of the particle showing considerable folding as oxygen species were removed during reduction process.
- The AFM GO sheets are thicker due to the presence of covalently bonded oxygen and the displacement of sp^3 hybridized carbon atoms slightly above and below the original graphene plane.
- The AFM height profile between GO and RGO indicates a single graphene oxide sheet due to intercalating of oxygen into the graphite gallery. This further confirms the reduction of graphene oxide into graphene.
- AFM images in 3D view supported the formation of rippled graphene layers and effect of reaction in each step.

- SEM images indicated the existence of rippled graphene layers instead of completely flat layers in a free standing state. The defects and holes on the RGO SEM image could be attributed to the removal of oxygen functional species.

5.3 Carbon nanotubes (CNTs)

5.3.1 Structural analysis

- The XRD has shown lattice structure at characteristic peaks while many other peaks were a result of impurities and amorphous carbon.
- It is then can be concluded that MgO has proved to be a better supporting material especially for Co-Sr and Co-Zn catalysts.
- T- band which is associated with sp^3 sites was evidenced.
- D- and G- bands in the Raman spectra of graphite and amorphous carbon were found to be the same..
- The G peak is due to the relative motion of sp^2 carbon atoms, while the D peak is linked to the breathing modes rings.
- The Raman spectra depend formally on the ordering/packing of the sp^2 sites due to the resonance enhancement of their vibrations.

5.3.2 Morphological analysis

The SEM images have shown that nanospheres were synthesized in all samples except in Co-Sr/Mg samples where elongated tubes are produced. These tubes were confirmed to be carbon nanotubes by TEM.

5.4 Recommendation

Further research must be thoroughly done on application of these carbon allotropes. Since graphene is hydroscopic a composite with it must be synthesized, characterized and applied to ensure its efficiency.

The carbon nanotubes are also hydroscopic and do not dissolve in water. It is therefore, important that CNTs must be functionalized to tune them to be compatible for various applications.

The GO which is hydrophilic is desirable for heavy metal removal because of readily attached functional groups, but more research can be done on it when it is in a composite to improve efficiency. However more intense research should be done to find out if indeed lead has been adsorbed by graphene oxide. It should also be appreciated that more techniques should be employed to confirm if indeed carbon material was really CNTs or just carbon fibres.